

**Control and eradication of migrating parasitic  
nematode larvae by innate effector cells**

**Dissertation**

with the aim of achieving a doctoral degree at the  
Faculty of Mathematics, Informatics and Natural Sciences

Department of Biology  
of the Universität Hamburg

submitted by

**Nikolas Rüdiger**

Hamburg, December 2018






## Eidesstattliche Versicherung

Hiermit erkläre ich an Eides statt, dass ich die vorliegende Dissertationsschrift selbst verfasst und keine anderen als die angegebenen Quellen und Hilfsmittel benutzt habe.

Hamburg, 11.12.2018



---

Nikolas Rüdiger

## Language certificate

My name is Daniel Nicholas Fairhurst and I am a native speaker.

I have read the present PhD thesis and I hereby confirm that it complies with the rules of the English language.

Hamburg, 01.12.2018



Daniel Nicholas Fairhurst

## **Danksagung**

Ich möchte mich ganz herzlich bei PD Dr. Minka Breloer bedanken für die exzellente wissenschaftliche Betreuung und unermüdliche Unterstützung bei dieser Arbeit.

Prof. Dr. Jörg Ganzhorn möchte ich für die Bereitschaft danken, als Gutachter diese Arbeit zu bewerten.

Marie-Luise, ich danke dir für alles was ich von dir lernen durfte. Martina, ich danke dir für deine große Hilfe, gerade in den letzten zwei Jahren der Doktorarbeit. Wiebke und Nadine, euch gilt ebenfalls ein großer Dank.

Liebe Zane, Frauke, Gesine und lieber Philipp, ich danke euch für die schöne Zeit in Borstel. Diese Zeit bleibt unvergessen.

Ein besonderer Dank geht an meine gesamte Familie für ihre Liebe und Unterstützung.

Mein tiefster Dank geht an meine Freundin Marie. Ich danke dir, dass du immer für mich da bist. Ich danke dir für deine Liebe, Unterstützung und Geduld. Ohne dich wäre es nicht möglich gewesen.

## Summary

Helminths are large multicellular parasites that represent a complex challenge for the mammalian immune system. In this thesis, the helminth parasite *Strongyloides ratti* is used as a model to study the immune response of intestinal helminths with tissue migration stages. *S. ratti* actively penetrates the skin of its rodent host and migrates via the tissue and the mouth to the small intestine where it lives and reproduces. Immune competent mice terminate the infection within one month in the context of a canonical type 2 immune response. Efficient killing of migrating larvae in the tissue depends on neutrophilic and eosinophilic granulocytes, whereas expulsion of adult parasites from the intestine is predominantly mediated by mast cells. During tissue migration of larvae, cell damage occurs, which is accompanied by the release of danger-associated molecules such as interleukin-33 (IL-33). IL-33 functions as an alarmin in the extracellular space to promote the initiation of the appropriate anti-helminth type 2 immune response.

The aim of this study was to define the fate and localization of migrating larvae during a primary and secondary infection in mice and to analyze the role of the alarmin IL-33 in the initiation and execution of the type 2 immune response against *S. ratti* in the tissue and the intestine.

The kinetic analysis of various tissues during *S. ratti* infection revealed that the larvae followed a defined migration route. After a rapid disappearance from the site of infection, the footpad, larvae migrated through skin and muscle tissue, via lung and head to the small intestine. In primary infected mice, larvae were killed during their entire tissue migration i.e. at the site of infection, in skin and in muscle tissues, while larvae were almost completely eradicated at the site of infection during a secondary infection.

Treatment of mice with recombinant IL-33 (rIL-33) resulted in site-specific divergent effects. rIL-33 induced an early initiation of type 2 immune response in the tissue that was indicated by Arginase-1 and IL-13 mRNA transcription in the lung. Nevertheless, killing of larvae in the tissue was impaired in rIL-33 treated mice. Depletion of granulocytes or the absence of eosinophils resulted in increased numbers of larvae in the tissue, as expected. However, rIL-33 mediated no further elevation of the tissue parasite burden in the absence of these effector cells, suggesting that rIL-33 treatment interfered with granulocyte effector functions.

Despite elevated numbers of larvae in the tissue, the parasite burden in the small intestine was drastically decreased in rIL-33 treated mice. Efficient expulsion of parasitic adults from the intestine of rIL-33 treated mice was dependent on the presence of mast cells and a functional IL-9 receptor and was associated with accelerated mast cell activation. Therefore, rIL-33 triggered rapid mast cell activation via IL-9 induction, either directly or indirectly via an IL-9 responsive cell.

Taken together, the results of this thesis provide evidence that rIL-33 treatment induces a potent type 2 immune response for efficient clearance of *S. ratti* from the small intestine, but at the same time, may interfere with granulocyte- and eosinophil-mediated killing of larvae in the tissue.



## Zusammenfassung

Helminthen sind große und vielzellige Parasiten, die eine komplexe Herausforderung für das Immunsystem von Säugetieren darstellen. In dieser Arbeit wird der Helminthen-Parasit *Strongyloides ratti* als Modell verwendet, um die Immunantwort gegen gastrointestinale Helminthen mit Gewebemigrationsstadien zu untersuchen. *S. ratti* dringt aktiv in die Haut seines Nagetier-Wirtes ein und wandert über das Gewebe und den Mund in den Dünndarm, um sich dort einzunisten und zu vermehren. Immunkompetente Mäuse beenden die Infektion im Rahmen einer kanonischen Typ-2-Immunantwort innerhalb eines Monats. Die effiziente Abtötung von wandernden Larven im Gewebe hängt von neutrophilen und eosinophilen Granulozyten ab, wohingegen die Ausstoßung adulter Parasiten aus dem Darm überwiegend durch Mastzellen vermittelt wird. Während der Gewebemigration von Larven kommt es zu einer Zellschädigung, die mit der Freisetzung von molekularen Gefahren- und Schadsignalen wie beispielsweise Interleukin-33 (IL-33) einhergeht. IL-33 fungiert als Alarmin im extrazellulären Raum, um eine geeignete Typ-2-Immunantwort gegen Helminthen zu initiieren.

Das Ziel dieser Studie war es, das Schicksal und die Lokalisation migrierender Larven während einer primären und sekundären Infektion bei Mäusen zu untersuchen und die Rolle des Alarmins IL-33 bei der Initiierung und Durchführung der Typ-2-Immunantwort gegen *S. ratti* im Gewebe und Darm zu analysieren.

Die kinetische Analyse verschiedener Gewebeproben während der Infektion mit *S. ratti* ergab, dass die Larven einer definierten Migrationsroute folgen. Die Larven wanderten schnell von der Infektionsstelle, der Hinterpfote, durch Haut- und Muskelgewebe, über Lunge und Kopf zum Dünndarm. In primär infizierten Mäusen wurden Larven während der gesamten Gewebemigration, d. h. in der Infektionsstelle, Haut- und Muskelgewebe abgetötet. In einer Sekundärinfektion wurden die Larven hingegen beinahe vollständig in der Infektionsstelle eliminiert.

Die Behandlung von Mäusen mit rekombinantem IL-33 (rIL-33) führte zu unterschiedlichen gewebespezifischen Effekten. rIL-33 induzierte eine frühe Initiierung der Typ-2-Immunantwort im Gewebe, die durch Arginase-1 und IL-13 mRNA-Transkription in der Lunge gekennzeichnet war. Allerdings wurde die Bekämpfung der Larven im Gewebe durch die Gabe von rIL-33 beeinträchtigt. Die Abwesenheit von

Granulozyten oder eine Eosinophilen-Defizienz führte erwartungsgemäß zu einer erhöhten Anzahl von Larven im Gewebe. In Abwesenheit dieser Effektorzellen konnte rIL-33 jedoch keine weitere Erhöhung der Parasitenlast im Gewebe bewirken, was darauf hindeutet, dass die Behandlung mit rIL-33 die Effektorfunktionen der Granulozyten beeinträchtigte.

Trotz einer erhöhten Anzahl von Larven im Gewebe war die Parasitenlast im Dünndarm bei rIL-33 behandelten Mäusen drastisch verringert. Die effiziente Ausstoßung von adulten Parasiten aus dem Darm in rIL-33 behandelten Mäusen war von Mastzellen und einem funktionellen IL-9-Rezeptor abhängig und ging mit einer beschleunigten Aktivierung der Mastzellen einher. Folglich löste rIL-33 eine schnelle IL-9 induzierte Mastzellaktivierung aus, entweder direkt oder indirekt über eine auf IL-9 reagierende Zelle.

Zusammenfassend liefern die Ergebnisse dieser Arbeit einen Beweis dafür, dass die Behandlung mit rIL-33 eine starke Typ-2-Immunantwort zur effizienten Ausstoßung von *S. rattii* aus dem Dünndarm induziert. Gleichzeitig geht diese Immunantwort jedoch mit einer Abschwächung der Larvenbekämpfung durch Granulozyten und Eosinophilen im Gewebe einher.

## List of abbreviations

°C	Degree Celsius
AAM	Alternative activated macrophages
APC	Allophycocyanin
APCs	Antigen presenting cells
Arg-1	Arginase-1
AS	Anti-sense
B cell	Bone-marrow derived lymphocyte
BAL	Bronchoalveolar lavage
BNITM	Bernhard Nocht Institute for Tropical Medicine
bp	Base pair
BSA	Bovine serum albumin
BV421	Brilliant Violet 421
BV510	Brilliant Violet 510
CCL1	CC-chemokine ligand 1
CD	Cluster of differentiation
cDNA	Complementary deoxyribonucleic acid
CO <sub>2</sub>	Carbon dioxide
Cpa3	Carboxypeptidase A3
C-TLs	C-type lectin
CXCL8	C-X-C Motif Chemokine Ligand 8
CXCR2	C-X-C chemokine receptor type 2
DAMP	Danger-associated molecular pattern
DMSO	Dimethyl sulfoxide
DNA	Deoxyribonucleic acid
EDTA	Ethylenediaminetetraacetate
ELISA	Enzyme linked immunosorbent assay
et al.	<i>et alia</i>
EtBr	Ethidium bromide
FACS	Flow activated cell sorting
FCS	Fetal calf serum
FITC	Fluorescein Isothiocyanate
g	Gram
GM- CSF	Granulocyte-macrophage colony-stimulating factor
Gr-1	Granulocyte receptor-1
h	Hours
H&E	Hematoxylin and eosin
HEPES	4-(2-hydroxyethyl)-1-piperazineethanesulfonic acid
HpARI	<i>H. polygyrus</i> alarmin release inhibitor
HRP	Horseradish peroxidase
i.p.	Intraperitoneal
Ig	Immunoglobulin
IL	Interleukin

IL-9R	Interleukin-9 receptor
ILC2	group 2 innate lymphoid cells
iNOS	Inducible nitric oxide synthase
JHD	J <sub>H</sub> region deletion
KOH	Potassium hydroxide
L	Liter
L1	First stage larvae
L2	Second stage larvae
L3	Third stage larvae
L3i	Infective third stage larvae
L4	Fourth stage larvae
Ly6C	Lymphocyte antigen 6C
Ly6G	Lymphocyte antigen 6G
M	Molar
MBP	Major basic protein
Mcpt8	Mast cell protease 8
MDSCs	Myeloid-derived suppressor cells
MHC	Major histocompatibility complex
mL	Milliliter
mMCPT-1	Mouse mast cell protease-1
MPO	Myeloperoxidase
MRI	Magnetic resonance imaging
mRNA	Messenger ribonucleic acid
NaCl	Sodium chloride
NaSDCI	Naphthol AS-D Chloroacetate esterase
NETs	Neutrophil extracellular traps
ng	Nanogram
ns	Not significant
OD	Optical density
p	Probability
p.i.	Post infection
PAMP	Pathogen associated molecular pattern
PBS	Phosphate buffered saline
PCR	Polymerase chain reaction
PE	Phycoerythrin
PerCP	Peridinin chlorophyll protein
pH	<i>potentia hydrogenii</i>
PRR	Pattern recognition receptor
qPCR	Quantitative polymerase chain reaction
RAG	Recombination activating gene 1
rIL-33	Recombinant Interleukin-33
rpm	Rounds per minute
RPMI	Roswell Park Memorial Institute
rRNA	Ribosomal ribonucleic acid

S	Sense
s.c.	Subcutaneous
SEA	Soluble egg antigen
SEM	Standard error of mean
SiglecF	Sialic acid-binding, Ig-like lectin F
spp.	<i>species pluralis</i>
ST2	Suppression of tumorigenicity-2
T cell	Thymus derived lymphocyte
T reg	regulatory T cell
TBE	Tris/borate/EDTA
Th2	T helper cell type 2
TLR	Toll-like receptor
TNF	Tumor necrosis factor
Tris	Tris(Hydroxymethyl)aminomethane
TSLP	Thymic stromal lymphopoietin
USA	United States of America
Wt	Wildtype
xg	relative centrifugal gravity force
µg	Microgram
µL	Microliter

## List of figures

Figure 1. The life cycle of <i>S. ratti</i> . .....	2
Figure 2. Alarmin-mediated activation of ILC2 in the initiation of type 2 immune response during helminth infection.....	8
Figure 3. Quantification of <i>S. ratti</i> parasites in host tissue.....	37
Figure 4. <i>S. ratti</i> L3 migration-induced tissue damage in the lung.....	39
Figure 5. <i>S. ratti</i> parasite burden in rIL-33 treated mice.....	41
Figure 6. Quantification of <i>S. ratti</i> parasites in rIL-33 treated mice.....	43
Figure 7. Quantification of erythrocytes in bronchoalveolar lavage of rIL-33 treated mice. .....	44
Figure 8. Quantification of <i>S. ratti</i> -derived DNA in feces of rIL-33 treated mice.....	45
Figure 9. Quantification of mMCP-1 concentrations in sera of rIL-33 treated mice. ....	47
Figure 10. <i>S. ratti</i> parasite burden and mast cell activation in rIL-33 treated mast cell-deficient <i>Cpa3<sup>Cre</sup></i> mice.....	50
Figure 11. <i>S. ratti</i> parasite burden and mast cell activation in rIL-33 treated IL-9R-deficient mice.....	52
Figure 12. <i>S. ratti</i> parasite burden and mast cell activation in rIL-33 treated basophil-deficient mice.....	54
Figure 13. Flow cytometric detection and quantification of neutrophils and eosinophils in the lung of rIL-33 treated mice.....	56
Figure 14. <i>S. ratti</i> parasite burden and mast cell activation in rIL-33 treated, granulocyte depleted mice.....	59
Figure 15. <i>S. ratti</i> parasite burden and mast cell activation in rIL-33 treated eosinophil-deficient mice.....	60
Figure 16. Lung mRNA expression in rIL-33 treated mice during <i>S. ratti</i> infection. ....	62

## List of tables

Table 1. Laboratory equipment.....	11
Table 2. Consumables.....	12
Table 3. Reagents. ....	13
Table 4. Buffers and solutions. ....	15
Table 5. DNA oligonucleotide primers. ....	17
Table 6. Kits.....	17
Table 7. Software. ....	17
Table 8. Mice.....	18
Table 9. PCR program.....	25
Table 10. PCR Cpa3 <sup>Cre</sup> mice.....	25
Table 11. PCR Mcpt8 <sup>Cre</sup> mice.....	25
Table 12. qPCR DNA program. ....	27
Table 13. qPCR DNA sample preparation.....	27
Table 14. Mastermix DNase treatment. ....	28
Table 15. RNA incubation with random primer mix.....	28
Table 16. cDNA synthesis reagents. ....	29
Table 17. Gene specific primers for gene expression qPCR analysis. ....	29
Table 18. qPCR cDNA program. ....	30
Table 19. qPCR reagents for gene expression analysis.....	30
Table 20. Fluorescence-labeled antibodies for flow cytometry.....	33

## Table of contents

1. Introduction.....	1
1.1 <i>Strongyloides ratti</i> as a model for a transient gastrointestinal nematode infection .	1
1.2 The type 2 immune response during helminth infection .....	3
1.3 Immune response to <i>Strongyloides</i> infections in rodents .....	4
1.4 Initiation of type 2 immune responses .....	5
1.5 The biology of interleukin-33 .....	9
1.6 Study aim .....	10
2. Materials and Methods .....	11
2.1 Materials.....	11
2.1.1 Laboratory equipment .....	11
2.1.2 Consumables .....	12
2.1.3 Reagents.....	13
2.1.4 Buffers and solutions.....	15
2.1.5 DNA oligonucleotides.....	16
2.1.6 Kits .....	17
2.1.7 Software .....	17
2.1.8 Parasite .....	18
2.1.9 Mice .....	18
2.1.10 Statistical Analysis .....	19
2.2 Methods.....	19
2.2.1 Parasitological methods and animal experiments .....	19
2.2.1.1 Maintenance of <i>S. ratti</i> life cycle and preparation of L3i.....	20
2.2.1.2 Experimental infections.....	20
2.2.1.3 Mice treatments .....	20
2.2.1.3.1 Recombinant IL-33 treatment .....	20
2.2.1.3.2 Anti-Gr-1 treatment.....	20
2.2.1.4 Quantification of L3 in the tissue .....	21
2.2.1.5 Quantification of adults in the small intestine .....	21
2.2.1.6 Collection of mice stool for quantification of <i>S. ratti</i> -derived DNA in the feces .....	21
2.2.1.7 Mouse serum .....	21



2.2.1.8 Quantification of erythrocytes in bronchoalveolar lavage (BAL) and cytopsin of BAL cells.....	22
2.2.1.9 Histology of lung tissue .....	22
2.2.2 Biochemical methods .....	23
2.2.2.1 ELISA quantification of mouse mast cell protease-1 (mMCPT-1) in sera .....	23
2.2.3 Molecular biological methods.....	23
2.2.3.1 DNA isolation from ear biopsy .....	23
2.2.3.2 DNA isolation from feces .....	23
2.2.3.3 DNA isolation from tissues and organs .....	24
2.2.3.4 DNA concentration.....	24
2.2.3.5 Polymerase chain reaction (PCR) for mice genotyping.....	24
2.2.3.6 Agarose gel electrophoresis .....	26
2.2.3.7 <i>Strongyloides</i> DNA real-time quantitative PCR (qPCR) .....	26
2.2.3.8 RNA isolation .....	27
2.2.3.9 DNase treatment and reverse transcriptase reaction.....	28
2.2.3.10 cDNA real-time quantitative PCR (qPCR).....	29
2.2.4 Cell biology methods.....	31
2.2.4.1 Cell count determination .....	31
2.2.4.2 Lung single cell suspension preparation .....	31
2.2.4.3 Blood cell preparation .....	31
2.2.4.4 Flow cytometry.....	32
2.2.4.4.1 Flow cytometry – staining procedure .....	32
3. Results.....	34
3.1 Quantification of <i>S. ratti</i> parasites in host tissue.....	34
3.2 <i>S. ratti</i> L3 migration-induced tissue damage in the lung .....	38
3.3 Quantification of <i>S. ratti</i> parasites in rIL-33 treated mice.....	40
3.4 Quantification of mMCPT-1 concentrations in sera of rIL-33 treated mice .....	46
3.5 <i>S. ratti</i> parasite burden and mast cell activation in rIL-33 treated mast cell-deficient Cpa3 <sup>Cre</sup> mice .....	48
3.6 <i>S. ratti</i> parasite burden and mast cell activation in rIL-33 treated IL-9R-deficient mice.....	51

3.7 <i>S. ratti</i> parasite burden and mast cell activation in rIL-33 treated basophil-deficient mice.....	53
3.8 Flow cytometric detection and quantification of neutrophils and eosinophils in the lung of rIL-33 treated mice .....	55
3.9 <i>S. ratti</i> parasite burden and mast cell activation in rIL-33 treated, granulocyte depleted mice and eosinophil-deficient mice .....	57
3.10 Lung mRNA expression in rIL-33 treated mice during <i>S. ratti</i> infection .....	61
4. Discussion .....	63
4.1 Migration of <i>S. ratti</i> .....	63
4.2 The impact of IL-33 on <i>S. ratti</i> infection .....	65
4.3 The impact of IL-33 on <i>S. ratti</i> infection in the small intestine.....	66
4.4 The impact of IL-33 on <i>S. ratti</i> in the tissue .....	69
5. Outlook .....	74
5.1 The impact of IL-33 on <i>S. ratti</i> infection .....	74
5.2 Migration of <i>S. ratti</i> .....	75
List of references .....	77

## 1. Introduction

### 1.1 *Strongyloides ratti* as a model for a transient gastrointestinal nematode infection

The genus *Strongyloides* encloses about 50 nematode species that parasitize in the gastrointestinal tract of vertebrates, including mammals, birds, reptiles and amphibians (Speare, 1989; Viney and Lok, 2007). Humans can be infected by two species, *Strongyloides stercoralis* and *Strongyloides fuelleborni* (Schad, 1989), whereas *S. fuelleborni* normally infects African primates (Hira and Patel, 1980; Pampiglione and Ricciardi, 1972). It is estimated that *S. stercoralis* infects 30 - 100 million individuals worldwide (Dogan et al., 2014). Infection with *Strongyloides* spp., called strongyloidiasis, is most commonly in South America, sub-Saharan Africa and South-East Asia. In these areas, the infection prevalence with over 20 % represents a major health concern (Siddiqui and Berk, 2001). To model *Strongyloides* infection in mice, the closely related pathogen *Strongyloides ratti* (*S. ratti*) is used for experimental infections (Dawkins et al., 1980). *S. ratti* was first described by Sandground in 1925 as a parasite of rats (*R. norvegicus*) (Sandground, 1925). *S. ratti* infections are widespread around the world that go along with the distribution of rats (Viney and Kikuchi, 2017). The life cycle of *Strongyloides* spp. is complex and includes parasitic and free-living phases (Viney, 1999; Viney and Lok, 2007). The following description is based on the life cycle of *S. ratti* (Fig. 1).

Host infections occur by skin penetration of infective third stage larvae (L3i). Third stage larvae (L3) migrate through the host, partially via the lung, to the naso-frontal region of the head within 2 days (Dawkins and Grove, 1981a; Dawkins et al., 1982b). After being swallowed, they reach the small intestine, where they develop to parasitic female adults via fourth stage larvae (L4) (Dawkins and Grove, 1981a). The adults reside in the intestinal mucosa and reproduce by parthenogenesis. Adults move along the intestine by creating epithelial tunnels, but they never penetrate the basement lamina (Dawkins et al., 1983; Viney and Lok, 2007). Eggs as well as hatched first stage larvae (L1) are released with the feces into the environment. Two alternative developments then can occur, termed homogenetic and heterogenetic. In homogenetic development, also known as direct development, L1 can develop via two stages to L3i. This L3i stage only develops further when it infects a new host. In heterogenetic development, also known as indirect

## 1. Introduction

development, L1 moult via 4 larval stages to free-living female and male adults. Free living adults reproduce by conventional sexual reproduction and females lay eggs in the environment. Hatched L1 moult via 2 larval stages to L3i again. These L3i are able to survive for a long period of time in the environment until finding a new host (Viney, 1999; Viney and Lok, 2007). Sex determination of L1 is based on a X chromosome system, in which XX parasitic females produce XX female and X0 male L1. XX females can undergo direct as well as indirect development, whereas X0 males are restricted to indirect development and become free-living male adults (Streit, 2008; Viney and Lok, 2007).

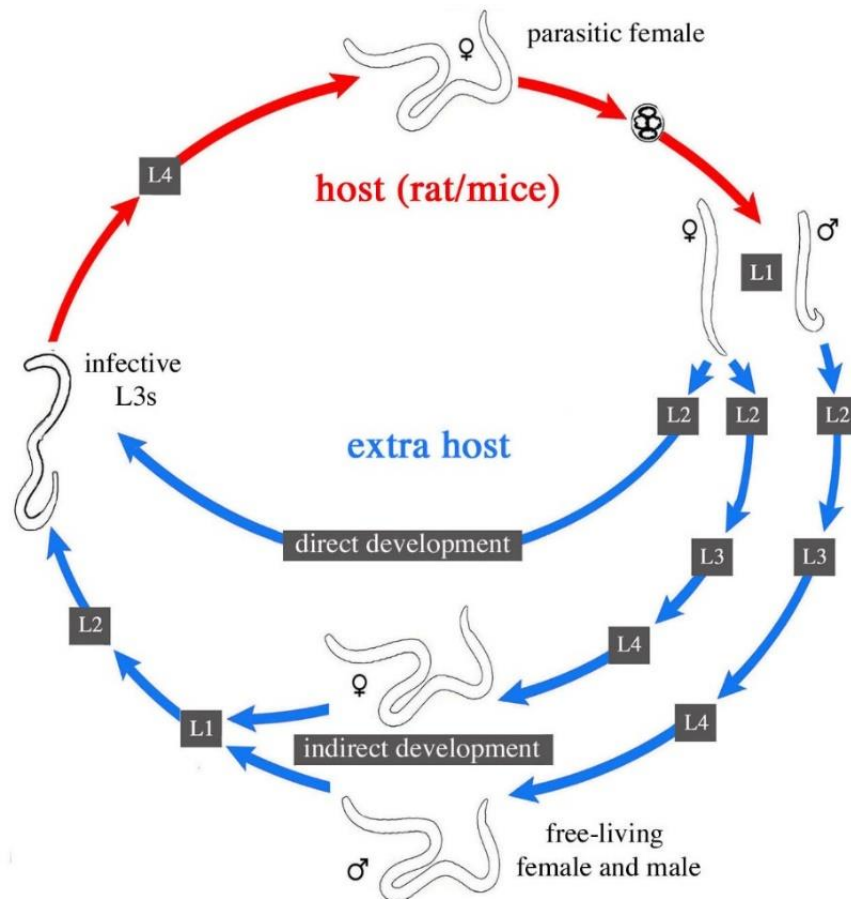


**Figure 1. The life cycle of *S. ratti*.**

The life cycle of *S. ratti* has parasitic and free-living life phases. Infective L3 actively penetrate the skin of a rodent host. Within the tissue, L3 migrate to the pharynx via head and lung within 2 days. After being swallowed, L3 develop in the gastrointestinal tract to adult females, that live embedded in the mucosa of the small intestine. Females adults reproduce by mitotic parthenogenesis and excrete eggs and hatched L1 with the stool into the environment. These L1 develop either directly into infective L3 or they moult to female or male adults that sexually produce L1. These genetically different L1 moult again to infective L3, ready to infect new hosts.

### **1.2 The type 2 immune response during helminth infection**

The immune system protects the host against a full spectrum of pathogens, including microorganisms such as viruses, bacteria or fungi and macropathogens, such as multicellular, large helminths or ectoparasites (Allen and Maizels, 2011). In contrast to the antimicrobial type 1 immune response against rapidly replicating microorganisms, helminths are controlled in a distinct immune response called type 2 immune response (Gause et al., 2013; Yap and Gause, 2018). As most helminths do not replicate in the mammalian host, the danger of rapid expansion is absent. During infection, larvae develop within the host to sexual mature adults that produce eggs or alive offspring for transmission to the next host. The type 2 immune response against helminths mediates containment, destruction and expulsion of the parasite and at the same time induces wound-healing as parasite migration through the host often results in tissue injury (Allen and Maizels, 2011; Gause et al., 2013). As many aspects are shared between injury repair pathways and parasite control, it is proposed that type 2 immunity evolved out of the innate immune response to tissue injury (Allen and Sutherland, 2014). Protective type 2 or T helper 2 (Th2) immune response to helminths is associated with cytokines interleukin (IL)-3, IL-4, IL-5, IL-9, IL-10 and IL-13, antibody isotype immunoglobulin (Ig)G1, IgG4 and IgE, expanded populations of eosinophils, basophils, mast cells and alternatively activated macrophages (AAM) and goblet cell hyperplasia for mucus production (Allen and Maizels, 2011; Oliphant et al., 2011; Sorobetea et al., 2018).

Although the exact defense mechanisms differ for individual helminth parasites some general mechanisms exist.

In the mucosal tissue of the intestine, Th2 cells release IL-4 and IL-13 that increase epithelial cell turnover, mucus production of goblet cells and intestinal muscle hypercontractility to dislodge resident worms from the intestine in a “weep and sweep” process. In tissues, helminths are opsonized by complement and antibodies and subsequently encapsulated by recruited neutrophils, eosinophils, basophils and macrophages that attack the parasite by release of granule proteins and reactive molecules like nitric oxide (Allen and Maizels, 2011; Maizels et al., 2012).

### 1.3 Immune response to *Strongyloides* infections in rodents

Protective immunity to *Strongyloides* infections is challenging. As different stages of the *Strongyloides* life cycle reside in specific tissue locations, the immune response requires different effector mechanisms to control the infection by either trapping and killing L3 in the tissue or to expel the parasitic adults from the intestine (Breloer and Abraham, 2017). *S. ratti* infection in mice is cleared in the context of a canonical Th2 immune response, as described above. This response is characterized by production of the IL-3, IL-4, IL-5, IL-10 and IL-13, mastocytosis, suppression of interferon- $\gamma$  (IFN- $\gamma$ ) secretion and the production of nematode antigen-specific IgG1 (Eschbach et al., 2010). Immune competent mice are able to control and clear a *Strongyloides* infection within 4 weeks and remain semi-resistant to reinfections (Dawkins and Grove, 1981a; Sato and Toma, 1990).

Protective immune response in the tissue against migrating L3 relies on parasite trapping, killing and disintegration of the L3 by recruited immune cells (Breloer and Abraham, 2017). Coming into contact with highly motile L3 is difficult for recruited cells. Neutrophils are capable to release neutrophil extracellular traps (NETs), consisting of nuclear DNA, by dying in a process called etosis (Bonne-Annee et al., 2014). Etosis is a recently discovered type of cell death different to apoptosis and necrosis. Similar to neutrophils other cell types such as eosinophils, monocytes/macrophages and mast cells can release extracellular traps (Guimaraes-Costa et al., 2012). This fibrous network of extracellular DNA ensnares *S. stercoralis* L3 *in vitro* and *in vivo*, consequently providing an immobile, but still alive target for the immune response for subsequent L3 killing (Bonne-Annee et al., 2014). Neutrophils and eosinophils are recruited to trap worms and kill them by the release of toxic molecules upon direct contact (O'Connell et al., 2011). Eosinophils not only attack the L3 but also serve as antigen presenting cells (APCs) for CD4<sup>+</sup> T cells to induce an adaptive immune response (O'Connell et al., 2011; Padigel et al., 2006; Stein et al., 2009). The adaptive immune response in secondary infected mice is very effective by eradicating more than 90 % of challenge L3 within 24 h (Abraham et al., 1995). Activated CD4<sup>+</sup> T cells release Th2 cytokines that activate eosinophils, B cells and alternatively activated macrophages (AAM) to interact with neutrophils to kill antibody and complement opsonized L3 in the tissue (Bonne-Annee et al., 2013; Herbert et al., 2002; O'Connell et al., 2011; Rotman et al., 1997).

In contrast to trapping and disintegration of L3 in the tissue, the immune response in the small intestine is focused on the expulsion of the adults from the host. During *S. ratti* and *S. venezuelensis* infection in mice and rats, mast cells are induced in the small intestine and mouse mast cell protease-1 (mMCPT-1), a mucosal mast cell degranulation marker, is elevated in sera of infected mice (Eschbach et al., 2010; Khan et al., 1993; Reynolds et al., 1990; Sasaki et al., 2005; Shintoku et al., 2013). Cpa3<sup>Cre</sup> mice, lacking mucosal and connective tissue mast cells, are unable to clear a *S. ratti* infection for more than 150 days, while mice deficient only for connective tissue mast cells clear the infection with kinetics that are comparable to wildtype mice. Mucosal and connective tissue mast cell-deficient mice show higher intestinal *S. ratti* burden and prolonged *S. ratti* fecal output, but no differences in migrating L3 numbers (Blankenhaus et al., 2014; Reitz et al., 2017). Therefore, it was concluded that mucosal mast cells represent essential effector cells that terminate a *S. ratti* infection (Reitz et al., 2017). The adaptive immune response against intestinal *S. ratti* adults clearly depends on T cells as in nude mice, that lack T lymphocytes, and in RAG1<sup>-/-</sup> mice that lack T and B cells, infection is drastically prolonged (Dawkins et al., 1982a; Reitz et al., 2017). Especially CD4<sup>+</sup> T cells are important for termination of the infection since CD4<sup>+</sup> T cell-deficient MHC-II<sup>-/-</sup> but not CD8<sup>+</sup> T cell-deficient MHC-I<sup>-/-</sup> mice show impaired intestinal clearance of *S. venezuelensis* (Goncalves et al., 2008; Rodrigues et al., 2013; Rodrigues et al., 2009). However, early intestinal control of *S. ratti* is independent of adaptive immune cells as T and B cell-deficient RAG1<sup>-/-</sup> mice show comparable adult numbers to wildtype mice at day 6 after infection (Breloer et al., 2015). Nevertheless, contribution of B cells specifically to intestinal immunity was shown by reduced numbers of adults and prolonged egg release in B cell-deficient JHD mice upon intra-duodenal implantation of *S. venezuelensis* adults (El-Malky et al., 2013).

### **1.4 Initiation of type 2 immune responses**

During homeostasis, the immune system requires a certain trigger to initiate an immune response. Innate and adaptive immune responses are based on the recognition of conserved molecular structures on pathogens, known as pathogen-associated molecular patterns (PAMPs). Recognition of these specific molecular patterns are mediated by pattern recognition receptors (PRRs) such as Toll-like receptors (TLRs), C-type lectin (CTLs) and intracellular Nod-like receptors (Mogensen, 2009; Perrigoue et al., 2008). PRR

mediated signaling in innate cells is essential for the recognition of viruses, bacteria, fungi and protozoa for subsequent development of anti-pathogen adaptive immune responses. In contrast, the signals initiating an immune response to helminths are less well defined (Gause et al., 2013).

Some helminths-derived molecules have Th2 cell inducing capacities, like excretory/secretory products or the helminth structural polymer chitin (Perrigoue et al., 2008). For instance, glycans of soluble egg antigen (SEA) of *Schistosoma mansoni* (*S. mansoni*) bind to TLR4 on dendritic cells that in turn promote CD4<sup>+</sup> T cell IL-4 production (Everts et al., 2009; Thomas et al., 2003). Another well studied Th2 initiating secretory glycoprotein is IPSE/alpha-1, which is released from *S. mansoni* eggs. IPSE/alpha-1 induces a pronounced antibody response and acts through IgE to induce IL4 production by basophils (Schramm et al., 2006; Schramm et al., 2007). However, the large size of the helminths and the tissue injury that occurs during their migration might be the most important factors for the induction of a type 2 immune response (Gause et al., 2013).

Upon tissue damage, the epithelium-derived alarmins IL-25, thymic stromal lymphopoietin (TSLP) and IL-33 are released (Saenz et al., 2008). These tissue-derived alarmins are strong inducers of type 2 immune responses (Ramalingam et al., 2009; Saenz et al., 2010; Smithgall et al., 2008).

TSLP is predominantly expressed by keratinocytes, small airway epithelial cells and intestinal epithelial cells (Saenz et al., 2008). Mice infected with *Trichuris muris* (*T. muris*) showed impaired initiation of type 2 immunity and impaired parasite clearance (Taylor et al., 2009). However, another study showed that TSLP had no functional impact on the development of protective Th2 immune response against *Nippostrongylus brasiliensis* (*N. brasiliensis*) and *Heligmosomoides polygyrus* (*H. polygyrus*) as infection clearance was similar in TSLP-deficient mice and wildtype control mice (Massacand et al., 2009). Therefore, the role of TSLP in initiating a type 2 immune response during helminth infection remains controversial. IL-25 is expressed by Th2 polarized CD4<sup>+</sup> T cells, basophils, eosinophils, mast cells and epithelial cells (Oliphant et al., 2011). IL-25-deficient mice showed delayed type 2 cytokine responses and impaired parasite



clearance of *N. brasiliensis*, whereas administration of exogenous IL-25 enhanced *N. brasiliensis* expulsion from the intestine (Fallon et al., 2006). IL-33 expression was reported in several tissues including lung, skin and lymph nodes but also by dendritic cells and macrophages (Saenz et al., 2008). Infection with *T. muris* increased early IL-33 mRNA expression and injection of exogenous IL-33 improved *T. muris* clearance by enhancing Th2 immune responses, indicating the importance of IL-33 in anti-helminth immunity (Humphreys et al., 2008).

Alarmins promote initiation of Th2 immunity by inducing recruitment and proliferation of type 2 innate lymphoid cells (ILC2s), that belong to a recently discovered group of immune cells closely related to T and B lymphocytes, but do not express antigen-specific receptors (Maizels et al., 2012; Nausch and Mutapi, 2018). ILC2s exert upon alarmin-mediated activation an anti-helminth immune responses like induction of eosinophilia by IL-5 secretion, mucus production by IL-13 secretion and activation of adaptive Th2 cells, B cells and alternative activated macrophages (Fig. 1) (Allen and Sutherland, 2014; Nausch and Mutapi, 2018).

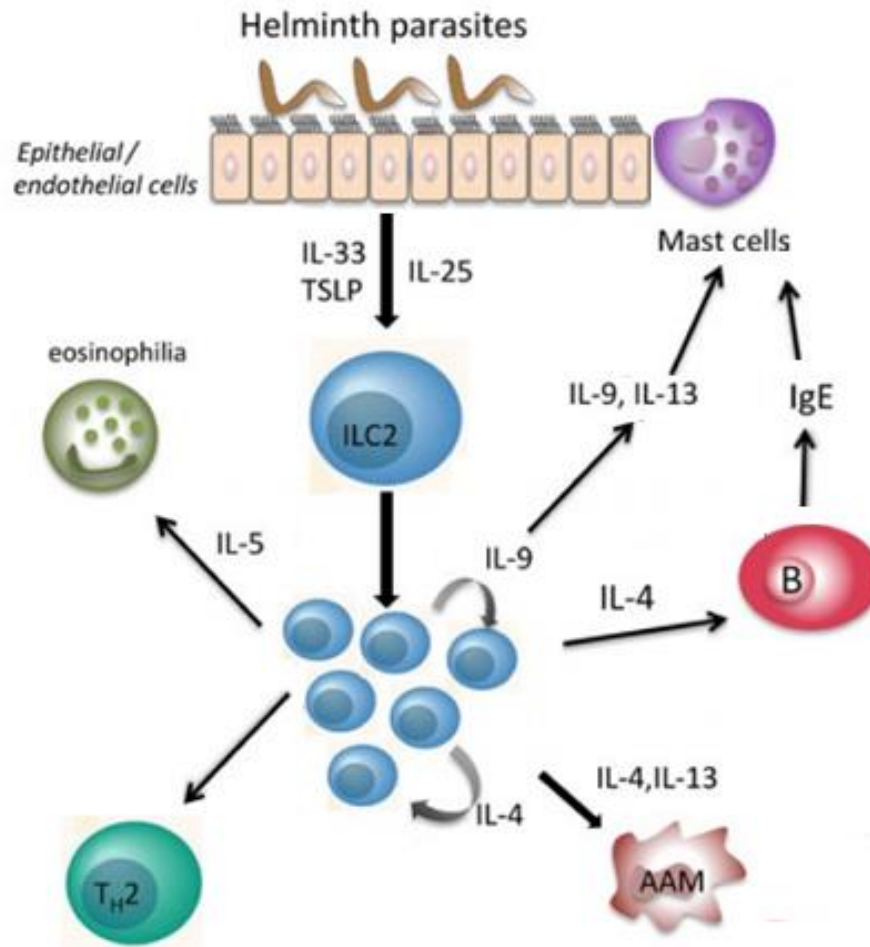


**Figure 2. Alarmin-mediated activation of ILC2 in the initiation of type 2 immune response during helminth infection.**

Helminth parasites trigger the secretion of alarmins by endothelial and epithelial cells (IL-33, TSLP and IL-25) activating ILC2. IL-4 and IL-9 act in an autocrine manner to maintain and emphasize ILC2 activation. ILC2 secrete type 2 cytokines, inducing eosinophilia by IL-5, IL-4 triggered B cell isotype switch to IgE, mucus production of goblet cells by IL-13, induction of alternative activated macrophages by IL-4 and IL-13 and activation of mast cells by IL-9 and IL-13. Further, ILC2 interact with Th2 cells to induce type 2 immune responses (adapted and modified from (Nausch and Mutapi, 2018)).

### 1.5 The biology of interleukin-33

IL-33 is a member of the IL-1 family of cytokines (Schmitz et al., 2005). IL-33 activates many immune cells involved in allergic reactions and type 2 immunity, such as ILC2, mast cells, Th2 cells, eosinophils, basophils, dendritic cells and alternatively activated macrophages (Cayrol and Girard, 2014; Liew et al., 2016; Molofsky et al., 2015). IL-33 binds to a heterodimeric receptor, consisting of suppressor of tumorigenicity 2 (ST2) and IL-1R accessory protein and signals through MyD88-mediated activation of MAP kinases and NF- $\kappa$ B (Chackerian et al., 2007; Luthi et al., 2009). ST2 belongs to the TLR/IL1-R superfamily (Miller, 2011) and high levels of ST2 are expressed on tissue resident mast cells, ILC2 and tissue Tregs (Cayrol and Girard, 2018).

Analysis of human and mouse tissues have revealed that IL-33 is mainly expressed in endothelial and epithelial cells, fibroblast-like cells and myofibroblasts during steady state and inflammation (Carriere et al., 2007; Kuchler et al., 2008; Moussion et al., 2008; Pichery et al., 2012). Within the cell, IL-33 protein binds to histones and chromatin, thereby accumulating in the nucleus (Baekkevold et al., 2003; Carriere et al., 2007; Roussel et al., 2008). If intact cells are destroyed by cellular or mechanical injury, nucleus-derived IL-33 is released into the extracellular space, however the exact mechanisms of IL-33 release *in vivo* remain incompletely defined (Cayrol and Girard, 2018). In the extracellular space, IL-33 functions as an alarmin or damage-associated molecular pattern (DAMP) to alert the immune system of cell or tissue damage. Initially, it was believed that the full-length IL-33 protein released from dying cells required processing to be biologically active (Schmitz et al., 2005). However, in 2009 it was shown that the full-length IL-33 protein is a biological active form and processing is not essential for activation of ST2 expressing cells (Cayrol and Girard, 2009; Luthi et al., 2009; Talabot-Ayer et al., 2009). Nevertheless, the full-length IL-33 protein was shown to be processed by serine proteases from neutrophils and mast cells in the extracellular space to shorter more bioactive products with 10 - 30-fold higher biological activity (Lefrancais et al., 2014; Lefrancais et al., 2012). These highly active shorter products of IL-33 seem to be biologically important as they were detected in bronchoalveolar lavage (BAL) fluid of mice upon acute lung injury (Lefrancais et al., 2012) or in the lung tissue in response to migrating helminths (Mohapatra et al., 2016).

### **1.6 Study aim**

*S. ratti* is a model for parasitic nematodes with tissue migrating and intestinal life phases. Only a small fraction of infecting L3 survive the immune attack during migration and reach the small intestine, where they reproduce.

The first aim of this study was to define the fate and localization of migrating L3 during a primary and secondary infection in mice to specifically determine the site where L3 are killed in the tissue.

The second aim was to define the role of the tissue-derived alarmin IL-33 in the initiation and execution of the type 2 immune response to both, migrating L3 in the tissue and adult parasites in the small intestine.

## 2. Materials and Methods

### 2.1 Materials

#### 2.1.1 Laboratory equipment

The following table describes the laboratory equipment, which was used in this study (Tab.1).

**Table 1. Laboratory equipment.**

<b>Equipment</b>	<b>Company</b>
Agarose gel documentation chamber	Bio-Rad Laboratories, USA
Agarose gel electrophoresis unit	PeqLab Biotechnology, Germany
Centrifuge "1-15K"	Sigma, Germany
Centrifuge "5415D"	Sigma, Germany
Centrifuge "Megafuge 2.0R"	Heraeus Instruments, Germany
Centrifuge "Minispin"	Eppendorf, Germany
Centrifuge "Multifuge 1 L-R"	Heraeus Instruments, Germany
Digital scale "Kern"	Kern & Sohn, Germany
ELISA Plate Shaker	IKA Labortechnik, Germany
ELISA Reader "MRX II"	Dynex Technologies, Germany
Flow Cytometer "LSRII"	Beckton Dickinson, Germany
Fridge and freezer	Liebherr, Germany
Incubator "37°C"	Heraeus Instruments, Germany
Incubator "CO <sub>2</sub> -incubator"	New Brunswick Scientific, The Netherlands
Laminar cabinet "Lamin Air HB 2448"	Heraeus Instruments, Germany
Light microscope "Wilovert"	Hund, Germany
Magnetic stirrer "IKAMAG® RCT"	IKA Labortechnik, Germany
Microscope "BX-51"	Olympus, Japan
Microscope digital camera "DP-25"	Olympus, Japan
Microtome	Leica, Germany
Microwave	Panasonic, Germany
PCR-Cycler "Px2 Thermal Cycler"	Thermo Scientific, USA
Pestle Mixer	Sigma, Germany
pH meter "WTW pH 537"	Labotec, Germany
Photometer "NanoDrop 2000c"	Thermo Scientific, USA

## 2. Materials and Methods

PipetBoy	Hirschmann, Germany
Pipettes (multi-channel)	Thermo Scientific, USA
Pipettes (single-channel)	Eppendorf, Germany
Pipettes Dispenser	Eppendorf, Germany
RT-Cycler “Corbett Rotor-Gene 6000“	Qiagen, Germany
Spectrophotometer “Multiscan GO”	Thermo Fisher Scientific, Finland
Thermomixer “Comfort”	Eppendorf, Germany
Vortexer	Heidolph Instruments, Germany
Water bath	GFL, Germany
Water deionization unit	TKA GmbH, Germany

### 2.1.2 Consumables

The following table describes the consumables, which were used in this study (Tab.2).

**Table 2. Consumables.**

<b>Consumables</b>	<b>Company</b>
Blood lancet	Megro GmbH, Germany
Cannulas	Braun, Germany
Cell strainer 70 µm	Becton Dickinson, Germany
EDTA tubes	Kabe Labortechnik, Germany
ELISA 96-well plate “Microlon”	Greiner bio-one, Germany
Falcon tubes 15, 50 mL	Sarstedt, Germany
Filter “Filtropur”	Sarstedt, Germany
Filter units “Stericup”	Millipore, USA
Flow Cytometer tube 5 mL	Sarstedt, Germany
Glass pipettes 5, 10, 20 mL	Brandt, Germany
Gloves	Braun, Germany
Insulin syringe “Micro-Fine” 0.3 mL	BD, Germany
Neubauer hemocytometer	Brandt, Germany
Petri dish	Sarstedt, Germany
Pipette filtered tips 10, 20, 200, 1000 µL	Biozym, Sarstedt and Greiner bio-one, Germany
Pipette tips 10, 20, 200, 1000 µL	Sarstedt, Germany

## 2. Materials and Methods

Plates 6-well, 12-well, 24-well, 96-well	Greiner bio-one, Germany
Schott glass bottles	Schütt Labortechnik, Germany
Syringe 1, 5 mL	Braun, Germany
Tracheal Cannula for mouse	Hugo Sachs Elektronik - Harvard Apparatus, Germany
Tubes 0.2, 0.5, 1.5 mL	Eppendorf, Sarstedt, Germany
Tubes PCR strips	Sarstedt, Germany

### 2.1.3 Reagents

The following table describes the reagents, which were used in this study (Tab.3).

**Table 3. Reagents.**

<b>Reagent</b>	<b>Company</b>
10 x PCR Puffer	Qiagen, Germany
2-Propanol	Merck, Germany
2x HS Taq Mix	Biozym, Germany
5x RT PCR buffer	Thermo Scientific, USA
AccuCheck Counting Beads	Life technologies, USA
Agar	Sigma, Germany
Agarose	Biomol, Germany
Ampuwa H <sub>2</sub> O	Fresenius Kabi, Germany
Bovine serum albumin (BSA)	Serva Feinbiochemika, Germany
Chloroform	Merck, Germany
Collagenase VIII	Sigma, Germany
Decosept	Dr. Schumacher GmbH, Germany
Dimethyl sulfoxide (DMSO)	Sigma, Germany
DNA 100 bp Ladder	Thermo Fischer Scientific, Germany
DNA Loading Dye	Thermo Fischer Scientific, Germany
DNase	Roche, Germany
dNTP's	Thermo Scientific, USA
DTT	Roth, Germany
EDTA	Roth, Germany
EDTA qPCR	Thermo Scientific, USA

## 2. Materials and Methods

Eosin	Merck, Germany
Ethanol	Merck, Germany
Ethidium bromide	Sigma, Germany
Fetal calf serum (FCS)	Sigma, Germany
Formalin	Merck, Germany
H <sub>2</sub> O	Braun, Germany
H <sub>2</sub> SO <sub>4</sub>	Roth, Germany
Hematoxylin	Merck, Germany
HEPES	Lonzo, Belgium
Hot Star Taq Polymerase	Qiagen, Germany
Incidin Liquid	Ecolab, Germany
Ketamine	Medistar, Germany
KOH	Merck, Germany
MgCl <sub>2</sub>	Qiagen, Germany
Na <sub>2</sub> HPO <sub>4</sub>	Roth, Germany
NaCl	Roth, Germany
NH <sub>4</sub> Cl	Roth, Germany
Penicillin/Streptomycin (Pen/Strep)	PAA, Austria
Percoll	GE Healthcare, Sweden
Protease inhibitor Cocktail Tablets (Complete Mini EDTA-free)	Roche, Germany
Proteinase K	Roth, Germany
Random Hexamer Primer	Thermo Scientific, USA
Recombinant Mouse IL-33 (carrier-free)	BioLegend, USA
RevertAid H Minus Reverse Transcriptase	Thermo Scientific, USA
RiboLock RNase Inhibitor	Thermo Scientific, USA
Rompun	Bayer, Germany
RPMI 1640 medium	PAA, Austria
Streptavidin-HRP	DAKO, Denmark
SybrGreen	Invitrogen/ Thermo Fischer Scientific, Germany
Tris	Merck, Germany
TRIzol	Sigma, Germany
Trypan blue	Sigma, Germany



## 2. Materials and Methods

---

Tween20	Sigma, Germany
---------	----------------

---

### 2.1.4 Buffers and solutions

Buffers and solutions were prepared with deionized H<sub>2</sub>O and were autoclaved (135 °C, 2 bar, 20 minutes). The following table describes the buffers and solutions, which were used in this study (Tab.4).

**Table 4. Buffers and solutions.**

Buffer/solution	Ingredients
1M KOH	56,1 g KOH Ad 1 L H <sub>2</sub> O
1M NaCl solution	58,44 g NaCl Ad 1 L H <sub>2</sub> O
1M Tris solution	121,14 g Tris-Base Ad 1 L H <sub>2</sub> O
4 % Formalin	55 mL formalin (36 %) filled up to 500mL 1x PBS
Complete RPMI 1640 medium	500 mL RPMI 1640 50 mL FCS 5 mL Glutamine (200 mM) 2.5 mL Penicillin/Streptavidin (100x)
Digestion solution	R10F <sup>+</sup> Lung medium Final conc. 0.5 mg/mL collagenase Final conc. 100 µg/mL DNase
ELISA stop solution	H <sub>2</sub> SO <sub>4</sub> (2,5 M)
ELISA wash buffer	0.05 % Tween 20 in 1x PBS
Erythrocyte lysis buffer	10 % Tris/HCl (0,1 M, pH 7,5) 90 % NH <sub>4</sub> Cl (0,16 M)
FACS buffer	1 % FCS 0,1 % Sodium azide In 1x PBS
Narcosis solution	9 mL PBS 1 mL Ketavet

---

## 2. Materials and Methods

---

	250 µL Rompun
PBS (10x)	80 g NaCl 2 g KH <sub>2</sub> PO <sub>4</sub> 2 g KCl 11.5 g Na <sub>2</sub> HPO <sub>4</sub> in 1L H <sub>2</sub> O
PBS containing protease inhibitor	1x tablet solved in 50 mL 1x PBS
PBS/Pen/Strep	PBS (1x) + Pen/Strep (final conc. 1x)
Percoll 37 %	37 mL percoll Ad to 1 1L H <sub>2</sub> O
R10F <sup>+</sup> Lung medium	RPML 1640 Medium 10 % FCS 1 % HEPES 1 % Pen/strep
TBE (10x)	216 g Tris base 110 g boric acid 80 mL 0,5M EDTA pH 8.0 Add 2 L H <sub>2</sub> O
Tissue lysis buffer	20 mL 1M Tris pH 8,5 4 mL 10% SDS 40 mL M NaCl Add 200 mL H <sub>2</sub> O (final use: add Proteinase K 100 µg/mL final conc.)
Trypan blue solution	2 % Trypan blue in 1x PBS
Wash buffer	1x PBS 1L 1 % FCS 1 mM EDTA

---

### 2.1.5 DNA oligonucleotides

The following table describes the DNA oligonucleotides, which were used in this study (Tab.5).

**Table 5. DNA oligonucleotide primers.**

Primer	Sequence
<i>S. rattii</i> 28S RNA coding DNA primer:	
StroS2	5'-TTAGAGTCGTGTTGCTTGGAA
StroAS1	5'-GTGCAACTGGCTCTGTATGC
Cpa3 <sup>Cre</sup> primer:	
Cpa3 common	5'-GGACTGTTTCATCCCCAGGAACC
CpaA3 Wt	5'-CTGGCGTGCTTTTCATTCTGG
Cpa3 KI	5'-GTCCGGACACGCTGAAGTTG
Mcpt8 <sup>Cre</sup> primer:	
Mcpt8 <sup>Cre</sup> -S	5'-CTGCAAACCCTATGCTACTC
Mcpt8 <sup>Cre</sup> -AS	5'-AGGACTCACAGGGATCATAG
Actin	
Actin-S	5'-AGAGGGAAATCGTGCGTGAC
Actin- AS	5'-CAATAGTGATGACCTGGCGGT

### 2.1.6 Kits

The following table describes the kits, which were used in this study (Tab.6).

**Table 6. Kits.**

Kit	Company
Diff-Quick staining Kit	DADE Diagnostics, USA
Mouse MCPT-1 Uncoated ELISA Kit	Invitrogen/ Thermo Fischer Scientific, Austria
Naphthol AS-D chloroacetate esterase (NE-Kit)	Sigma, Germany

### 2.1.7 Software

The following table describes the software, which was used in this study (Tab.7).

**Table 7. Software.**

Software	Company
Cell^A software	Olympus, Japan
EndNote 8	Clarivate Analytics, USA

## 2. Materials and Methods

FlowJo X	Tree Star, USA
Microsoft Office 365	Microsoft, USA
Prism5	GraphPad, USA
qPCR Software	Corbett Life Science, Germany

### 2.1.8 Parasite

The rodent-specific nematode *Strongyloides ratti* was used for infection of mice in this study. The life cycle of the parasite is maintained at the BNITM.

### 2.1.9 Mice

The following table describes the mouse strains, which were used in this study (Tab.8).

**Table 8. Mice.**

Mice	Description	Origin
BALB/c (H-2 <sup>d</sup> )	Wildtype	BNITM Animal facility, Germany Janvier labs, France Charles River, Germany
BALB/c Cpa3 <sup>Cre</sup>	Heterozygous Cpa3 <sup>Cre</sup> mice express Cre recombinase under the control of the Cpa3 promoter deleting all mucosal and connective tissue mast cells by genotoxic mechanisms (Feyerabend et al., 2011).	Heterozygous breeding at BNITM Animal Facility, Germany
BALB/c IL-9R <sup>-/-</sup>	IL-9R <sup>-/-</sup> mice were generated by substitution of the <i>KpnI-SpeI</i> fragment containing exons 2, 3, 4, 5, and 6, with a neomycin resistance gene (Steenwinckel et al., 2007).	Homozygous breeding at BNITM Animal Facility, Germany
BALB/c Mcpt8 <sup>Cre</sup>	Heterozygous bacterial artificial chromosome (BAC) transgenic mice express Cre recombinase under control of	Heterozygous breeding at BNITM Animal Facility, Germany

## 2. Materials and Methods

---

regulatory elements for basophil-specific mast cell protease 8 (Mcpt8), resulting in constitutively deletion of basophils (Ohnmacht et al., 2010).

---

BALB/c $\Delta$ dblGATA	The $\Delta$ dblGATA model was generated by deletion of a high-affinity GATA-binding site in the hematopoietic promoter. GATA-1 gene deletion results in loss of the eosinophil lineage (Yu et al., 2002)	Kind gift from M. P. Hübner, Institute for Medical Microbiology, Immunology, and Parasitology, University Hospital Bonn, Germany
-------------------------	---	--

---

### 2.1.10 Statistical Analysis

Statistical analysis was performed with GraphPad Prism 5 software. All data were assessed for normality and two groups were compared by using Student's t-test (parametric) or Mann-Whitney U test (non-parametric). More than two groups were compared by ANOVA (parametric) or Kruskal-Wallis test (non-parametric). P values of  $\leq 0.05$  were considered to indicate statistical significance.

## 2.2 Methods

### 2.2.1 Parasitological methods and animal experiments

All animal experimentations were performed at the animal facility of the Bernhard Nocht Institute for Tropical Medicine agreed by the German animal welfare act. Experimental protocols have been reviewed and approved by the responsible federal health Authorities of the State of Hamburg, Germany. Mice were sacrificed by carbon dioxide (CO<sub>2</sub>) euthanasia with subsequent cervical dislocation. Mice were housed in individually ventilated cages under specific pathogen-free conditions. For all experiments, male and female mice were used at 6 to 14 weeks of age and experimental groups were matched for gender and age.

### **2.2.1.1 Maintenance of *S. ratti* life cycle and preparation of L3i**

Parasite life cycle was maintained by serial passage of *S. ratti* in Wistar rats. Stool samples of *S. ratti* infected rats were collected over a period of 24 h. Collected feces was soaked with 10 ml H<sub>2</sub>O and mixed with water-soaked charcoal in a glass beaker. The beaker was covered with parafilm and incubated for 6 days at 25 °C. During this period of time *S. ratti* L1 develop into L3i. *S. ratti* L3i were collected from the cultures with a Baermann apparatus. Collected L3i were washed three times with PBS supplemented with penicillin (100 U/mL) and streptomycin (100 µg/mL). Each washing step was followed by a sedimentation phase of the L3i for at least one hour at 4 °C. Washed L3i were stored at 4 °C for a maximum of 24 h. The L3i were microscopically counted, aliquoted and used for experimental infections.

### **2.2.1.2 Experimental infections**

Mice were injected subcutaneously (*s.c.*) with 2000 *S. ratti* L3i in 40 µL PBS (Pen/Strep) in the left hind footpad for experimental infections. Secondary infection was performed in immune mice that already cleared a *S. ratti* infection and established a protective memory immunity. Mice were infected 4 weeks before the secondary infection with 2000 *S. ratti* L3i as described above.

Wistar rats were injected subcutaneously with 2500 *S. ratti* L3i in 200 µL PBS (Pen/Strep) in the right flank for maintenance of the parasite life cycle.

### **2.2.1.3 Mice treatments**

#### **2.2.1.3.1 Recombinant IL-33 treatment**

Mice were injected intraperitoneally (*i.p.*) 3 h before and at day 1 p.i. with 1 µg recombinant mouse IL-33 (rIL-33) (BioLegend, Germany).

#### **2.2.1.3.2 Anti-Gr-1 treatment**

Mice were injected intraperitoneally (*i.p.*) 1 day before the infection with 350 µg anti-Gr-1 antibody to deplete Gr-1<sup>+</sup> cells. Depletion of Gr-1<sup>+</sup> cells was controlled by analyzing blood samples with flow cytometry at day 1 p.i.

### **2.2.1.4 Quantification of L3 in the tissue**

The numbers of viable L3 were counted in the foot, leg-derived skin and muscle tissue, lung, head, kidney and small intestine. The procedure of counting parasites in small intestine is stated in 2.2.1.5. Tissues and organs were prepared from mice. Fur and skin were removed from the head. Foot, leg-derived skin, leg-derived muscle and head were cut in small pieces and put into 6-well plates. Lung and kidney were cut in small pieces and put into 24-well plates. Organs and tissues were covered with H<sub>2</sub>O (tap water) and incubated for 3 h at 37 °C. After each hour well-plates were shaken gently. During this incubation viable L3 emigrate out of the tissue. After 3 h of incubation, tissues and organs were removed and L3 were counted microscopically.

### **2.2.1.5 Quantification of adults in the small intestine**

The numbers of viable L4 and adults were counted in the small intestine at day 5 and day 6, respectively. The small intestines were prepared from mice and sliced longitudinally open and washed with H<sub>2</sub>O (tap water) to remove feces and put into a petri dish. The small intestine was covered with H<sub>2</sub>O and incubated for 3 h at 37 °C. After each hour petri dishes were shaken gently. After the incubation, small intestine was shaken to loosen the mucus. After removing the small intestine, L4 and adults were counted microscopically.

### **2.2.1.6 Collection of mice stool for quantification of *S. ratti*-derived DNA in the feces**

*S. ratti*-derived DNA was quantified in stool samples of infected mice. Mice were placed on cellulose papers for 24 h and feces was collected in tubes for further DNA isolation. Feces samples were stored until further use at 4 °C.

### **2.2.1.7 Mouse serum**

Blood of mice was collected by puncture of the facial vein (*Vena facialis*) with a lancet or *post mortem* with a syringe from the heart. Blood was incubated for at least 1 h at room temperature. Coagulated blood samples were centrifuged with 10000 xg for 10 minutes to remove serum from cellular components. Serum was transferred into new tube and stored until further use at -20 °C.

### **2.2.1.8 Quantification of erythrocytes in bronchoalveolar lavage (BAL) and cytopsin of BAL cells**

Mice were sacrificed in this experiment by an *i.p.* injected overdose of narcosis solution to exclude unintended side effects in the lung upon CO<sub>2</sub> euthanasia. For the preparation of the bronchoalveolar lavage (BAL), a cannula was inserted into the exposed trachea and lungs were rinsed with 1 mL cold PBS containing protease inhibitor (Roche, Germany). Lavages were centrifuged at 10000 xg for 10 minutes and resuspended in 300 µL FACS buffer. 100 µL were cytopsined on a microscope slide and stained with Diff-Quick staining kit (DADE Diagnostics, Germany). A 1:3 dilution from the lavage was made with AccuCheck Counting Beads (Life Technologies, USA) and samples were analyzed on a LSRII flow cytometer (BD, Germany). Erythrocyte gate was determined by analyzing several dilutions of blood samples. The erythrocyte cell count was calculated according to AccuCheck Counting Beads protocol formula:

$$absolute\ cell\ count = \left( \frac{number\ of\ cells\ counted}{number\ of\ beads\ counted\ total} \right) \times beads/\mu L$$

### **2.2.1.9 Histology of lung tissue**

Mice were sacrificed in this experiment by an *i.p.* injected overdose of narcosis solution to exclude unintended side effects in the lung upon CO<sub>2</sub> euthanasia. A cannula was inserted into the exposed trachea. 1 mL of 4 % formalin was injected through the cannula into the lungs. After removal of the whole lung, a constant fixation fluid pressure with 4 % formalin followed for 20 minutes. The trachea was tied off and the lungs were stored in 50 mL Falcons filled with 10 mL 4 % formalin. After removal of the heart, the lungs were embedded in 2 % agar and cut into vertical sections. All tissue samples were embedded in paraffin. For histological analysis, 2 µm sections were cut, dewaxed and stained with Hematoxylin & Eosin (H&E) or Naphthol AS-D Chloroacetate Esterase (NE-Kit, Sigma, Germany). Photographs were taken with a digital camera (DP-25 Olympus, Japan) attached to a microscope (BX-51 Olympus, Japan) using Olympus cell<sup>A</sup> software.



### 2.2.2 Biochemical methods

#### 2.2.2.1 ELISA quantification of mouse mast cell protease-1 (mMCPT-1) in sera

Quantification of Mouse mast cell protease 1 (mMCPT-1) in sera of mice was performed by using the Mouse MCPT-1 Uncoated ELISA Kit (Invitrogen/Thermo Fisher Scientific, Austria). Coating of 96-well plates were performed with capture antibody, 1:250 diluted in coating buffer, in 50  $\mu$ L per well overnight at 4°C. Plates were washed with ELISA wash buffer and blocked for 2 h with 100  $\mu$ L 1x Assay-Diluent per well. Plates were washed with ELISA wash buffer and incubated with 50  $\mu$ L serum, 1:20 diluted in 1x Assay-Diluent, per well overnight at 4°C. Plates were washed with ELISA wash buffer and incubated with 50  $\mu$ L detection antibody per well, 1:250 diluted in 1x Assay-Diluent, for 1 h at room temperature. Plates were washed with ELISA wash buffer and incubated with 50  $\mu$ L Avidin-HRP antibody per well, 1:250 diluted in 1x Assay-Diluent, for 30 minutes at room temperature. Plates were washed with ELISA wash buffer and samples were developed with 50  $\mu$ L TMB substrate and stopped after 10 minutes with 25  $\mu$ L ELISA stop solution. Samples were measured in duplicates. OD was determined on a photometer at a wavelength of 450 nm. mMCPT-1 concentrations of sera were calculated using a serial dilution of a standard with known concentrations.

### 2.2.3 Molecular biological methods

#### 2.2.3.1 DNA isolation from ear biopsy

Ear biopsies of mice were incubated with 20  $\mu$ L tissue lysis buffer containing 100  $\mu$ g/mL proteinase K for 15 minutes at 75 °C. Samples were incubated for proteinase K inactivation for 10 minutes at 95 °C. Samples were vortexed and 180  $\mu$ L 10 mM Tris buffer was added. 2  $\mu$ L of this solution were used for further PCR genotyping.

#### 2.2.3.2 DNA isolation from feces

DNA isolation from feces of infected *S. ratti* mice was performed using a modified KOH-Method (Katzwinkel-Wladarsch et al., 1994). 200 mg feces were suspended in 1.4 mL H<sub>2</sub>O, 100  $\mu$ L 1 M KOH and 30  $\mu$ L 1 M DTT were added and mixed well by vortexing until complete homogenization. After incubation at 65 °C for 30 minutes, samples were vortexed again. After centrifugation at 13000 xg for 10 minutes, 400  $\mu$ L supernatant of

each sample was transferred into a new tube containing 10  $\mu\text{L}$  of 10 mg/mL proteinase K. Samples were vortexed and incubated for 15 minutes at 56  $^{\circ}\text{C}$ . Reaction was stopped by storing the samples for 10 minutes at 4  $^{\circ}\text{C}$ . 400  $\mu\text{L}$  isopropanol was added to precipitate DNA in the samples and stored for 30 minutes at -20  $^{\circ}\text{C}$ . After centrifugation at 13000  $\times g$  for 10 minutes, supernatant was discarded, and DNA was washed with 100  $\mu\text{L}$  80 % ethanol. After centrifugation, ethanol was discarded, and DNA was dried at room temperature. The DNA was suspended in 200  $\mu\text{L}$  Millipore  $\text{H}_2\text{O}$ . DNA concentration was adjusted to 100 ng/ $\mu\text{L}$ .

### **2.2.3.3 DNA isolation from tissues and organs**

Tissue and organs were cut into small pieces and incubated over night with 1 mL (foot and tongue), 2 mL (leg-derived skin, leg-derived muscle, kidney and lung) or 4 mL (small intestine and head) lysis buffer containing 100  $\mu\text{g}/\text{mL}$  proteinase K at 56  $^{\circ}\text{C}$ . After centrifugation at 13000  $\times g$  for 10 minutes at 4  $^{\circ}\text{C}$ , 0.5 mL (foot and lung) or 1 mL (leg-derived skin tissue, leg-derived muscle tissue, kidney, head and small intestine) supernatant was transferred into a new tube. Saturated NaCl in 25 % final concentration was added to the samples, vortexed and stored for 10 minutes at 4  $^{\circ}\text{C}$ . After centrifugation at 13000  $\times g$  for 15 minutes at 4  $^{\circ}\text{C}$ , 0.5 mL supernatant was transferred into new tube. 20  $\mu\text{g}/\text{mL}$  RNase A was added and incubated for 15 minutes at 37  $^{\circ}\text{C}$ . DNA was precipitated with 500  $\mu\text{L}$  isopropanol and centrifuged at 13000  $\times g$  for 5 minutes at 4  $^{\circ}\text{C}$ . DNA was washed with 500  $\mu\text{L}$  of 80 % ethanol then allowed to dry at room temperature. The DNA was resuspended in 200  $\mu\text{L}$  (foot, leg-derived skin and leg-derived muscle) or 400  $\mu\text{L}$  (lung, head, kidney and small intestine) Millipore  $\text{H}_2\text{O}$ . DNA concentration was adjusted to 5 ng/ $\mu\text{L}$ .

### **2.2.3.4 DNA concentration**

DNA concentrations were determined by using a UV-Vis Spectrophotometer (Nanodrop, Thermo Scientific).

### **2.2.3.5 Polymerase chain reaction (PCR) for mice genotyping**

The polymerase chain reaction is a rapid and accurate technique to amplify exponentially a specific DNA sequence by using oligonucleotide sequences as primers (Mullis, 1990). Transgenic mice were genotyped by polymerase chain reaction (PCR) with the DNA from

## 2. Materials and Methods

ear biopsies. Three primers were used to screen the heterozygous bred Cpa3<sup>Cre</sup> mice. The primers amplified the wildtype gen (320 bp) and the transgenic gen (450 bp). Two primers were used to screen the heterozygous bred Mcpt8<sup>Cre</sup> mice for the transgenic gen and additional two primers were used to amplify actin. Primer sequences are described in 2.1.5.

The following table describes the PCR program, which was used for DNA amplification (Tab. 9).

**Table 9. PCR program.**

PCR reaction step	Temperature	Time
Polymerase activation	95 °C	15 minutes
Denaturation	95°C	30 seconds x 40 cycles
Primer annealing	57 °C	30 seconds x 40 cycles
Elongation	72 °C	40 seconds x 40 cycles

The following table describes PCR sample preparations of Cpa3<sup>Cre</sup> mice (Tab. 10)

**Table 10. PCR Cpa3<sup>Cre</sup> mice.**

PCR reagent	Volume (total 20 µL)
2x HS Taq Mix	10 µL
Cpa3 common	0.8 µL
Cpa3 Wt	0.8 µL
Cpa3 KI	0.8 µL
H <sub>2</sub> O	5.6 µL
DNA	2 µL

The following table describes PCR sample preparations of Mcpt8<sup>Cre</sup> mice (Tab. 11).

**Table 11. PCR Mcpt8<sup>Cre</sup> mice.**

PCR reagent	Volume (total 20 µL)
2x HS Taq Mix	10 µL
Mcpt8-S or Actin-S	0.8 µL
Mcpt8-AS or Actin-S	0.8 µL

## 2. Materials and Methods

---

H <sub>2</sub> O	6.4 $\mu$ L
DNA	2 $\mu$ L

---

### 2.2.3.6 Agarose gel electrophoresis

Amplified DNA fragments were separated using a 1 % agarose gel (containing 0.001 % ethidium bromide) in TBE buffer. 10 - 20  $\mu$ L sample volume was mixed with 3  $\mu$ L DNA loading dye, loaded on the gel and separated for 45 - 60 minutes at 90 V. The gel was analyzed with UV light in an agarose gel documentation device and the DNA fragment sizes were analyzed using a 100 bp DNA ladder.

### 2.2.3.7 *Strongyloides* DNA real-time quantitative PCR (qPCR)

The *S. ratti* 28S ribosomal RNA (rRNA) coding DNA was quantified by real-time quantitative PCR (qPCR) using a Corbett RotorGene 6000 (Qiagen, Germany). DNA amplification is based on the PCR principle. qPCR allows the quantitation of specific DNA products, generated during each cycle of the PCR process (Higuchi et al., 1993). Sequences of the *Strongyloides*-specific primers are described in table 5. A plasmid (TOPO TA cloning kit, Invitrogen) containing a 180 bp fragment of the *S. ratti* 28S rRNA gene produced by PCR was used as calibrator. SYBR<sup>®</sup> Green I, a double stranded DNA binding fluorescence dye, was used to quantify DNA in the samples. SYBR<sup>®</sup> Green I exhibits little fluorescence when unbound in solution. By intercalation in generated double stranded DNA products, the fluorescence becomes measurable. Fluorescence signal is proportional to the generated DNA products of each cycle and the fluorescence signal increases over the baseline fluorescence. A fluorescence signal above this threshold can be considered as a real signal and the numbers of PCR cycles needed to exceed this threshold is called cycle threshold value (Ct-value) (Arya et al., 2005). A low Ct-value indicates that amplification was achieved in earlier cycles and that DNA starting material was abundant in the sample. Comparative quantification (efficiency-corrected Ct method) was used to transform the difference in Ct values between the test samples and the calibrator sample into a copy number ratio. Samples were measured in duplicates and a negative control, master mix with no template DNA, was included. To ensure the specificity in each reaction tube, a melting curve analysis was performed for each run.

## 2. Materials and Methods

The following table describes the qPCR program used for DNA quantification (Tab. 12).

**Table 12. qPCR DNA program.**

PCR reaction step	Temperature	Time
Polymerase activation	95 °C	15 minutes
Denaturation	95°C	10 seconds x 35 cycles
Primer annealing	50 °C	15 seconds x 35 cycles
Elongation	72 °C	20 seconds x 35 cycles
Melting curve	62 °C – 95 °C, in 1 °C steps	

The following table describes the qPCR sample preparation for DNA quantification (Tab. 13).

**Table 13. qPCR DNA sample preparation.**

PCR reagent	Volume (total 10 µL)
10x PCR Buffer	1 µL
BSA (1 µg/µL)	0.4 µL
SYBR Green (1:1000)	0.1 µL
BSA (1 µg/µL)	1 µL
10 mM dNTPs	0.2 µL
StroS2	0.3 µL
StroAS1	0.3 µL
<i>Taq</i> -Polymerase	0.05 µL
H <sub>2</sub> O	4.65 µL
DNA or calibrator	2 µL

### 2.2.3.8 RNA isolation

Mice were sacrificed and lungs were removed. Half of the lung was stored in 200 µL TRIzol reagent at -20 °C until further use. For isolation of total RNA, tissues were homogenized by using a Pestles mixer (Sigma, Germany). After homogenization, 800 µL of TRIzol reagent was added. After mixing, the samples were incubation for 5 minutes at room temperature. 200 µL of chloroform were added and mixed for 15 seconds and incubated for 3 minutes at room temperature. Centrifugation at 12000 xg for 15 minutes at 4 °C was

performed. 500  $\mu\text{L}$  of supernatant was transferred to a new tube containing 500  $\mu\text{L}$  isopropanol. After mixing and incubation for 10 minutes at room temperature, centrifugation was performed at 12000  $\times g$  for 15 minutes at 4  $^{\circ}\text{C}$ . Supernatant was discarded and pellet was washed with 200  $\mu\text{L}$  80 % ethanol and centrifuged at 7500  $\times g$  for 5 minutes at 4  $^{\circ}\text{C}$ . Supernatant was discarded and the RNA was allowed to dry at room temperature. RNA was resuspended in 50  $\mu\text{L}$  Ampuwa  $\text{H}_2\text{O}$  and RNA concentration was measured by using the Spectrophotometer (Nanodrop) and adjusted to 10  $\mu\text{g}/40\mu\text{L}$ .

### 2.2.3.9 DNase treatment and reverse transcriptase reaction

1  $\mu\text{g}$  RNA was used for DNase treatment and reverse transcriptase reaction to perform cDNA (complementary DNA) synthesis. DNase treatment was performed by incubating the samples with a mastermix (Tab. 14) for 30 minutes at 37  $^{\circ}\text{C}$ . After addition of 1  $\mu\text{L}$  50 mM EDTA, samples were incubated for 10 minutes at 65  $^{\circ}\text{C}$ .

**Table 14. Mastermix DNase treatment.**

Reagent	Volume (total 9 $\mu\text{L}$ )
10x DNase buffer	1 $\mu\text{L}$
DNase I	3 $\mu\text{L}$
Ampuwa	1 $\mu\text{L}$
RNA	4 $\mu\text{L}$

cDNA was prepared after DNase treatment using random primer and RevertAid H Minus reverse transcriptase (Thermo Scientific, USA) (Tab. 15 and 16). DNase treated RNA was incubated with random primer mix for 5 minutes at 65  $^{\circ}\text{C}$ . After addition of the cDNA synthesis mix, samples were incubated for 10 minutes at 25  $^{\circ}\text{C}$ , followed by 42  $^{\circ}\text{C}$  for 60 minutes and last 10 minutes at 70  $^{\circ}\text{C}$ .

**Table 15. RNA incubation with random primer mix.**

Reagent	Volume (total 12.5 $\mu\text{L}$ )
Random Hexamer Primer	1 $\mu\text{L}$
Ampuwa	1,5 $\mu\text{L}$
RNA (DNase treated)	10 $\mu\text{L}$

**Table 16. cDNA synthesis reagents.**

Reagent	Volume (total 7.5 $\mu$ L)
5x RT rxn buffer	4 $\mu$ L
RNase inhibitor	0.5 $\mu$ L
10 mM dNTPs	2 $\mu$ L
Ampuwa	0.5 $\mu$ L
Reverse transcriptase	0.5 $\mu$ L

### 2.2.3.10 cDNA real-time quantitative PCR (qPCR)

10 ng of cDNA were used for qPCR analyses. qPCR method is described in more detail in 2.2.3.7. All samples were measured in duplicates and a negative control, master mix with no template DNA, was included. To ensure the specificity in each reaction tube, a melting curve analysis was performed for each run. Housekeeping gene GAPDH was used as internal control and to calculate delta Ct. The relative expression of the target genes was calculated using the comparative Ct method ( $\Delta\Delta$ Ct method) using naïve PBS treated mice as reference group.

The following table describes the gene specific primers, which were used in this study (Tab. 17).

**Table 17. Gene specific primers for gene expression qPCR analysis.**

Primer	Sequence
GAPDH primer:	
GAPDH-S	5'-ATTGTCAGCAATGCATCCTG
GAPDH-AS	5'-ATGGAAGTGGTCATGAGCC
Arg-1 primer:	
Arg-1-S	5'-CAGAAGAATGGAAGAGTCAG
Arg-1-AS	5'-CAGATATGCAGGGAGTCACC
iNOS primer:	
iNOS-S	5' -TTTGGGAATGGAGACTGTCCCAGCAATG
iNOS-AS	5'- GTTGCATTGGAAGTGAAGCGTTTCGGGAT
mMCPT-1 primer:	
mMCPT-1-S	5'-TGCAGGCCCTACTATTCCTG

## 2. Materials and Methods

mMCPT-1-AS	5'-CCATGTAAGGACGGGAGTGT
IL-13 primer:	
IL-13-S	5'-AGACCAGACTCCCCTGTGCA
IL-13-AS	5'-TGGGTCCTGTAGATGGCATTG

qPCR analyses were performed using a Corbett RotorGene 6000 (Qiagen, Germany) with the following cycle conditions (Tab. 18).

**Table 18. qPCR cDNA program.**

PCR reaction step	Temperature	Time
Polymerase activation	95 °C	15 minutes
Denaturation	95°C	20 seconds x 45 cycles
Primer annealing	60 °C	15 seconds x 45 cycles
Elongation	72 °C	30 seconds x 45 cycles
Melting curve	67 °C – 95 °C, in 1 °C steps	

The following table describes qPCR sample preparations for gene expression quantification (Tab. 19).

**Table 19. qPCR reagents for gene expression analysis.**

Reagent	Volume (total 10 µL)
Ampuwa	5.65 µL
10 x PCR buffer	1 µL
25 mM MgCl <sub>2</sub>	0.4 µL
10 mM dNTPs	0.2 µL
Primer-S	0.3 µL
Primer-AS	0.3 µL
SYBR Green (1:1000)	0.1 µL
Taq Polymerase	0.05 µL
cDNA	2 µL



### 2.2.4 Cell biology methods

#### 2.2.4.1 Cell count determination

To determine the cell count in samples, Neubauer cell counting chambers (hemocytometer) were used. Single cell suspensions were prepared from lungs and diluted 1:10 with trypan blue. Dead cells can be distinguished from viable cells. Dead cells appear blue as the dye diffuses through the membrane. Cells were counted in one set of 16 squares. The total cell count per milliliter was determined by following formula:

$$\text{cell number/mL} = \text{counted cells} \times \text{dilution factor} \times 10^4$$

#### 2.2.4.2 Lung single cell suspension preparation

Lungs were removed from sacrificed mice and placed in a petri dish filled with PBS. Lungs were cleaned from adherent blood and transferred into the lid of the petri dish. Lungs were cut into pieces and transferred into a 15 mL tube with 2 mL R10F+ lung medium. 2 mL of R10F+ lung medium containing Collagenase VIII, final concentration 0.5 mg/mL, and DNase, final concentration 100 µg/mL were added. After incubation for 45 minutes at 37 °C, samples were filtered through a 70 µm nylon mesh in a 50 mL tube. Nylon mesh were rinsed twice with 5 mL washing buffer. After centrifugation at 360 xg for 7 minutes at 4 °C, supernatant was discarded. Cell pellets were resuspended in 5 mL 37 % percoll solution and transferred to 15 ml tube and centrifuged without breaks for 15 minutes at room temperature. After discard of supernatant, pellets were resuspended in 1 mL erythrocyte lysis buffer and incubated for 5 minutes. Lysis was stopped with 10 mL washing buffer and centrifuged at 360 xg for 7 minutes at 4 °C. Pellets were washed with 5 mL washing buffer and again centrifuged. Cells were resuspended in 1 mL washing buffer and cell count was performed. 5x10<sup>6</sup> cells of each sample were transferred into a FACS tube and cells were stored at 4°C until further use.

#### 2.2.4.3 Blood cell preparation

Blood was collected from mice in EDTA tubes. Blood was transferred in 15 ml tubes with 200 µL FACS buffer. 2 mL erythrocyte lysis buffer was added and incubated for 5 minutes at room temperature. Lysis was stopped by adding 10 mL FACS buffer. After centrifugation at 12000 xg for 5 minutes at 4 °C, cells were washed with 2 mL FACS buffer

and centrifuged again. Cells were resuspended in 200  $\mu$ L FACS buffer and transferred into a FACS tube.

### **2.2.4.4 Flow cytometry**

Flow cytometry provides accurate and rapid analysis of multiple characteristics of single cells. Flow cytometry measures optical and fluorescence characteristics of the cell such as the size, which is represented by the forward angle light scatter, and granularity or internal complexity, which is represented by the sideward angle light scatter. By the differentiation between these characteristics, cells can be resolved into distinct cell populations. Cells can be targeted by antibodies conjugated to fluorescent dyes, which can bind for example to membrane bound proteins such as receptors or they can bind to intracellular component such as DNA or other proteins. Fluorescence labeled cells pass a light source in a laminar flow, the fluorescent dyes are stimulated and excited to a higher energy state. Upon returning to their resting state, the fluorochromes emit a specific wavelength. Multiple fluorochromes, each with specific excitation wavelength and different emission wavelengths can be used simultaneously to analyze different cell properties (Brown and Wittwer, 2000).

#### **2.2.4.4.1 Flow cytometry – staining procedure**

Lung single cell suspensions or blood cells were transferred in FACS tubes. After centrifugation at 360 xg for 5 minutes at 4 °C, supernatant was discarded. Cells were resuspended in 1 mL PBS containing ZombieUV dye to stain dead cells for 30 minutes at 4 °C in darkness. After centrifugation at 360 xg for 5 minutes at 4 °C, supernatant was discarded. Cells were washed with 2 mL FACS buffer and centrifuged again. After discard of supernatant, cells were resuspended in 50  $\mu$ L Fc-block containing monoclonal antibodies (Tab. 13) and incubated for 30 minutes at 4 °C in darkness. Cells were washed twice with 2 mL FACS buffer and centrifugated at 360 xg for 5 minutes at 4 °C. Cells were resuspended in 200  $\mu$ L FACS buffer and were analyzed on a LSRII Flow Cytometer. Flow cytometry data was analyzed using FlowJo software.

The following table describes the fluorescence-labeled antibodies, which were used in this study (Tab. 20).

**Table 20. Fluorescence-labeled antibodies for flow cytometry.**

<b>Antibody (clone)</b>	<b>Company</b>
Anti-mouse CD8-FITC (53-6.7)	BioLegend, Germany
Anti-mouse CD4-FITC (RM4-5)	BioLegend, Germany
Anti-mouse CD19-BV510 (6D5)	BioLegend, Germany
Anti-mouse/human CD11b-PerCp-Cy5.5 (M1/70)	BioLegend, Germany
Anti-mouse IgE-PE (RME-1)	BioLegend, Germany
Anti-mouse Gr-1-BV421 (RB6-8C5)	BioLegend, Germany
Anti-mouse Siglec-F-APC (E50-2440)	BD Pharmingen, Germany

### 3. Results

#### 3.1 Quantification of *S. ratti* parasites in host tissue.

Free-living *S. ratti* L3i actively penetrate the skin of their mammalian host and migrate within 2 days on yet not fully defined migration routes through skin and muscle tissue and partially also via the lung to the nasofrontal region of the head. After being swallowed, L3 arrive in the small intestine at day 3 post infection (p.i.) (Dawkins and Grove, 1981a; Dawkins et al., 1982b). Here they moult via a L4 stage to parasitic female adults on day 5 p.i., which live embedded in the mucosa of the small intestine (Dawkins et al., 1983). Thereby, only 10 - 20 % of *S. ratti* L3 that penetrate the skin embed themselves in the small intestine during a primary infection and less than 5 % upon secondary infection in immune mice, indicating that host defense mechanisms actively participate in their elimination (Dawkins and Grove, 1981a, b). The fate and localization of the L3 that are successfully attacked and killed during the tissue migration has not been investigated so far.

To follow the fate of migrating L3 *in vivo*, naïve BALB/c mice (primary infection) and immune BALB/c mice (secondary infection) were infected with 2000 *S. ratti* L3i by *s.c.* injection into the footpad and sacrificed at different time points to analyze foot, leg, leg-derived skin, lung, head, small intestine and kidney for presence of viable and dead parasites. Viable L3, L4 and adults that emigrated out of the tissues were directly counted and complete *S. ratti*-derived DNA within the tissue samples was quantified by qPCR as indicator of both, viable and dying/dead parasites.

During a primary infection, *S. ratti*-derived DNA and viable L3 were immediately present after the injection in the footpad (Fig. 3). The numbers of viable L3 in the foot rapidly declined within 10 minutes and no viable L3 were present at day 1 p.i. or later. By contrast, *S. ratti*-derived DNA in the foot peaked at 30 min p.i. and was detected until day 6 p.i., suggesting that this remaining *S. ratti*-derived DNA was derived by killed and degrading *S. ratti* L3. Analysis of leg-derived skin and muscle tissues revealed presence of *S. ratti*-derived DNA and viable L3 at 10 min after injection of L3 i.e. the time point when the viable L3 had left the foot. Viable L3 declined in the leg after 60 min p.i., whereas *S. ratti*-derived DNA was detected until day 6 p.i., This remaining *S. ratti*-derived DNA again most likely reflected the presence of dead *S. ratti* L3-derived material for several days after the rapid

### 3. Results

---

emigration of viable L3 from the leg. Analysis of lung- and head-derived tissues showed viable L3 were first present 2 days (lung) or 1 day (head) after the infection with maximal numbers in both tissues at day 2 p.i. and rapid decline in numbers at day 3 p.i. Interestingly, *S. ratti*-derived DNA in the lung and head was detected before the presence of viable L3, i.e. in the lung already at 10 min p.i. and in the head at day 1 p.i. *S. ratti*-derived DNA was maximal in lung and head at day 2 p.i. and declined simultaneously with the numbers of viable L3, suggesting that no dead L3 remained in lung and head tissue. Viable *S. ratti* L3 immigrated from day 3 p.i. onwards into the small intestine and adult numbers peaked at day 6 p.i. *S. ratti*-derived DNA was detectable from day 2 p.i. onwards in the intestine, was maximal at day 6 p.i. and no longer present at 14 p.i. Therefore, analysis of viable adults was not performed after day 6 p.i. Analysis of kidney- and tongue-derived tissues revealed no detectable *S. ratti*-derived DNA or viable L3 throughout infection.

The analysis of parasite burden in the footpad of secondary infected mice closely resembled mice that were infected for the first time. Again, the numbers of viable L3 were maximal immediately after the injection and rapidly declined within 10 minutes. *S. ratti*-derived DNA was maximal between 10 and 60 min p.i. and was detectable until day 6 p.i. However, in comparison to the primary infection, *S. ratti*-derived DNA declined more pronounced from 30 min p.i. until day 2 p.i. The analysis of leg-, lung- and head-derived tissues showed that only very few viable L3 were present and the quantity of *S. ratti*-derived DNA was drastically reduced compared to the primary infection. Viable L3, L4, adults or *S. ratti*-derived DNA were absent in the small intestine. Consistent with the results of the primary infection, no viable L3 or *S. ratti*-derived DNA was detectable in kidney-derived tissues throughout the infection.

In summary these results show that *S. ratti* migration was restricted to the infection site (here the foot), the leg-derived skin and muscle tissues, lung, head and intestine, whereas other tissues such as the kidney and tongue remained parasite free. Thus, L3 did not migrate randomly through their host, but followed a specific route via the tissue to the intestine. Viable L3 were first present in the foot, arrived 10 minutes later in the leg-derived tissues and 2 days later in the lung and head. At day 3 after the infection L3 arrived at the small intestine. *S. ratti*-derived DNA was detected for a noticeable longer time period in

### 3. Results

---

foot and leg-derived tissues than viable L3, suggesting that the local killing of L3 predominantly occurred in these tissues and not in the lung and the head where viable L3 and *S. ratti*-derived DNA declined simultaneously. In immune mice, L3 were directly retained and killed at the site of re-infection, as almost no viable *S. ratti* L3 or *S. ratti*-derived DNA were detectable in other tissues than the footpad.

### 3. Results

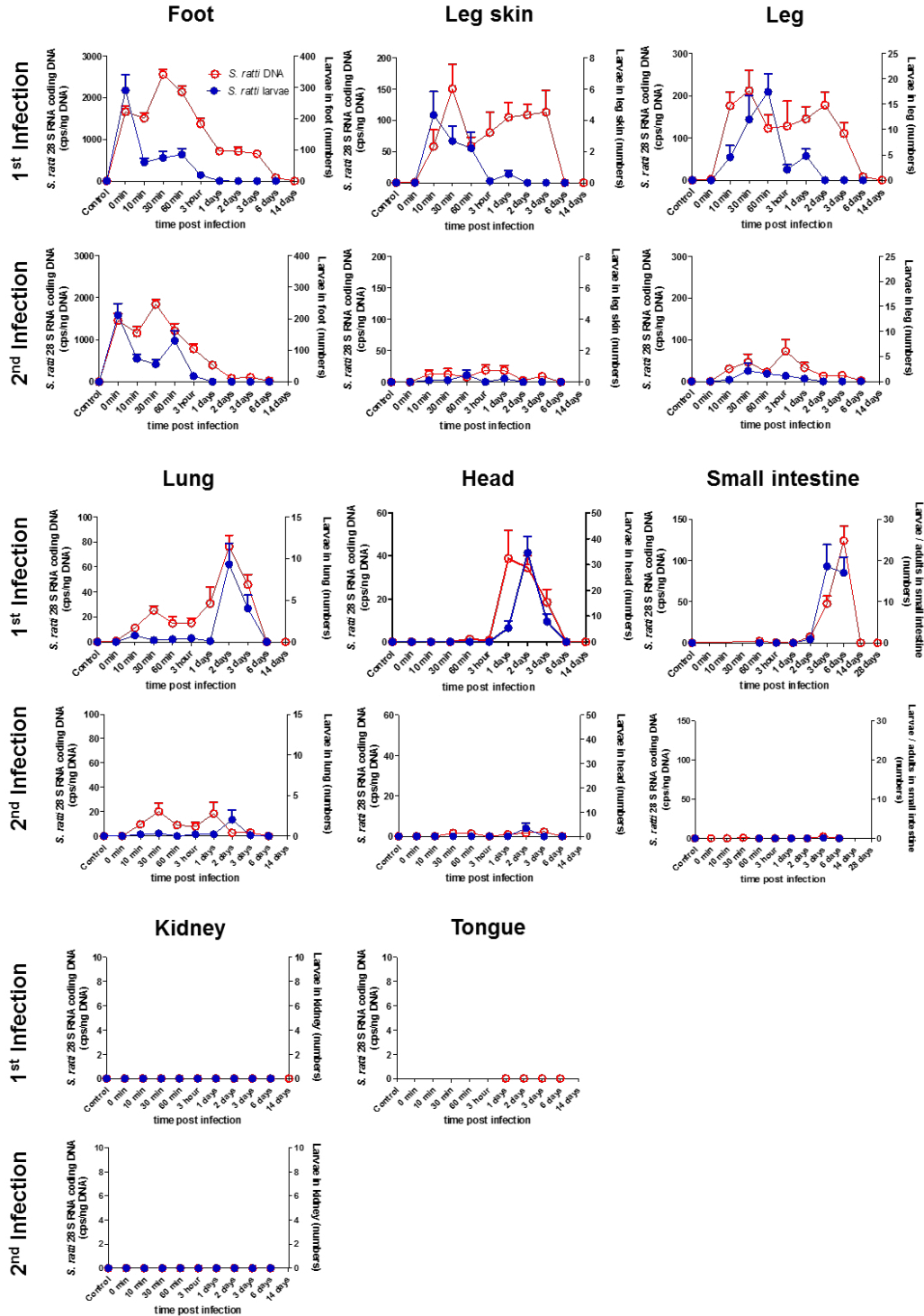


**Figure 3. Quantification of *S. rattii* parasites in host tissue.**

Naïve BALB/c (primary infection) mice and immune BALB/c (secondary infection) mice were infected with 2000 *S. rattii* L3i by s.c. injection into the footpad and sacrificed at indicated time points. *S. rattii*-derived DNA (open red circles - left ordinate) was quantified in the indicated tissues by qPCR. Viable *S. rattii* L3, L4 and adults (filled blue circles - right ordinate) that emigrated out of indicated tissues were counted. Graphs shown mean of combined results derived out of 2 experiments with 3 - 5 mice per time point, group and experiment, error bars show +SEM.

#### **3.2 *S. ratti* L3 migration-induced tissue damage in the lung**

At the time point of maximal parasite burden in the lung, day 2 p.i., it was observed that primary infected mice showed macroscopic hemorrhagic lung lesions while in uninfected control mice these lung lesions were absent (Fig. 4A). For this reason, lung pathology was investigated in more detail.

The presence of erythrocytes in alveolar spaces of histological sections and in cytospin-prepared bronchoalveolar lavage (BAL) samples indicated tissue damage (Fig. 4B). Histological tissue staining with Naphthol AS-D Chloroacetate (NaSDCI) identified granule containing cells around L3, however some L3 remained intact and free in lung tissue (Fig. 4C). These granule containing cells, i.e. granulocytes, are important for the tissue parasite control (Watanabe et al., 2000). BAL fluid samples were additionally analyzed by flow cytometry to determine erythrocyte numbers. Erythrocyte numbers were elevated in primary infected mice at day 2 p.i. compared to uninfected control mice and to secondary infected mice. Lung pathology was transient as erythrocyte numbers declined at day 6 p.i. when L3 had left the lung (Fig. 4E).



### 3. Results

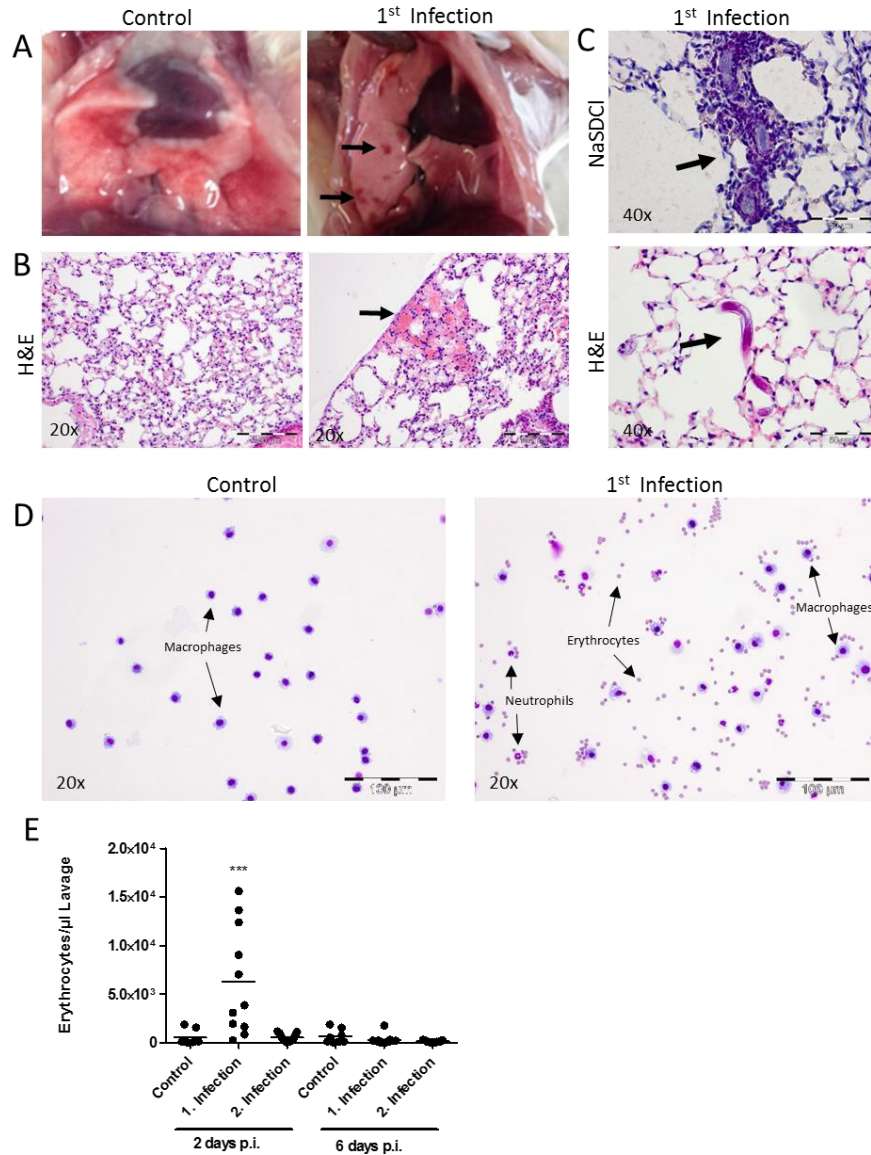


**Figure 4. *S. ratti* L3 migration-induced tissue damage in the lung.**

Naïve (primary infection) and immune (secondary infection) BALB/c mice were infected with 2000 *S. ratti* L3i by s.c. injection into the footpad and sacrificed at indicated time points. (A) Representative lung photographs and (B) representative H & E stained lung sections of uninfected (Control) and primary (1<sup>st</sup> Infection) infected mice at day 2 p.i. are shown. Hemorrhagic lung lesions are indicated by black arrows. (C) Representative NaSDCl (top) and H & E (bottom) stained lung sections with *S. ratti* L3, indicated by black arrow, of primary infected mice at day 2 p.i. are shown. (D) Representative cytopsin-prepared BAL fluid cells, stained with Diff-Quick, of uninfected (Control) and primary (1<sup>st</sup> Infection) infected mice at day 2 p.i. are shown. BAL fluid cells show macrophages, erythrocytes and neutrophils. (E) Erythrocyte count was analyzed in BAL fluid by flow cytometry. (A-D) Representative sections are shown of 2 experiments with 2 - 3 mice per time point, group and experiment. (E) Graph shows mean of combined results derived out of 2 experiments with 4 - 6 mice per time point, group and experiment, each symbol represents an individual mouse. Statistical analysis was performed by one-way ANOVA with Dunnett's post hoc test. Asterisks indicate significant differences between the groups (\*\*\*) p < 0.001).

#### **3.3 Quantification of *S. ratti* parasites in rIL-33 treated mice**

The alarmin IL-33 is mainly released by stromal cells such as epithelial and endothelial cells as a danger signal that contributes to initiation and amplification of innate and adaptive immune responses (Miller, 2011). IL-33 was shown to promote ILC2 expansion, lung eosinophilia and to improve host defense in mice during infection with *S. venezuelensis* (Yasuda et al., 2012), a helminth parasite that is closely related to *S. ratti*. In order to evaluate the role of IL-33 during *Strongyloides* infection more precisely, IL-33-induced changes in parasite burden were analyzed in different tissues. To this end BALB/c mice received 1 µg rIL-33 or PBS *i.p.* 3 h before and one day after *S. ratti* infection and the numbers of L3 in the lung and head at day 2 p.i. and parasitic adults in the small intestine at day 6 p.i. were counted (Fig. 5).

Surprisingly, the numbers of migrating L3 in lung and head of rIL-33 treated mice were significantly elevated compared to untreated mice (Fig. 5B), while parasitic adult numbers in the small intestine of rIL-33 treated mice were significantly decreased compared to untreated mice (Fig. 5C).

### 3. Results

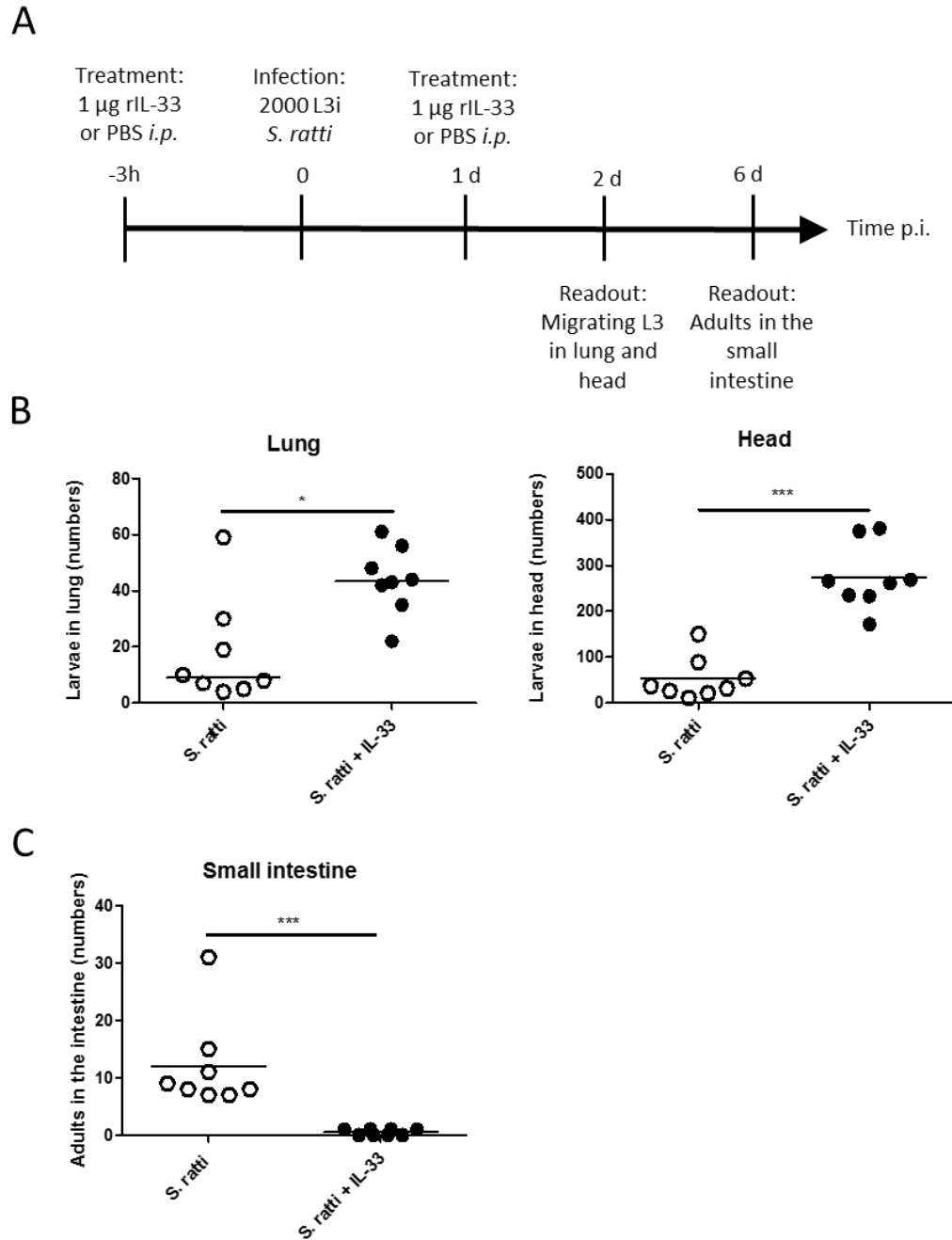


**Figure 5. *S. ratti* parasite burden in rIL-33 treated mice.**

(A) Experimental setup is shown. BALB/c mice were treated 3 h before infection and at day 1 p.i. with 1  $\mu$ g rIL-33 *i.p.* (black circles) or were left untreated (open circles). Mice were infected with 2000 *S. ratti* L3i by s.c. injection into the footpad and sacrificed at indicated time points. (B) Viable *S. ratti* L3 were counted in lung and head at day 2 p.i. (C) *S. ratti* adults were counted in the small intestine at day 6 p.i. Graphs show mean of combined results derived out of 2 experiments with 4 mice per time point, group and experiment, each symbol represents an individual mouse. Statistical analysis was performed by Mann-Whitney U test. Asterisks indicate significant differences between the groups (\*  $p < 0.05$ , \*\*\*  $p < 0.001$ ).

### 3. Results

---

Thus, rIL-33 treatment had different, tissue-specific effects. To analyze this unexpected finding more closely, the parasite burden in rIL-33 treated and untreated mice was compared in foot and leg-derived skin and muscle tissue, lung, head and small intestine over time and by differentiating between viable L3 and complete *S. ratti*-derived DNA (Fig. 6).

The analysis of the footpad showed that *S. ratti*-derived DNA and viable L3 were immediately present after injection. The number of viable L3 rapidly declined within 10 minutes and no viable L3 were present at day 1 p.i. or later in rIL-33 treated or untreated mice. In contrast, *S. ratti*-derived DNA was still increased in the footpad of untreated mice compared to rIL-33 treated mice at day 2 - 4 p.i., indicating that fewer parasites remained in the footpad of rIL-33 treated mice. Analysis of leg-derived skin and muscle tissues showed that viable L3 were first detectable at 10 min p.i. in rIL-33 treated and untreated mice. rIL-33 treatment significantly increased viable L3 numbers already at day 1 p.i. in both tissues compared to untreated mice. Interestingly, *S. ratti*-derived DNA was again increased at day 2 - 4 p.i. in leg-derived skin and muscle tissues in untreated mice compared to rIL-33 treated mice. This shows again that fewer parasites remained in leg-derived tissues of rIL-33 treated mice and could indicate that killing of migrating L3 in leg-derived tissues was less efficient upon rIL-33 treatment. Viable L3 simultaneously arrived in the lung- and head-derived tissues of rIL-33 treated and untreated mice showing that rIL-33 treatment did not change larval overall mobility. At day 2 p.i., viable L3 and *S. ratti* derived-DNA were significantly increased in lung and head in rIL-33 treated mice compared to untreated mice. Increased numbers of L3 in the lung were correlated with increased lung damage indicated by elevated erythrocyte numbers in BALF samples (Fig. 7). *S. ratti*-derived DNA declined in lung and head at day 3 p.i., together with viable L3 numbers, showing that no dead L3 remained in these tissues in rIL-33 treated and untreated mice. The analysis of parasite burden in the small intestine showed that viable L3 arrived simultaneously at day 3 p.i. in rIL-33 treated and untreated mice. However, at day 4 - 6 p.i. viable L4 and adults were decreased in rIL-33 treated mice and *S. ratti*-derived DNA was reciprocally increased in the intestine of untreated mice.

### 3. Results

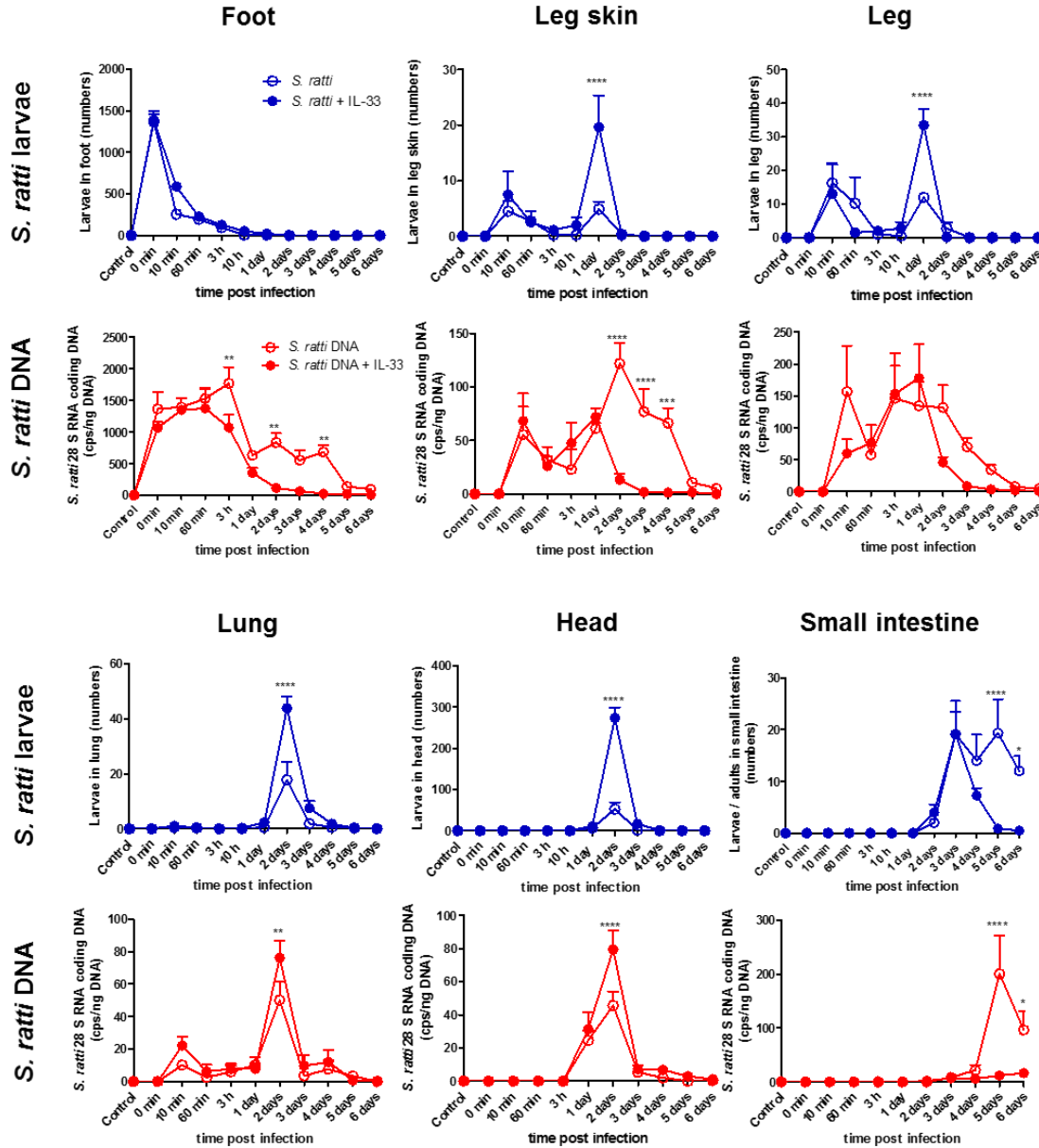


**Figure 6. Quantification of *S. ratti* parasites in rIL-33 treated mice.**

BALB/c mice were treated 3 h before the infection and at day 1 p.i. with 1  $\mu$ g rIL-33 *i.p.* (filled circles) or were left untreated (open circles). Mice were infected with 2000 *S. ratti* L3i by *s.c.* injection into the footpad and sacrificed at indicated time points. *S. ratti*-derived DNA (red circles) was quantified in the indicated tissues by qPCR. Viable *S. ratti* L3, L4 and adults (blue circles) that emigrated out of the indicated tissues were counted. Graphs show mean of combined results derived out of 2 experiments with 4 mice per time point, group and experiment, error bars show +SEM. Statistical analysis was performed by two-way ANOVA with Bonferroni's post hoc test. Asterisks indicate significant differences between the groups (\*  $p < 0.05$ , \*\*  $p < 0.01$ , \*\*\*  $p < 0.001$ , \*\*\*\*  $p < 0.0001$ ).

### 3. Results

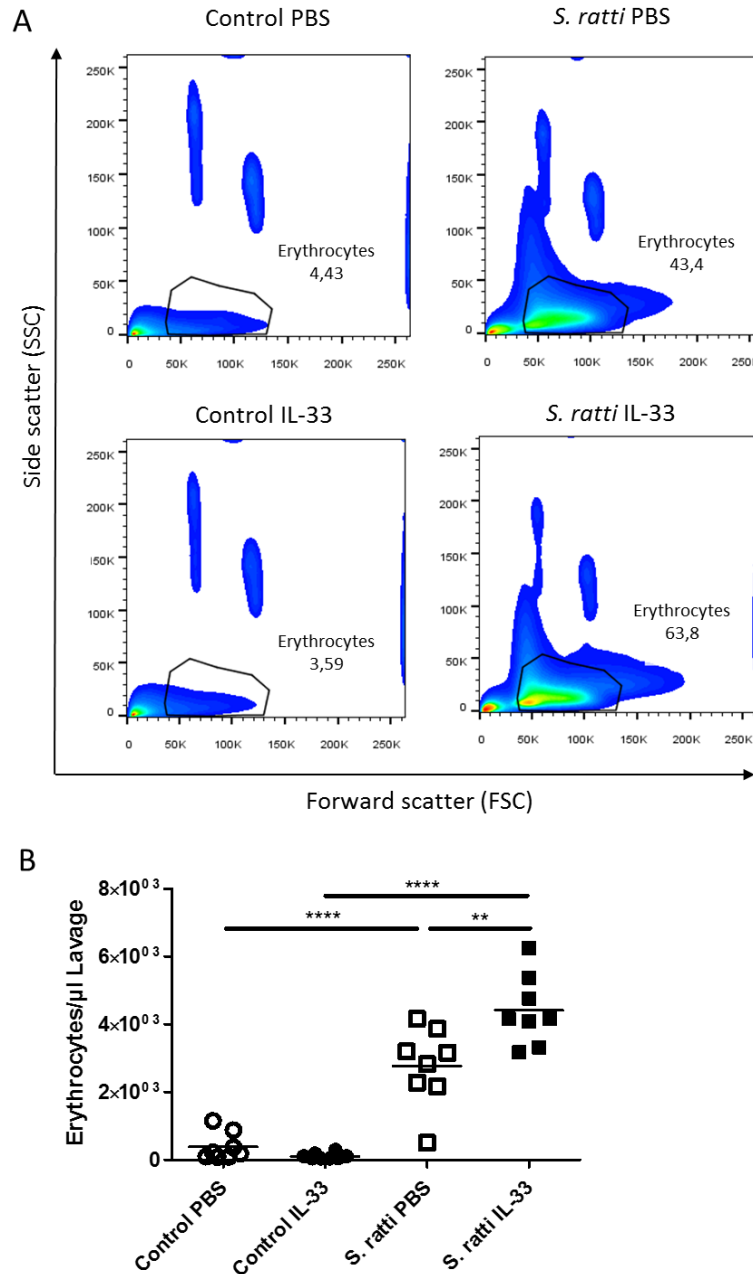


**Figure 7. Quantification of erythrocytes in bronchoalveolar lavage of rIL-33 treated mice.** BALB/c mice were treated 3 h before the infection and at day 1 p.i. with 1  $\mu\text{g}$  rIL-33 or PBS *i.p.* Control mice remained uninfected but rIL-33 or PBS treated. Mice were infected with 2000 *S. ratti* L3i by *s.c.* injection into the footpad and sacrificed at day 2 p.i. BAL fluid samples were analyzed by flow cytometry. (A) Representative dot plots are shown of uninfected PBS or rIL-33 treated mice (left) and *S. ratti* infected PBS or rIL-33 treated mice (right). (B) Corresponding quantification of erythrocyte count in the lavage is shown. Graph shows mean of combined results derived out of 2 experiments with 4 mice per time point, group and experiment, each symbol represents an individual mouse. Statistical analysis was performed by one-way ANOVA with Bonferroni's post hoc test. Asterisks indicate significant differences between the groups (\*\*  $p < 0.01$ , \*\*\*\*  $p < 0.0001$ ).

### 3. Results

To understand how the parasite burden changes from higher L3 numbers in the lung and head to fewer adults in the small intestine in rIL-33 treated mice, *S. ratti*-derived DNA was additionally quantified in the feces by qPCR (Fig. 8).

*S. ratti*-derived DNA in the feces was not detectable at day 2 p.i., the time point when first L3 arrived at the intestine. *S. ratti*-derived DNA was significantly increased in rIL-33 treated mice at day 3 and 4 p.i., indicating an early release of *S. ratti*-derived material with the feces. In contrast, *S. ratti*-derived DNA in the feces of untreated mice was first detected at day 4 p.i.

Taken together, these results show that treatment with rIL-33 increased the numbers of viable L3 during the tissue migration phase suggesting impaired killing of L3 in foot and leg-derived tissues. Nevertheless, the numbers of adults in the intestine was decreased in rIL-33 treated mice (Fig. 8B). This could reflect a rapid expulsion of *S. ratti* L3, immediately upon arrival in the intestine and before they embed themselves in the mucosa, in rIL-33 treated mice. This might be supported by the initially increased detection of *S. ratti* DNA in the feces and reduced numbers of mucosa attached adults at day 6 in rIL-33 treated mice.

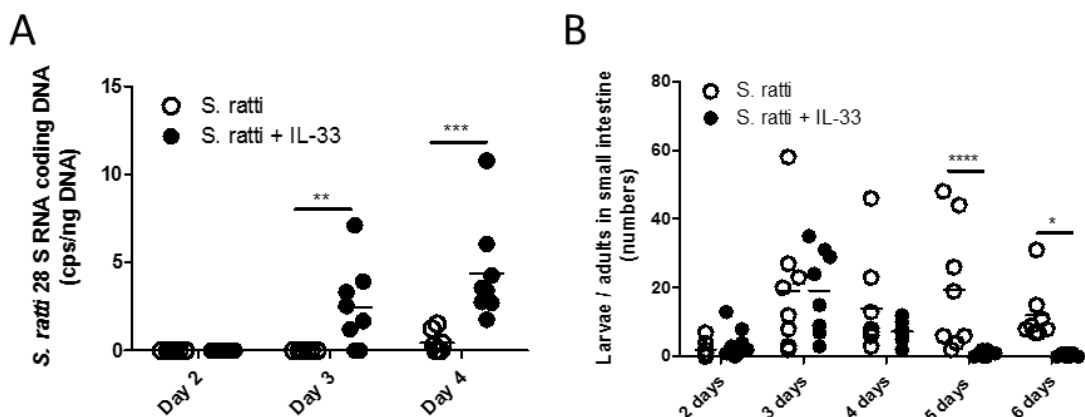


**Figure 8. Quantification of *S. ratti*-derived DNA in feces of rIL-33 treated mice.**

BALB/c mice were infected with 2000 *S. ratti* L3i by *s.c.* injection into the footpad and treated 3 h before and at day 1 p.i. with 1  $\mu$ g rIL-33 (black circles) or PBS (open circles) *i.p.* (A) Feces samples were analyzed at indicated time points for quantification of *S. ratti*-derived DNA by qPCR. (B) Viable *S. ratti* L3, L4 and adults that emigrated out of the small intestine were counted at indicated time points. Graphs show mean of combined results derived out of 2 experiments with 4 mice per time point, group and experiment, each symbol represents an individual mouse. Statistical analysis was performed by Mann-Whitney U test. Asterisks indicate significant differences between the groups (\*  $p < 0.05$ , \*\*  $p < 0.01$ , \*\*\*  $p < 0.001$ , \*\*\*\*  $p < 0.0001$ ).

#### **3.4 Quantification of mMCPT-1 concentrations in sera of rIL-33 treated mice**

To test the hypothesis that rIL-33 accelerates expulsion of *S. ratti* from the intestine, mast cells were analyzed in more detail. Mucosal mast cells are important intestinal effector cells mediating expulsion of *S. ratti* from the intestine (Khan et al., 1993). Activation of mucosal mast cells leads to degranulation and thereby to the release of mast cell-specific protease 1 (mMCPT-1). Therefore, measurement of mMCPT-1 is frequently used as a marker for degranulation of mucosal mast cells *in vivo*. Infection with *S. ratti* and *S. venezuelensis* elevated mMCPT-1 sera concentrations (Eschbach et al., 2010; Reynolds et al., 1990; Sasaki et al., 2005). To analyze the impact of IL-33 on mast cell activation, mMCPT-1 sera concentration of *S. ratti* infected and uninfected control mice were analyzed (Fig. 9).

The analysis showed a drastic increase of mMCPT-1 sera concentrations in *S. ratti* infected mice treated with rIL-33 from day 2 - 4 p.i. compared to PBS treated infected mice. mMCPT-1 concentrations of PBS and rIL-33 treated infected mice were comparable again at day 6 p.i. Interestingly, rIL-33 induced mast cell degranulation also in the absence of *S. ratti* infection.

This result shows that mucosal mast cells were rapidly activated in response to rIL-33 treatment.



### 3. Results

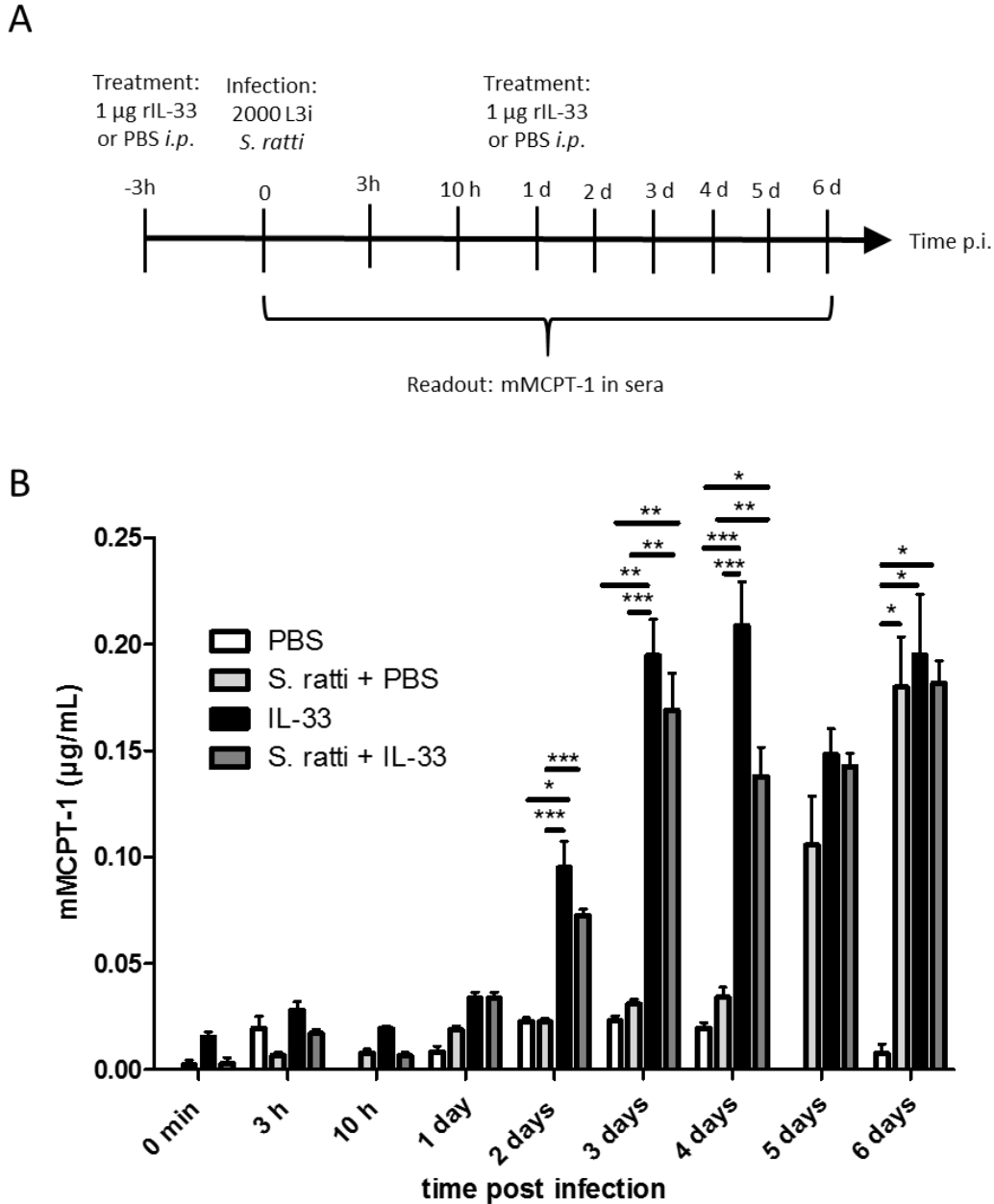


**Figure 9. Quantification of mMCPT-1 concentrations in sera of rIL-33 treated mice.**

(A) Experimental setup is shown. BALB/c mice were infected with 2000 *S. ratti* L3i by s.c. injection into the footpad and blood was collected at indicated time points for analysis of mMCPT-1 concentration. Mice were treated 3 h before and at day 1 p.i. with 1  $\mu$ g rIL-33 (dark grey bars) or PBS (light grey bars) *i.p.* Uninfected control mice were treated with rIL-33 (black bars) or PBS (white bars) (B) mMCPT-1 concentrations in sera were analyzed by ELISA. Graph shows mean of combined results derived out of 3 experiments with 4 mice per time point and experiment (*S. ratti* + PBS, *S. ratti* + IL-33), 2 experiments with 4 mice per time point and experiment (IL-33) and 1 experiment with 4 mice per time point (PBS), error bars show +SEM. Statistical analysis was performed by Kruskal-Wallis test with Dunn's post hoc test. Asterisks indicate significant differences between the groups (\*  $p < 0.05$ , \*\*  $p < 0.01$ , \*\*\*  $p < 0.001$ ).

So far, it was shown that rIL-33 treatment increased tissue parasite burden while the numbers of adults in the small intestine were decreased. Mucosal mast cells were rapidly activated to degranulate, indicated by elevated serum mMCPT-1 concentration and *S. ratti* fecal release was accelerated by rIL-33 treatment.

To elucidate the underlying mechanism of rIL-33-mediated changes in parasite burden, mice deficient for specific immune cells or receptors were used in following experiments.

#### **3.5 *S. ratti* parasite burden and mast cell activation in rIL-33 treated mast cell-deficient Cpa3<sup>Cre</sup> mice**

To analyze the importance of mast cells for the rIL-33-mediated changes in the parasite burden, the Cpa3<sup>Cre</sup> mouse model for mast cell deficiency was used. Heterozygous Cpa3<sup>Cre</sup> mice express Cre recombinase under the control of the Cpa3 promoter deleting all mucosal and connective tissue mast cells by genotoxic mechanisms (Feyerabend et al., 2011). *S. ratti* burden in mast cell-deficient Cpa3<sup>Cre</sup> mice and their mast cell-competent Cpa3<sup>wt</sup> (wildtype) littermates were compared between PBS and rIL-33 treatment (Fig. 10).

Adult numbers in the small intestine were not decreased by rIL-33 treatment in mast cell-deficient Cpa3<sup>Cre</sup> mice, compared to rIL-33 treated Cpa3<sup>wt</sup> littermates. Interestingly, rIL-33 treatment increased numbers of L3 also in the absence of mast cells in the head but not in the lung. In general, mast cell deficiency did not change the number of migrating L3 in the tissue, while the number of adults in the small intestine was increased as described before (Reitz 2016).

Although no mast cell activation was expected in mast cell-deficient mice under any circumstances a very low concentration of mMCPT-1 was measured in sera of mast cell-deficient Cpa3<sup>Cre</sup> mice that, although still on very low level, was significantly increased by rIL-33 treatment. This could either indicate the presence of residual mucosal mast cells in Cpa3<sup>Cre</sup> mice or mMCPT-1 release by another cell type. Nevertheless, the strong increase in mMCPT-1 concentration that was correlated to decreased parasite burden in rIL-33-treated mice was selectively observed in mast cell competent mice.

### 3. Results

---

These results show that the rIL-33-induced reduction in parasite burden in the small intestine was dependent on mast cells and associated with mast cell activation. rIL-33-induced elevation of L3 numbers in the tissue, by contrast was independent of mast cells.

### 3. Results

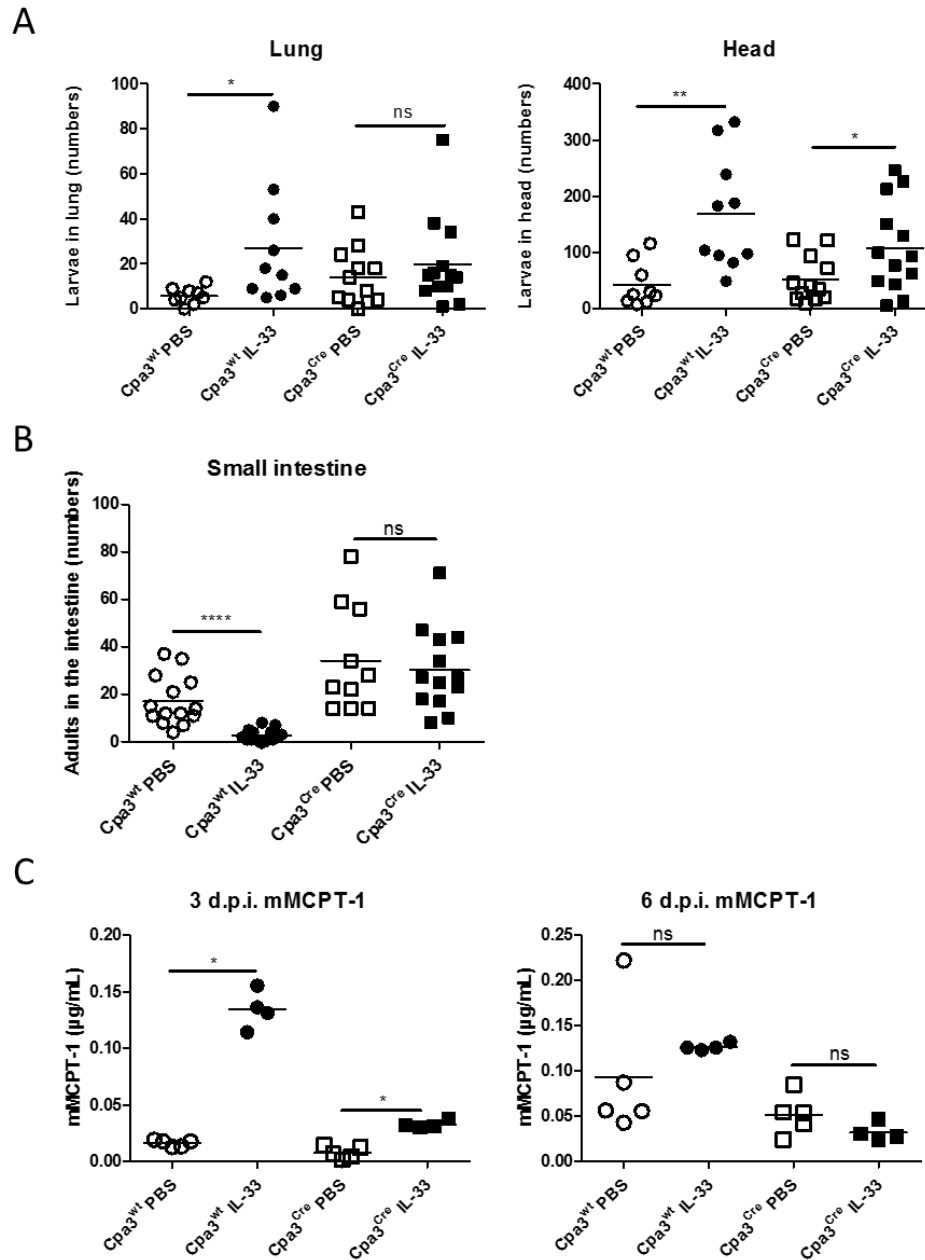


**Figure 10. *S. ratti* parasite burden and mast cell activation in rIL-33 treated mast cell-deficient *Cpa3*<sup>Cre</sup> mice.**

BALB/c *Cpa3*<sup>wt</sup> (circles) and *Cpa3*<sup>Cre</sup> mice (squares) were treated 3 h before and at day 1 p.i. with 1 µg rIL-33 (black symbols) or PBS *i.p.* (open symbols). Mice were infected with 2000 *S. ratti* L3i by *s.c.* injection into the footpad. (A) Viable *S. ratti* L3 in lung and head at day 2 p.i. and (B) adults in the intestine at day 6 p.i. were counted. (C) mMCPT-1 concentrations in sera at day 3 and 6 p.i. were analyzed by ELISA. Graphs show mean of combined results derived out of 2 (A) and 3 (B) experiments with 4 - 7 mice (A) and 3 - 6 mice (B) per group and experiment, each symbol represents an individual mouse. (C) Graphs show data from one experiment with 4 - 5 mice per group and time point, bars indicate the mean. Statistical analysis was performed by Student's t-test or Mann-Whitney U test. Asterisks indicate significant differences between the groups (\*  $p < 0.05$ , \*\*  $p < 0.01$ , \*\*\*\*  $p < 0.0001$ , ns=not significant).

#### **3.6 *S. rattii* parasite burden and mast cell activation in rIL-33 treated IL-9R-deficient mice.**

IL-9 is an important activator of mast cells and injection of exogenous IL-9 reduced intestinal parasite burden in *S. rattii* infection (Blankenhaus et al., 2014; Noelle and Nowak, 2010). To elucidate the mechanism of improved and accelerated mast cell activation by rIL-33 treatment, parasite burden in IL-9R-deficient mice and BALB/c wildtype mice was compared between PBS and rIL-33 treatment (Fig. 11).

Consistent with the results obtained using mast cell-deficient mice, treatment with rIL-33 failed to reduce parasite burden in the small intestine in IL-9R-deficient mice at day 6 p.i. compared to wildtype mice. Viable L3 in rIL-33 treated IL-9R-deficient mice were increased in the head but not in the lung, compared to wildtype mice. In general, IL-9R deficiency increased the number of migrating L3 in the tissue and adults in the intestine as described before (Reitz et al., 2018). Treatment with rIL-33 increased mMCP-1 concentration in IL-9R-deficient mice at day 6 p.i., but not at day 2 p.i., indicating that early mast cell activation was not established in the absence of IL-9R signaling.

These results show that the rIL-33-induced acceleration of mast cell activation and reduction in parasite burden in the small intestine was dependent on functional IL-9R signaling. However, the elevation of L3 numbers in the tissue was not altered in the absence of IL-9R signaling.

### 3. Results

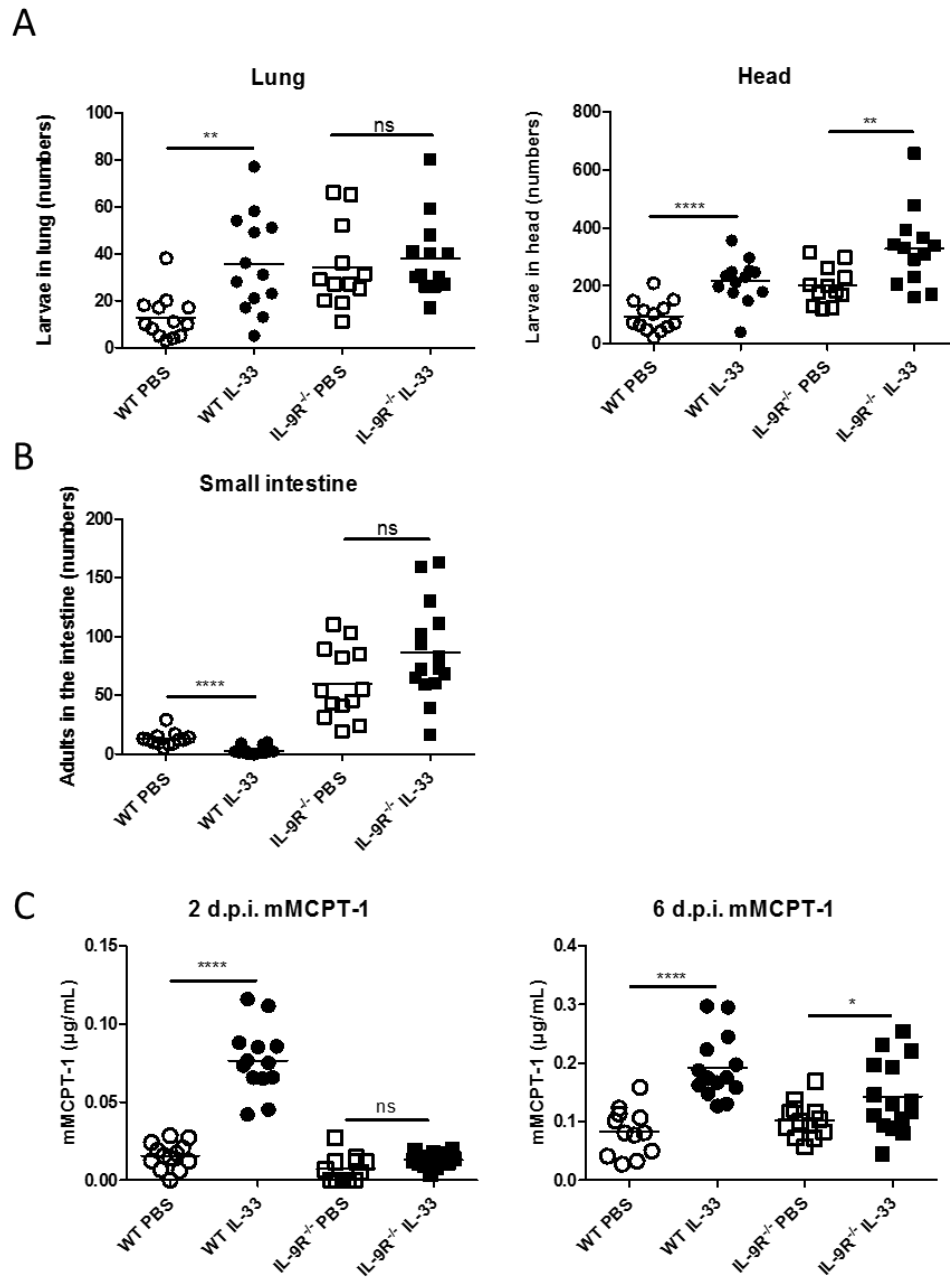


**Figure 11. *S. ratti* parasite burden and mast cell activation in rIL-33 treated IL-9R-deficient mice.**

BALB/c wildtype (circles) and IL-9R<sup>-/-</sup> mice (squares) were treated 3 h before and at day 1 p.i. with 1 µg rIL-33 (black symbols) or PBS *i.p* (open symbols). Mice were infected with 2000 *S. ratti* L3i by *s.c.* injection into the footpad. (A) Viable *S. ratti* L3 in lung and head at day 2 p.i. and (B) adults in the intestine at day 6 p.i. were counted. (C) mMCPT-1 concentrations in sera at day 2 and 6 p.i. were analyzed by ELISA. Graphs show mean of combined results derived out of 2 experiments with 6 - 7 mice (A and C left) and 7 - 8 mice (B and C right) per group and experiment, each symbol represents an individual mouse. Statistical analysis was performed by Student's t-test or Mann-Whitney U test. Asterisks indicate significant differences between the groups (\* p < 0.05, \*\* p < 0.01, \*\*\*\* p < 0.0001, ns=not significant).

#### **3.7 *S. ratti* parasite burden and mast cell activation in rIL-33 treated basophil-deficient mice.**

Basophils play a role in the contribution to early expulsion of the *S. ratti* adults from the intestine, however they are redundant for final control and termination of the infection (Reitz et al., 2017). Basophils have overlapping functions with mast cells (Voehringer, 2013). As mast cells are important for the IL-33-induced reduction in the intestinal parasite burden, the contribution of basophils was examined as well. Therefore, parasite burden in Mcpt8<sup>Cre</sup> basophil-deficient mice and basophil-competent Mcpt8<sup>wt</sup> littermates was compared between PBS and rIL-33 treatment (Fig. 12). Heterozygous bacterial artificial chromosome (BAC) transgenic mice express Cre recombinase under control of regulatory elements for basophil-specific mast cell protease 8 (Mcpt8), resulting in constitutively deletion of basophils (Ohnmacht et al., 2010).

The treatment with rIL-33 efficiently reduced the parasite burden in the small intestine and increased the numbers of viable L3 in lung and head in Mcpt8<sup>Cre</sup> basophil-deficient mice to the same extend as in basophil-competent Mcpt8<sup>wt</sup> littermates. Basophil deficiency as such increased the number of adults in the intestine, but parasite burden in the tissue remained unchanged as previously described (Reitz et al., 2018). mMCPT-1 concentrations were elevated in rIL-33 treated Mcpt8<sup>Cre</sup> basophil-deficient mice at day 2 p.i., indicating that rIL-33-mediated acceleration of mast cell degranulation functioned independently of basophils.

Thus, neither the rIL-33-induced increased tissue parasite burden nor the decrease in the intestinal parasite burden were mediated by basophils.

### 3. Results

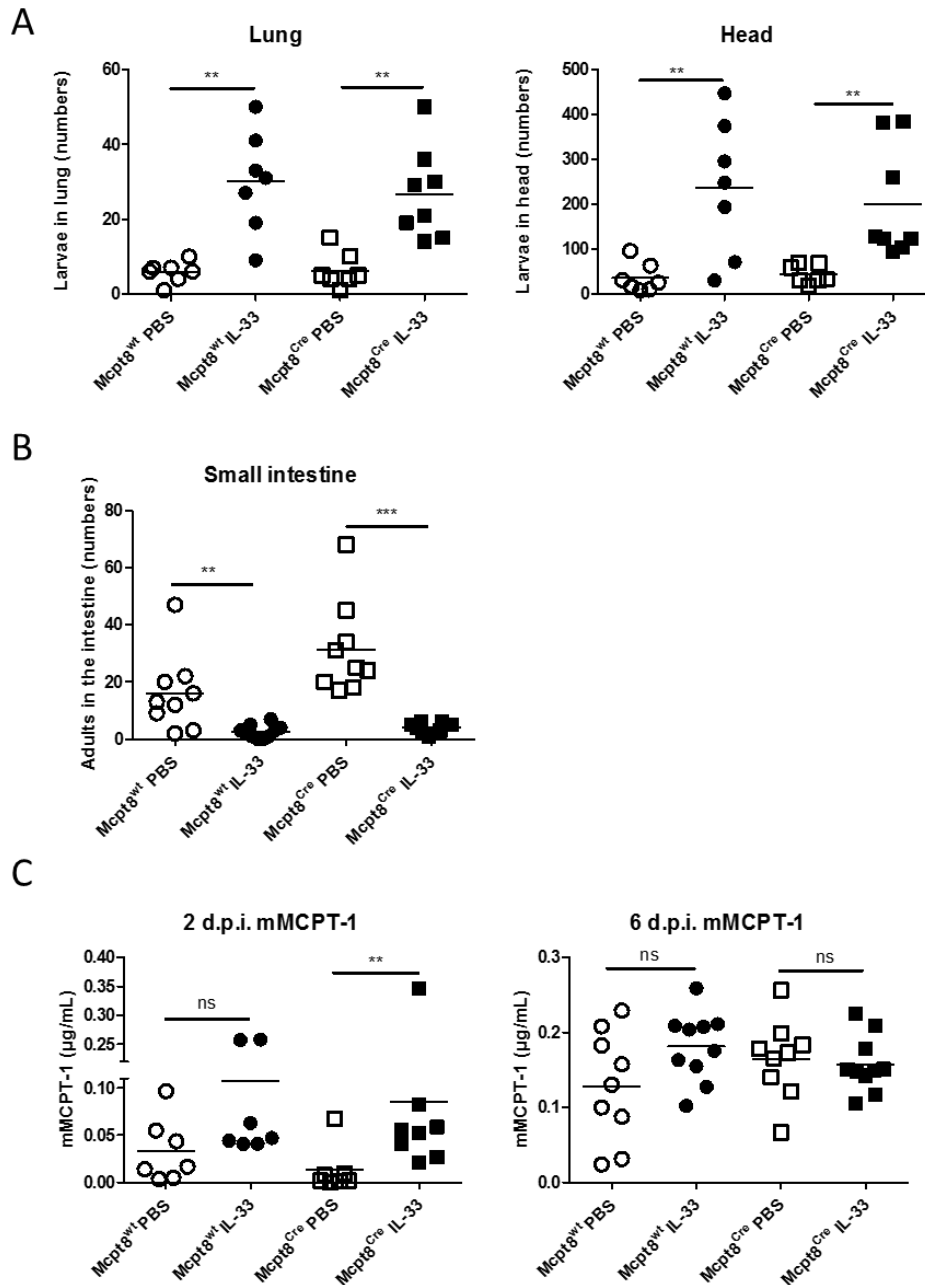


**Figure 12. *S. ratti* parasite burden and mast cell activation in rIL-33 treated basophil-deficient mice.**

BALB/c wildtype (circles) and basophil-deficient mice (squares) were treated 3 h before the infection and at day 1 p.i. with 1 µg rIL-33 (black symbols) or PBS *i.p.* (open symbols). Mice were infected with 2000 *S. ratti* L3i by *s.c.* injection into the footpad. (A) Viable *S. ratti* L3 in lung and head at day 2 p.i. and (B) adults in the intestine at day 6 p.i. were counted. (C) Expression levels of mMCPT-1 in sera at day 2 and 6 p.i. were analyzed by ELISA. Graphs show mean of combined results derived out of 2 experiments with 3 - 4 mice (A and C left) and 4 - 5 mice (B and C right) per group and experiment, each symbol represents an individual mouse. Statistical analysis was performed by Mann-Whitney U test. Asterisks indicate significant differences between the groups (\*\*  $p < 0.01$ , \*\*\*  $p < 0.001$ , ns=not significant).



In conclusion, these findings show that rIL-33-mediated reduction of intestinal *S. ratti* parasite burden was independent of basophils but strictly dependent on the presence of mast cells and intact IL-9R signaling. Thereby, IL-9R was needed for rIL-33-mediated acceleration of mast cell activation indicated by increased mMCPT-1 release.

The rIL-33-mediated interference with larval killing in the leg-derived tissues and subsequent elevation of L3 numbers in the head was independent of basophils, mast cells and IL-9R mediated signaling. The analysis of tissue parasite burden in mast cell-deficient mice and IL-9R-deficient mice treated with rIL-33 revealed different results for head and lung derived tissues. The parasite burden in lung tissue was more comparable to the results of the small intestine, indicating that the lung tissue behaved more like a mucosal tissue.

#### **3.8 Flow cytometric detection and quantification of neutrophils and eosinophils in the lung of rIL-33 treated mice**

To understand how rIL-33 treatment modulated the immune response to migrating *S. ratti* L3 in the tissue, the cellular composition of lungs derived from rIL-33 or PBS treated infected and uninfected mice at day 2 p.i. was analyzed by flow cytometry (Fig. 13).

rIL-33 treatment of uninfected mice decreased the frequency and total cell number of neutrophils at day 2 p.i. compared to PBS treated uninfected and infected mice. However, the eosinophil cell population remained unchanged in frequency and total cell number in rIL-33 compared to PBS treated infected and uninfected mice.

This result indicates that rIL-33 treatment decreased neutrophil numbers in the lung also in the absence of parasite infection. Despite the unchanged neutrophil numbers in rIL-33 treated *S. ratti* infected mice compared to PBS treated infected or uninfected mice, possible neutrophil effector functions might be altered by rIL-33.

### 3. Results

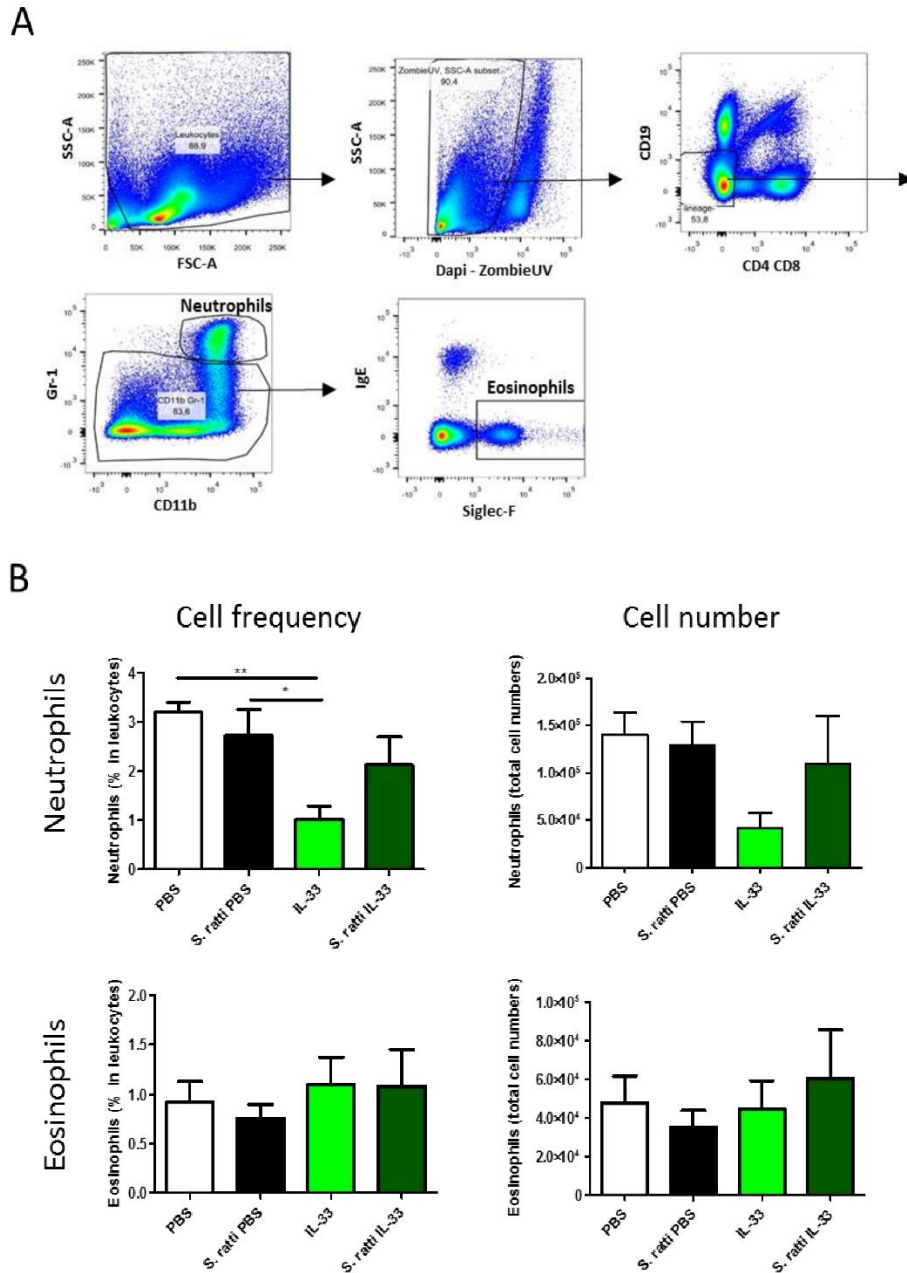


**Figure 13. Flow cytometric detection and quantification of neutrophils and eosinophils in the lung of rIL-33 treated mice.**

BALB/c mice were infected with 2000 *S. rattii* L3i by s.c. injection into the footpad. Lungs were removed for analysis of neutrophil and eosinophil populations by flow cytometry at day 2 p.i. Mice were treated 3 h before and at day 1 p.i. with 1  $\mu$ g rIL-33 (dark green bars) or PBS (black bars) i.p. Uninfected control mice were treated with rIL-33 (light green bars) or PBS (white bars). (A) Lung single cell suspensions were prepared for cell surface staining of neutrophils and eosinophils with BV421 labeled Gr-1; clone RB6-8C5 and APC labeled Siglec-F; clone E50-2440 and PerCP-Cy5.5 labeled CD11b; clone M1/70. Gating strategy is shown. (B) Cell frequency and total cell number of neutrophils and eosinophils are shown. Graphs show mean of combined results derived out of 2 experiments with 4 mice per group, time point and experiment, error bars show +SEM. Statistical analysis was performed by one-way ANOVA with Bonferroni's post hoc test. Asterisks indicate significant differences between the groups (\*  $p < 0.05$ , \*\*  $p < 0.01$ ).

#### **3.9 *S. ratti* parasite burden and mast cell activation in rIL-33 treated, granulocyte depleted mice and eosinophil-deficient mice**

Neutrophilic and eosinophilic granulocytes are important effector cells contributing to the control of migrating *S. ratti* L3 in the tissue (Watanabe et al., 2000; Watanabe et al., 2003). To investigate whether rIL-33 treatment interfered with granulocyte mediated killing of L3 in the tissue, the impact of IL-33 treatment on parasite burden was analyzed in granulocyte depleted and eosinophil-deficient mice (Fig. 14 and 15).

Granulocytes were efficiently depleted by administration of anti-Gr-1 antibody in blood at day 1 p.i. (Fig. 14E). Granulocyte depletion elevated the numbers of viable L3 in the tissue and of intestinal adults as described (Watanabe et al., 2000), highlighting their function in L3 control. Interestingly, rIL-33 treatment did not elevate L3 numbers in the tissue of granulocyte-depleted mice any more while wildtype mice displayed elevated L3 numbers upon rIL-33 treatment in the same experiment. Furthermore, intestinal parasite burden was reduced by rIL-33 treatment in the presence and absence of granulocytes to the same extent. Reduced parasite burden was correlated to increased mast cell degranulation suggesting that rIL-33-mediated acceleration of mast cell activation was independent of granulocytes.

Anti-Gr-1 antibody binds to granulocyte surface marker Ly6G and Ly6C targeting not only neutrophils and eosinophils but also monocytes/macrophages and dendritic cells (Daley et al., 2008; Percopo et al., 2017; Watanabe et al., 2000; Wojtasiak et al., 2010). To exclude unintended effects of non-granulocytic cells, specific eosinophil-deficient  $\Delta$ dbIGATA mice were analyzed (Fig. 15).

Eosinophil deficiency elevated the numbers of viable L3 in the tissue and intestinal adults. However, rIL-33 treatment did not further increase L3 numbers in the tissue of eosinophil-deficient mice, while wildtype mice displayed elevated L3 numbers upon rIL-33 treatment in the same experiment. Intestinal adult numbers were reduced by rIL-33 treatment in the presence and absence of eosinophils to the same extent. Reduction of intestinal parasite burden was correlated to mast cell degranulation, indicating that eosinophils are dispensable for the rIL-33-mediated accelerated mast cell activation.

### 3. Results

---

Together, these results show that the absence of granulocytes, specifically eosinophils, abolished the additional rIL-33-mediated increase of L3 numbers in the lung and head, while the mast cell-mediated decrease of adult numbers in the small intestine was unaffected.

### 3. Results

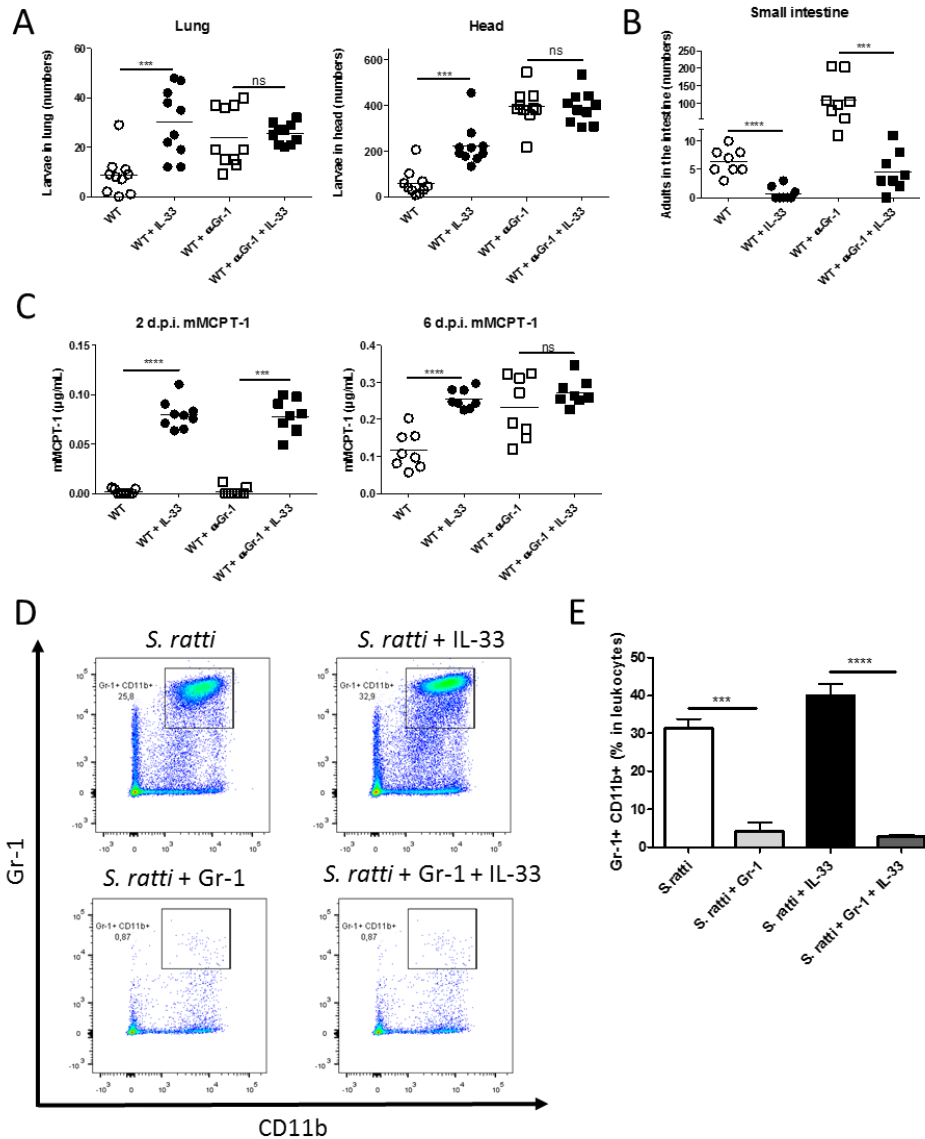


**Figure 14. *S. ratti* parasite burden and mast cell activation in rIL-33 treated, granulocyte depleted mice.**

BALB/c wildtype mice were treated 3 h before and at day 1 p.i. with 1 µg rIL-33 *i.p.* (black symbols (A - C), black respectively dark grey bar (E)) and/or were treated 1 day before infection with 350 µg anti-Gr-1 antibody (clone RB6-8C5) to deplete Gr-1<sup>+</sup> cells (squares (A - C), light grey respectively dark grey bar (E)). Mice were infected with 2000 *S. ratti* L3i by *s.c.* injection into the footpad. (A) Viable *S. ratti* L3 in lung and head at day 2 p.i. and (B) adults in the intestine at day 6 p.i. were counted. (C) Expression levels of mMCPT-1 in sera at day 2 and 6 p.i. were analyzed by ELISA. (D and E) Depletion of Gr-1<sup>+</sup> cells was confirmed by flow cytometry. Representative dot plots showing CD11b/Gr-1 expression of cells in blood samples at day 1 p.i. Graphs show mean of combined results derived out of 2 experiments with 4 - 5 mice (A and C left), 4 mice (B and C right) and 3 - 5 mice (D) per group and experiment, each symbol represents an individual mouse. Statistical analysis was performed by Student's t-test or Mann-Whitney U test. Asterisks indicate significant differences between the groups (\*\*\*)  $p < 0.001$ , \*\*\*\*  $p < 0.0001$ , ns=not significant).

### 3. Results

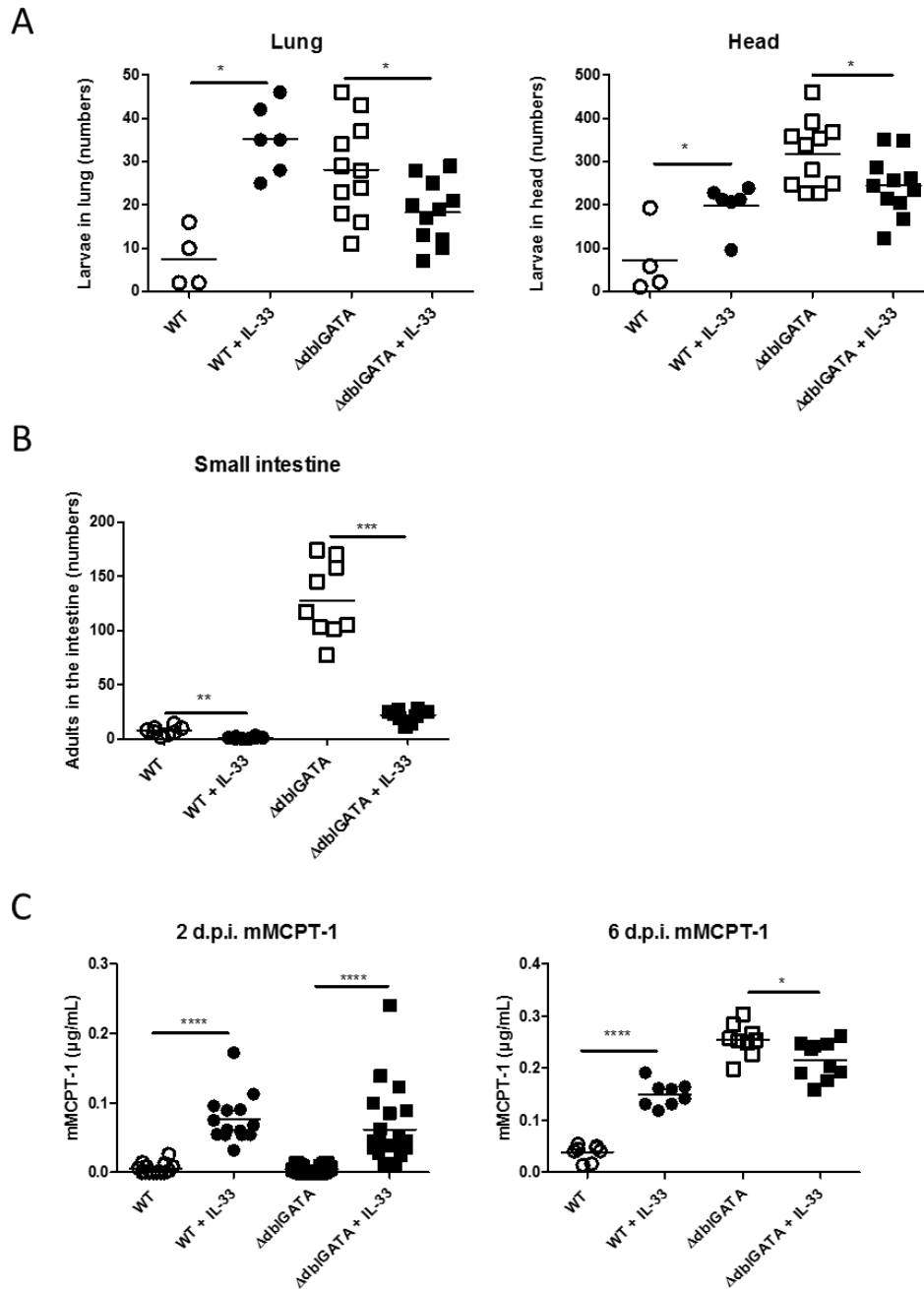


**Figure 15. *S. ratti* parasite burden and mast cell activation in rIL-33 treated eosinophil-deficient mice.**

BALB/c wildtype (circles) and eosinophil-deficient  $\Delta$ dblGATA mice (squares) were treated 3 h before and at day 1 p.i. with 1  $\mu$ g rIL-33 (black symbols) or PBS *i.p.* (open symbols). Mice were infected with 2000 *S. ratti* L3i by *s.c.* injection into the footpad. (A) Viable *S. ratti* L3 in lung and head at day 2 p.i. and (B) adults in the intestine at day 6 p.i. were counted. (C) Expression levels of mMCPT-1 in sera at day 2 and 6 p.i. were analyzed by ELISA. Graphs show mean of combined results derived out of 2 experiments with 2 - 6 mice (A and C left) and 4 - 5 mice (B and C right) per group and experiment, each symbol represents an individual mouse. Statistical analysis was performed by Student's t-test or Mann-Whitney U test. Asterisks indicate significant differences between the groups (\*\*  $p < 0.01$ , \*\*\*  $p < 0.001$ , ns=not significant).

#### **3.10 Lung mRNA expression in rIL-33 treated mice during *S. rattii* infection**

IL-33 is a potent inducer of type 2 immune responses by driving naïve T cells into a Th2 phenotype that secrete IL-5 and IL-13 (Rank et al., 2009). IL-33 can activate a wide range of innate immune cells, e.g. macrophages respond to IL-33 by polarization into an alternative activated phenotype (Kurowska-Stolarska et al., 2009). To further address the question how rIL-33 modulates the local immune response, RNA was prepared from lung tissue. mRNA expression of Arginase-1 (Arg-1), inducible nitric oxide synthase (iNOS), mMCPT-1 and IL-13 was quantified by qPCR at day 2 and 4 p.i. in the lung (Fig. 16).

rIL-33 treatment increased the transcription of Arg-1 mRNA, a marker for alternative activated macrophages, in the lung at day 2 and day 4 p.i. In contrast, iNOS mRNA, a marker for classically activated macrophages, was unchanged by rIL-33 treatment compared to PBS treated mice. Thus, rIL-33 treatment promoted the early type 2 polarization of macrophages. Also, the transcription of mMCPT-1 and the canonical Th2 cytokine IL-13 mRNA was increased by rIL-33 treatment at day 4 p.i.

Taken together, these results show that rIL-33 treatment mediated the initiation of a type 2 immune response in the lung.

### 3. Results

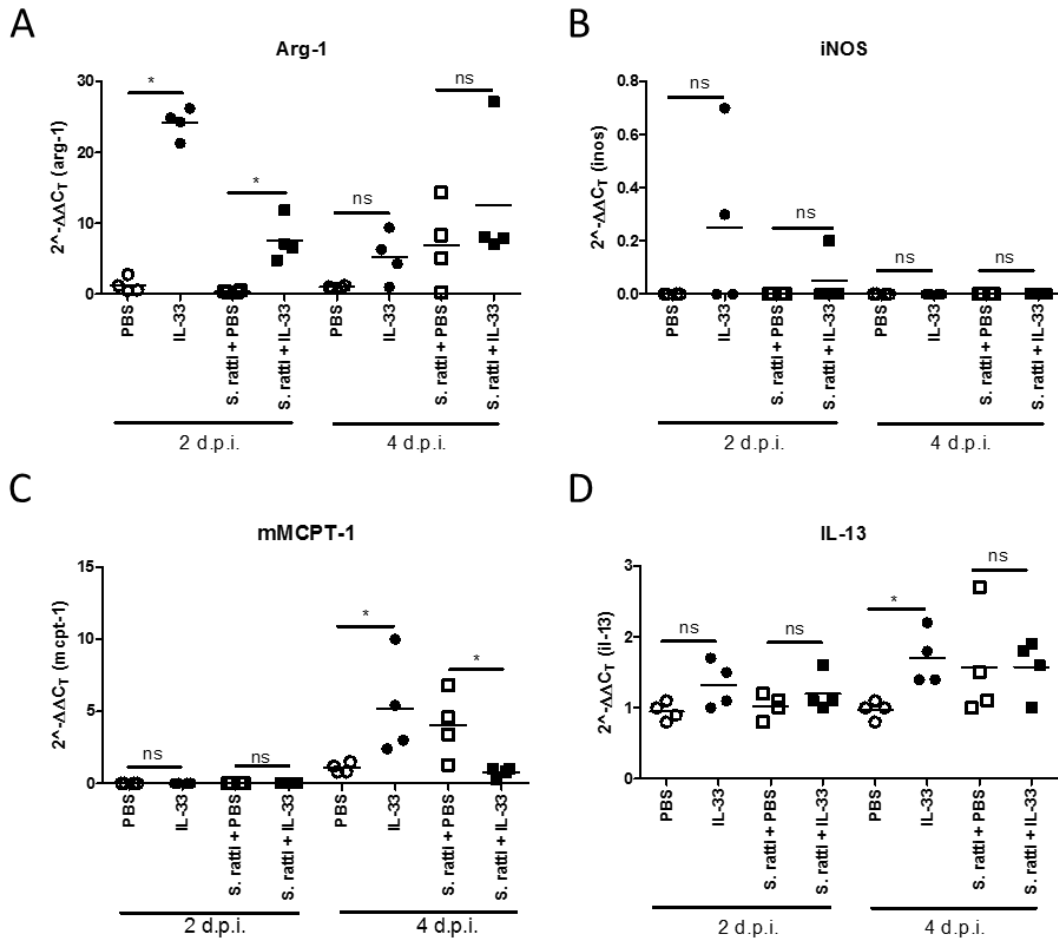


**Figure 16. Lung mRNA expression in rIL-33 treated mice during *S. rattii* infection.**

BALB/c mice were infected with 2000 *S. rattii* L3i by *s.c.* injection into the footpad and treated 3 h before and at day 1 p.i. with 1  $\mu$ g rIL-33 (black squares) or PBS (open squares) *i.p.* Uninfected control mice were treated with rIL-33 (black circles) or PBS (open circles). RNA was isolated from the lung. Relative expression of (A) Arg-1, (B) iNOS, (C) mMCP-1 and (D) IL-13 mRNA was quantified by qPCR and calculated using comparative Ct method. Results are shown as  $2^{-\Delta\Delta C_T}$  using expression of GAPDH as internal control and naïve PBS treated mice as reference group. Graph shows mean of 1 experiment with 4 mice per group and time point, each symbol represents an individual mouse. Statistical analysis was performed by Mann-Whitney U test. Asterisks indicate significant differences between the groups (\*  $p < 0.05$ , ns=not significant).



### 4. Discussion

#### 4.1 Migration of *S. ratti*

In this study, the migration route of the parasitic nematode *S. ratti* within the murine host was investigated in detail. During a *S. ratti* infection, the elicited anti-*S. ratti* immune response attacks migrating L3 in the tissue, limiting the numbers of parasites that reach the small intestine. The first aim of this study was to define the fate and tissue localization of killed L3 during a primary and secondary infection in mice.

The migration of *S. ratti* was investigated in this study by counting viable L3 that emigrated out of the different tissue after incubation in water. A disadvantage of this method is that only viable L3 migrate out of the tissue and dead L3 might remain in it. Therefore, quantification of *S. ratti*-derived DNA with qPCR was performed. This includes the detection of dead and viable parasite DNA at the same time. Combining these two methods a comprehensive picture emerges about where killing of L3 occurs during the migration phase.

*S. ratti* L3 rapidly migrated from the foot, which was the site of infection, through the leg to the lung and head subsequently reaching the small intestine during a primary infection. As no parasites were found in other tissues like the kidney or the tongue, a random migration of *S. ratti* through the host is unlikely. The collected data further suggest that the site of L3 killing is the foot and leg-derived tissues but not the lung or head in a primary infection. This assumption is supported by a decline of *S. ratti*-derived DNA together with viable L3 numbers at the same time in lung and head. In contrast, *S. ratti*-derived DNA was still increased in foot and leg-derived tissues, when viable L3 had already left the tissue. Most L3 were retained in the foot during a secondary infection, thus indicating that L3 killing occurred directly at the site of reinfection.

Low concentrations of *S. ratti*-derived DNA was detectable prior to viable L3 in the lung. This might be explained by the rapid transport of *S. ratti*-derived fragments from the footpad via the blood to the lungs during the infection process.

These findings extend several previous studies in mice and rats that were performed decades ago to investigate the migration of *S. ratti*. Migration routes of *S. ratti* were in that time mostly investigated by classical recovery of L3 from the tissue i.e., incubation of

tissue samples in water or by tissue homogenization and subsequent parasite microscopically counting or by tissue histology. Data was obtained without the use of more sensitive molecular biological techniques such as the quantification of parasite DNA within tissue samples. The advantage of molecular methods nowadays gives the possibility to reevaluate and extend previous findings.

Previous described migration routes of *S. ratti* in mice and rats resembled in general the findings of this thesis regarding migration kinetics and parasite tissue occurrence.

In 1981, Dawkins et al. demonstrated by counting parasite numbers in minced and homogenized tissue samples that *S. ratti* L3 rapidly migrated out of the infected skin during the first 24 h after infection of mice (Dawkins and Grove, 1981a). This confirms the finding of this thesis that *S. ratti* L3 rapidly emigrated out of the site of infection, the footpad, after infection. Another study by Dawkins et al. one year later reported that *S. ratti* larval migration through skin and subcutaneous tissue was not observed in mice. Instead, L3 were found in muscle tissue and cerebrospinal fluid 1 - 2 days after infection. A few L3 were found in blood, liver, spleen, kidney and brain. It was suggested that *S. ratti* L3 migrated via muscles to reach the lungs in mice (Dawkins et al., 1982b). By contrast, data obtained in this study suggest that *S. ratti* L3 indeed migrated partially via the skin, but they were not present in the kidney. However, studies are consistent about *S. ratti* L3 migration through muscle tissue. Abadie recovered L3 from blood and lung tissue 9 – 12 h after infection in rats (Abadie, 1963). Data of this study show the presence of a few viable L3 in the lung prior maximal arrival at day 2 p.i., however L3 presence in blood was not observed (data not shown) and well perfused organs such as kidney or liver were negative for L3 and *S. ratti*-derived DNA. Dawkins et al. reported that *S. ratti* L3 were detected from day 1 - 3 after the infection in the lung and head with maximal numbers at day 2 after infection in mice (Dawkins and Grove, 1981a; Dawkins et al., 1982b), which is in close correlation to the results of this study. Comparing the data of this thesis with previous studies, it is likely that *S. ratti* L3 migrates to the head before passing on to the intestine. Arrival of L3 in the intestine was recorded from day 2 after infection onwards. L3 developed to female adults by day 5 after infection in mice (Dawkins and Grove, 1981a; Dawkins et al., 1982b). In line with that, data of this study show first L3 arrived in the small intestine at day 2 p.i. and parasitic adults have developed at day 6 p.i.

Thus, overall migration kinetics of *S. ratti* in mice during the course of infection are comparable between older studies and this thesis. However, some migration phases remain unclear, for instance the route from the head region to the intestine or whether L3 migrate via the bloodstream.

In line with older studies (Dawkins and Grove, 1981a), it was shown in this thesis that the parasite burden during a secondary *S. ratti* infection was drastically decreased. Once a host experiences a helminth infection, a protective immune responses against reinfections is established. However, the site where this acquired protection is executed remains poorly understood. This thesis clearly shows that most *S. ratti* L3 were retained in the foot during a secondary infection, suggesting that improved L3 killing during adaptive immune response was executed directly at the site of reinfection. Consistent with this finding, a study from Obata-Ninomiya et al. showed that infecting *N. brasiliensis* L3 were retained in the skin of mice during reinfection. L3 were surrounded by skin infiltrating cells that prevented migration out of the site of infection. Thereby, confirming the data of this thesis, L3 were retained at the site of infection specifically in the secondary but not in the primary infection, indicating improved host resistance in the tissue by acquired immunity (Obata-Ninomiya et al., 2013).

### **4.2 The impact of IL-33 on *S. ratti* infection**

The second aim of this study was to define the role of the tissue-derived alarmin IL-33 during the immune response against *S. ratti* parasites in the tissue and small intestine. In light of the established role of IL-33 as enhancer of type 2 immune responses (Oboki et al., 2010) it was expected that rIL-33 treatment would improve parasite killing already during the tissue migration. Surprisingly, treatment with rIL-33 elevated the numbers of viable *S. ratti* L3 in leg-derived skin and muscle tissue, lung and head. Viable L3 arrived with same time kinetics in all investigated tissues, thereby ruling out that rIL-33 treatment increased L3 migration mobility. *S. ratti*-derived DNA was increased in leg-derived tissues of untreated mice, indicating that dead L3 remained in these tissues. In contrast, the killing of L3 in leg-derived tissues of rIL-33 treated mice was impaired, indicated by a reduction of *S. ratti*-derived DNA. This suggests that L3 migrated easily through the tissue to the intestine upon rIL-33 treatment and tissue parasite control in rIL-33 treated mice is diminished.

Despite this rIL-33-mediated interference with L3 control in the tissue, analysis of the parasite burden in the small intestine showed that rIL33 treatment resulted in a decrease of L4 and parasitic adults numbers. rIL-33 treatment accelerated *S. ratti* expulsion from the intestine indicated by increased *S. ratti*-derived DNA at early time points in feces and promoted mast cell activation, indicated by increased mMCPT-1 concentrations at early time points in the sera.

Thus, rIL-33 treatment improved overall infection outcome compared to untreated infected mice.

Interestingly, it should be noted that rIL-33 treatment in mast cell-deficient and IL-9R-deficient mice revealed different results for the parasite burden in lung and head. rIL-33 treatment mediated the additional increase of L3 numbers in the head but not in the lung tissue. As the rIL-33-mediated changes in parasite burden were also absent in the small intestine in these mice, lung tissue seemed to behave more like the mucosal tissue of the small intestine. Lung tissue might be more attributed to tissue with mucosal characteristics, while head tissue might be more attributed to common muscle tissue.

In the following sections it will be discussed how rIL-33 may facilitate the L3 migration through the tissue to the intestine by downregulation of immune responses to L3 in the tissue and how rIL-33 may improve anti-*S. ratti* immunity in the small intestine leading to fast clearance from the host by activated mast cells.

### **4.3 The impact of IL-33 on *S. ratti* infection in the small intestine**

This study clearly shows that rIL-33 treatment accelerated clearance of *S. ratti* from the small intestine dependent on the presence of mast cells and functional IL-9R signaling. In contrast, basophils and granulocytes were dispensable for the rIL-33-mediated reduction of adult numbers in the small intestine.

Efficient parasite expulsion from the intestine of rIL-33 treated mice was correlated with increased mast cell degranulation. Absence of IL-9R in rIL-33 treated mice impaired not only the improved expulsion of *S. ratti* from the intestine but also abrogated mast cell degranulation. Therefore, it is hypothesized that rIL-33 activates mucosal mast cells via IL-9.

As mucosal mast cells are a target of IL-9 (Townsend et al., 2000a) and mediate intestinal expulsion of *S. ratti* (Reitz et al., 2017), Reitz et al. suggested that IL-9 is an important cytokine for mucosal mast cell activation (Reitz et al., 2018), confirming the results of this thesis. A possible cellular source for IL-9 are ILC2 (Rauber et al., 2017; Wilhelm et al., 2011) which are activated by IL-33 to produce type 2 cytokines (Xu et al., 2017), including IL-9 (Mohapatra et al., 2016). Another possible source of IL-9 are Th9 cells that have been reported to facilitate parasite expulsion from the intestine during *N. brasiliensis* infection (Licona-Limon et al., 2013).

Mucosal mast cell-deficient mice displayed higher intestinal parasite burden and failed to timely terminate *S. ratti* infection (Reitz et al., 2017). Also, IL-9R-deficient mice displayed an increased intestinal parasite burden (Reitz et al., 2018). Investigating bone-marrow chimeras, it was shown that early expulsion of *S. ratti* from the intestine depended on IL-9R-mediated signaling on hematopoietic cells, ruling out any direct effects of IL-9 on intestinal epithelial or smooth muscle cells during infection (Reitz et al., 2018). Increased parasite burden in IL-9R-deficient mice was accompanied by decreased mast cell degranulation and impaired intestinal IL-13 expression, suggesting that IL-9 mediated mast cell activation and promoted Th2 polarization in the wildtype situation. Consistent with these findings, neutralization of endogenous IL-9 increased the number of parasitic adults in the intestine in the context of decreased mast cell degranulation (Blankenhaus et al., 2014). These cited studies confirm the results of this thesis that IL-9 is crucial for the activation of mast cells that in turn contributes to the clearance of *S. ratti* from the intestine.

Mast cells were also important for intestinal immunity against another gastrointestinal helminth parasite, *H. polygyrus*, as an enhanced parasite expulsion correlated with increased numbers of mast cells (Behnke et al., 1993). Mast cell deficiency resulted in an impaired resistance to *H. polygyrus* and reduced the host capacity to initiate type 2 immune responses (Hepworth et al., 2012). Khan et al. showed that neutralization of IL-9 resulted in less worm expulsion during an infection with *T. muris* (Khan et al., 2003). In addition, IL-9R deficiency delayed worm expulsion indicated by increased egg numbers in the feces and parasitic adults in the intestine during *N. brasiliensis* infection (Turner et al., 2013). However, another study demonstrated that clearance of *N. brasiliensis* in IL-9-

deficient mice was comparable to wildtype mice (Townsend et al., 2000a). These studies show the importance of mast cells and IL-9 for protective immunity against additional other helminths. However, the importance of IL-9 for parasite expulsion might differ between *N. brasiliensis* and *S. ratti*.

In line with the results of this thesis, Yasuda et al., demonstrated in 2012 that IL-33-deficient mice showed an increased fecal egg release during *S. venezuelensis* infection. Administration of exogenous IL-33 into IL-33-deficient mice showed a reciprocal phenotype. The mice demonstrated a decreased fecal egg release again (Yasuda et al., 2012). Furthermore, a role of IL-33 for protective immunity in mice during a primary and secondary infection with *N. brasiliensis* was shown by Hung et al. in 2013. IL-33-deficient mice showed an impaired clearance of *N. brasiliensis*, despite a strong induction of type 2 immunity in terms of IL-4 and IgE induction as well as basophil and mast cells responses. IL-33 was essential for the expansion of ILC2 that produced IL-13. It was concluded that IL-33 promoted *in vivo* production of IL-13 that contributed to parasite expulsion independent of a canonical type 2 immune response (Hung et al., 2013). During an infection with *T. muris*, IL-33 was rapidly produced within the caecum during the initial phase of parasite intestinal arrival. Additionally, the administration of rIL-33 promoted the expulsion of *T. muris* (Humphreys et al., 2008). Another study showed that mice deficient for the receptor of IL-33 failed to initiate a type 2 immune response to form granuloma around *S. mansoni* eggs in the lung (Townsend et al., 2000b). These cited studies are in line with data of this thesis and together they provide evidence that IL-33 contributes to a protective immunity against helminth infections.

This thesis shows that mast cells were activated *in vivo* upon rIL-33 treatment. Interestingly, mast cells respond not only to IL-33 but can also serve as a cellular source of it. Shimokawa et al. demonstrated that also mast cells secreted IL-33 upon ATP-mediated activation. ATP was released by damaged intestinal epithelial cells during the infection with *H. polygyrus*. IL-33 being released by mast cells activated ILC2 to produce IL-13, resulting in increased goblet cells and mucus production for expulsion of *H. polygyrus* (Shimokawa et al., 2017). This might indicate a positive feedback loop of mast cells to intensify the function of IL-33 during helminth infections. It should be noted that the definitive proof that IL-33 from mast cells contributed to *H. polygyrus* resistance was

investigated in mast cell-deficient Kit<sup>W-sh/W-sh</sup> mice. These Kit dependent murine models display immunological defects that extend beyond a mast cell deficiency such as reduced basophils numbers (Grimbaldeston et al., 2005). Therefore, the mast cell phenotype represented by these mice might be misinterpreted (Reber et al., 2012; Rodewald and Feyerabend, 2012) and final proof of mast cell contribution to IL-33 release within kit-independent mouse models for mast cell deficiency remains to be performed. However, also in an *in vitro* model for cell injury, mast cells served as sensor cells of cellular damage through the recognition of extracellular IL-33. Mast cells were activated by IL-33 to initiate a proinflammatory response (Enoksson et al., 2011). Helminth infection goes along with host tissue injury and release of IL-33, suggesting that mast cells contribute to early cell injury responses *in vivo*. IL-33 activates also human mast cells to secrete type 2 cytokines and chemokines including IL-13, IL-5, IL-6, IL-10, TNF, GM-CSF, CXCL8 and CCL1 (Allakhverdi et al., 2007), suggesting a role of IL-33 during helminth infection also in humans.

The collective results of this thesis and the cited studies agree with a proposed model that rIL-33 induces IL-9 production by either Th9 or ILC2 or both cell types. This IL-9 would subsequently mediate mast cell degranulation either directly via IL-9R expression on mast cell or indirectly via other IL-9 responsive cells contributing to the expulsion of *S. ratti* from the intestine. An additional direct activation of mast cells via IL-33R ST2 is conceivable (Wang et al., 2014). However, the fact that rIL-33-treatment did not increase early mast cell activation in IL-9R-deficient mice argues against that notion.

### **4.4 The impact of IL-33 on *S. ratti* in the tissue**

The absence of granulocytes or eosinophils elevated the numbers of viable L3 in the lung and head. Besides the elevation of L3 numbers in the tissue, the numbers of parasitic adults were also increased in the small intestine, which might be a consequence of the impaired immune response to L3 in the tissue and reflect the increased numbers of L3 progressing to the intestine. Treatment with rIL-33 increased the numbers of L3 in the tissue. Furthermore, L3 were less efficiently retained and killed in the tissue of rIL-33 treated mice, indicating a rIL-33-mediated impairment of tissue parasite control and facilitation of L3 migration to the intestine.

The notion that rIL-33 might interfere with proper effector mechanisms attacking L3 in the tissue is in sharp contrast to the established idea of IL-33 promoting type 2 immunity at all sites. Indeed, also in this thesis the rIL-33 treatment increased type 2 polarization in the lungs, indicated by transcription of Th2 cytokines IL-13 and the AAM associated Arg-1. Yasuda et al. specifically proposed that anti-*S. venezuelensis* immunity was efficiently initiated and amplified by IL-33 production in the lung. During *S. venezuelensis* infection, the production and release of the alarmin IL-33 from the nucleus of alveolar epithelial lung cells was triggered (Yasuda et al., 2012). IL-33 triggered the expansion of IL-5 producing ILC2 that in turn induced lung eosinophilia. Treatment with exogenous IL-33 reduced parasite burden in the small intestine recorded as fecal egg release. The authors hypothesized that IL-33 would improve the killing of *S. venezuelensis* L3 in the lung by increased eosinophil numbers and therefore less L3 would reach the small intestine. However, the analysis of L3 burden in the lung was not assessed in that study as only fecal egg release was shown. rIL-33 treatment during *S. rattii* infection, as performed in this thesis, did not reduce the parasite burden in the lung. Contrary to the hypothesis of Yasuda et al. in 2012, increased numbers of L3 in the lung were observed. However, the response to rIL-33 treatment in mediating changes in the tissue parasite burden might be different during *S. rattii* and *S. venezuelensis* infection.

In a wildtype situation, granulocytes are important effector cells against L3 during tissue migration (Allen and Maizels, 2011). In 1995, Abraham et al. showed that neutrophils, eosinophils and macrophages were present in the microenvironment of *S. stercoralis* L3, which were implanted in diffusion chambers into mice (Abraham et al., 1995). Depletion of neutrophils and eosinophils resulted in impaired *S. stercoralis* L3 killing (O'Connell et al., 2011). Infections with *S. rattii* showed that neutrophils, eosinophils and macrophages were found in the skin in response to invading L3 in rodents (Dawkins et al., 1981; McHugh et al., 1989). The depletion of granulocytes by anti-Gr-1 administration resulted in increased *S. rattii* L3 numbers and increased eggs secretion with the feces (Watanabe et al., 2000), confirming the results of this study. Eosinophils are directly recruited to *S. stercoralis* L3 by chitin or proteins, which are released by the L3 (Stein et al., 2009). Mice overexpressing IL-5 have elevated numbers of eosinophils and increased capacity to kill the L3. Reciprocally, mice deficient for IL-5 showed increased larval survival (Herbert et



al., 2000). Eosinophils kill L3 through a mechanism dependent on the release of granular protein major basic protein (MBP) (O'Connell et al., 2011). Besides eosinophils, neutrophils are also efficiently recruited to *S. stercoralis* L3 (Abraham et al., 1995). Recruitment of neutrophils to the L3 is dependent on the chemokine receptor CXCR2 and the protein Gai2. Implantation of *S. stercoralis* L3 in diffusion chamber into mice resulted in neutrophil-mediated killing of L3 (Galioto et al., 2006). Neutrophils kill *S. stercoralis* L3 through a mechanism dependent on the granular protein myeloperoxidase (MPO) (O'Connell et al., 2011).

In line with these reports, granulocyte depletion or absence of eosinophils in this study elevated *S. ratti* L3 numbers in head and lung tissue. However, the additional increase of L3 numbers mediated by rIL-33 treatment in the tissue was abolished by granulocyte depletion or in mice deficient for eosinophils. Therefore, it is conceivable that rIL-33 treatment interfered with granulocyte effector functions that mediated killing and control of tissue migrating L3 in the wildtype situation. In the absence of granulocytes, this putative rIL-33-mediated interference with L3 killing would be irrelevant and L3 numbers would not be increased any further. However, it is not possible to rule out that numbers of L3 in the tissue during absence of granulocytes are already increased to a maximal parasite burden *in vivo* and an additional increase of this parasite burden is simply not achievable.

IL-33 can mobilize neutrophils as intraperitoneal administration of IL-33 *in vivo* resulted in a rapid recruitment of neutrophils to the peritoneum, dependent on IL-33 receptor expressing peritoneal mast cells (Enoksson et al., 2013). As neutrophils are also activated by rIL-33 administration (Le et al., 2012; Yazdani et al., 2017), it is possible that rIL-33 treatment in this study resulted in hyperactivation and thus depletion of the short-lived neutrophil repertoire before the infection, thereby indirectly increasing L3 burden in the tissue. However, Gr-1<sup>+</sup> cells, including neutrophils, were increased in blood samples of rIL-33 treated *S. ratti* infected mice as controlled during granulocyte depletion experiments at day 1 p.i., thus arguing against a simple activation induced depletion of neutrophils during the relevant time of tissue migration at day 1 - 3 p.i. in rIL-33 treated mice.

The analysis of the local immune response in the lung upon rIL-33 treatment in this thesis showed an increase of Arg-1 mRNA transcription. Arg-1 is a marker for AAM and suppresses inflammatory pathways by inhibiting iNOS (Allen and Sutherland, 2014).

Consequently, the transcription of iNOS, a marker for classically activated macrophages was not increased, while type 2 associated cytokine IL-13 and protease mMCP-1 mRNAs were elevated upon rIL-33 treatment in the lung. Thus, rIL-33 treatment polarized the immune response towards a type 2 phenotype. Helminth infections are normally cleared by a canonical type 2 immune response. However, it is conceivable that rIL-33-induced type 2 immune response downregulated effector functions of granulocytes, which are also needed for parasite tissue control in wildtype mice, during *S. rattii* infection.

The literature provides evidence that IL-33 can interfere with immune responses by induction of regulatory immune cells. IL-33 was shown to induce immunosuppressive neutrophils via an ILC2/IL-13/STAT6 axis in viral hepatitis (Liang et al., 2018). IL-33 promoted the expression of Arg-1 in neutrophils via ILC2-derived IL-13. These Arg-1 expressing neutrophils were able to inhibit CD8<sup>+</sup> T cell responses, thereby diminishing immunopathology in the liver during hepatitis (Liang et al., 2018). Unfortunately, the cellular source expressing Arg-1 mRNA was not determined in this study as complete lung tissue homogenates were used for cDNA preparation. Additionally, IL-33 was shown to expand myeloid-derived suppressor cells (MDSCs) and Foxp3<sup>+</sup> regulatory T cells (Gajardo et al., 2015; Turnquist et al., 2011), both cell types with immunosuppressive capacities.

In contrast, other studies showed that IL-33 established a pro inflammatory immune response by enhancing neutrophil functions. Treatment with IL-33 protected mice during a model for sepsis that was introduced to mice by cecal ligation and puncture procedure. rIL-33 treated mice showed increased neutrophil influx into the peritoneal cavity and more efficient bacterial clearance than untreated mice (Alves-Filho et al., 2010). In another study, IL-33 was released by sinusoidal endothelial cells in a model of liver ischemia and reperfusion. Released IL-33 activated neutrophils to form neutrophil extracellular traps, which exacerbates liver inflammation and damage (Yazdani et al., 2017). Another interesting study indicated that IL-33 recruited neutrophils to the skin in a model for skin autoimmune disease, enhancing inflammatory responses. Neutrophil recruitment was dependent on chemokine CXCL1 (Hueber et al., 2011).

Nevertheless, it should be noted that little is known about the role of IL-33/ST2 signaling in neutrophils. Although IL-33 induces activation and recruitment of neutrophils, it is still

controversial whether neutrophils express ST2 (Alves-Filho et al., 2010; Cherry et al., 2008; Verri et al., 2010; Yazdani et al., 2017). Evaluating the cited studies, it seems that IL-33 has a functional impact on neutrophil recruitment and activation. However, in comparison to the results of this thesis, IL-33 might act differently on neutrophils dependent on the disease context. It is conceivable that rIL-33 treatment induces an immunosuppressive phenotype of neutrophils and eosinophils during *S. ratti* infection, thereby contributing to impaired larval killing during the migrations phase. Another possibility is that rIL-33 treatment indirectly inhibits granulocyte effector functions by establishing an immunosuppressive environment, downregulating the immune response to *S. ratti* L3 in the tissue. The exact molecular mechanism of rIL-33-mediated interference with effective killing of L3 will be the topic of future investigations.

### 5. Outlook

#### 5.1 The impact of IL-33 on *S. ratti* infection

Treatment with rIL-33 induced an elevation of *S. ratti* L3 numbers in the tissue during this thesis. This result is in contrast the proposed hypothesis by Yasuda et al., that IL-33 might improve tissue parasite killing by eosinophilia in the lung during *S. venezuelensis* infection. Therefore, it would be interesting to repeat the key experiment of this thesis comparing *S. venezuelensis* and *S. ratti*. Further, it would be interesting to investigate whether rIL-33 treatment induces changes in the tissue parasite burden also in additional nematode infections models that display a tissue migrating phase such as *N. brasiliensis*. This would embed the results of this study in a broader context to understand whether the observed rIL-33-mediated increase of L3 tissue burden would be a *S. ratti*-specific feature or reflect a general function of IL-33 during nematode infections in the tissue.

As discussed above, IL-33 can induce polarization of neutrophils towards an immunosuppressive phenotype (Liang et al., 2018). Therefore, it would be interesting to analyze whether rIL-33 treatment inhibited neutrophil and also eosinophil effector functions by inducing an immunosuppressive phenotype during a *S. ratti* infection. Future experiments could test this by recording the impact of rIL-33 on *in vitro* stimulations of neutrophils and eosinophils using effector functions such as the release of MPO for neutrophils or MBP for eosinophils as readout. Likewise, the impact of rIL-33 stimulation on neutrophil- and eosinophil-mediated killing of *S. ratti* L3 can be studied *in vitro*. In addition, the impact of rIL-33 treatment on the local immune response in leg-derived skin and muscle tissue during infection should be analyzed by quantification of mRNA transcription by qPCR.

Interestingly, the gastrointestinal helminth *H. polygyrus* secretes products that interfere with IL-33 function. In 2017, Osbourn et al. identified an IL-33-suppressive protein, named *H. polygyrus* Alarmin Release Inhibitor (HpARI) (Osbourn et al., 2017). *In vivo* administration of HpARI resulted in binding of IL-33 and abrogation of IL-33 signaling. HpARI impaired type 2 immune responses during allergen challenge by suppressing allergic airway inflammation. Furthermore, HpARI administration suppressed eosinophil-mediated immune response to *N. brasiliensis* infection impairing parasite clearance from the intestine. (Osbourn et al., 2017). Future experiments should address the question

whether *S. ratti* also excretes/secretates products that actively suppress IL-33 activity *in vivo*, as this would prolong parasite survival in the host.

The results of this study show that mast cells and IL-9R are essential for the rIL-33-mediated decrease of parasitic adults in the small intestine. Therefore, it is assumed that rIL-33 treatment activates mast cells via IL-9 to expel the worm from the intestine. IL-9 might be delivered by activated ILC2 upon rIL-33 treatment. Other putative sources of IL-9 are Th9 cells (Licona-Limon et al., 2017) regulatory T cells (Eller et al., 2011) and mast cells (Chen et al., 2015). Future experiments should identify the cellular source of IL-9 in response to rIL-33 treatment during *S. ratti* infection. For instance, the production of IL-9 by ILC2 or other cells might be investigated with flow cytometric analyses of cell suspensions derived from IL-9 fate reporter mice. A study using IL-9 fate reporter mice demonstrated that IL-9 during papain-induced lung inflammation was predominately produced by ILCs (Wilhelm et al., 2011).

This study demonstrates that treatment with rIL-33 improved the parasite clearance from the intestine. Therefore, it might be interesting to examine whether other epithelium-derived alarmins such as IL-25 or TSLP have also a protective role during *S. ratti* infection. IL-25- and TSLP-deficient mice could be infected with *S. ratti* and analyzed whether these alarmins play a role in anti-*S. ratti* immunity. Additionally, recombinant IL-25 or TSLP might be administrated during the infection to investigate whether this would mirror the results of this study. To evaluate the results of this study more precisely, analysis of *S. ratti* infected IL-33 receptor-deficient mice or neutralization of endogenous IL-33 by inhibitors would be interesting.

### **5.2 Migration of *S. ratti***

Within this thesis, the migration of *S. ratti* L3 was monitored by counting viable L3 and measuring *S. ratti*-derived DNA. It should be noted that attempts failed to investigate the migration in more detail by histology. It turned out that a detection of L3 in the tissues was infrequent and time consuming, and it was difficult to get additional information out of these experiments. Another attempt to follow *in vivo* migration of *S. ratti* L3 with Magnetic Resonance Imaging (MRI) failed as well. It was not possible to observe *in vivo* migration after infecting mice with iron beads-labeled viable L3.

In future experiments, other labeling methods of L3 should be examined to analyze *in vivo* migration of *S. ratti* in more detail, as this might confirm and extend the results of this study. A possible approach might be the labeling of *S. ratti* L3 with fluorescent agents that allow tracing of the fluorescent dye *in vivo* as it was shown for *Schistosoma* spp. (Krautz-Peterson et al., 2009). Other approaches described the infection of mice with transgenic protozoan parasites like *Toxoplasma gondii* or *Plasmodium* spp. expressing for instance the firefly luciferase. Next, mice were injected with a specific substrate that interacted with luciferase to generate bioluminescent parasites which can be detected by special *in vivo* imaging camera (Franke-Fayard et al., 2006; Saeij et al., 2005). Another recent study in 2018, described a new method to analyze intact transparent mice with a whole-mouse immunolabeling technology. With this method it is possible to visualize complex biological systems in the body such as the neuronal connectivity or subcellular details or even single cells in deeper tissue through enhancing fluorescent proteins (Cai et al., 2018). It would be interesting to target L3 with antibodies conjugated to these fluorescent proteins, inject them into mice and follow the migration via this new whole-body imaging method to extend previous findings about the migration processes of *S. ratti*.

## List of references

- Abadie, S.H. (1963). The life cycle of *Strongyloides ratti*. *J. Parasitol.* *49*, 241-248.
- Abraham, D., Rotman, H.L., Haberstroh, H.F., Yutanawiboonchai, W., Brigandi, R.A., Leon, O., Nolan, T.J., and Schad, G.A. (1995). *Strongyloides stercoralis*: protective immunity to third-stage larvae in BALB/cByJ mice. *Exp. Parasitol.* *80*, 297-307.
- Allakhverdi, Z., Smith, D.E., Comeau, M.R., and Delespesse, G. (2007). Cutting edge: The ST2 ligand IL-33 potently activates and drives maturation of human mast cells. *J. Immunol.* *179*, 2051-2054.
- Allen, J.E., and Maizels, R.M. (2011). Diversity and dialogue in immunity to helminths. *Nat. Rev. Immunol.* *11*, 375-388.
- Allen, J.E., and Sutherland, T.E. (2014). Host protective roles of type 2 immunity: parasite killing and tissue repair, flip sides of the same coin. *Semin. Immunol.* *26*, 329-340.
- Alves-Filho, J.C., Sonogo, F., Souto, F.O., Freitas, A., Verri, W.A., Jr., Auxiliadora-Martins, M., Basile-Filho, A., McKenzie, A.N., Xu, D., Cunha, F.Q., *et al.* (2010). Interleukin-33 attenuates sepsis by enhancing neutrophil influx to the site of infection. *Nat. Med.* *16*, 708-712.
- Arya, M., Shergill, I.S., Williamson, M., Gommersall, L., Arya, N., and Patel, H.R. (2005). Basic principles of real-time quantitative PCR. *Expert Rev. Mol. Diagn.* *5*, 209-219.
- Bækkevold, E.S., Roussigne, M., Yamanaka, T., Johansen, F.E., Jahnsen, F.L., Amalric, F., Brandtzaeg, P., Erard, M., Haraldsen, G., and Girard, J.P. (2003). Molecular characterization of NF-HEV, a nuclear factor preferentially expressed in human high endothelial venules. *Am. J. Pathol.* *163*, 69-79.
- Behnke, J.M., Wahid, F.N., Grecis, R.K., Else, K.J., Ben-Smith, A.W., and Goyal, P.K. (1993). Immunological relationships during primary infection with *Heligmosomoides polygyrus* (*Nematospiroides dubius*): downregulation of specific cytokine secretion (IL-9 and IL-10) correlates with poor mastocytosis and chronic survival of adult worms. *Parasite Immunol.* *15*, 415-421.
- Blankenhaus, B., Reitz, M., Brenz, Y., Eschbach, M.L., Hartmann, W., Haben, I., Sparwasser, T., Huehn, J., Kuhl, A., Feyerabend, T.B., *et al.* (2014). Foxp3(+) regulatory T cells delay expulsion of intestinal nematodes by suppression of IL-9-driven mast cell activation in BALB/c but not in C57BL/6 mice. *PLoS Pathog.* *10*, e1003913.
- Bonne-Annee, S., Kerepesi, L.A., Hess, J.A., O'Connell, A.E., Lok, J.B., Nolan, T.J., and Abraham, D. (2013). Human and mouse macrophages collaborate with neutrophils to kill larval *Strongyloides stercoralis*. *Infect. Immun.* *81*, 3346-3355.
- Bonne-Annee, S., Kerepesi, L.A., Hess, J.A., Wesolowski, J., Paumet, F., Lok, J.B., Nolan, T.J., and Abraham, D. (2014). Extracellular traps are associated with human and mouse neutrophil and macrophage mediated killing of larval *Strongyloides stercoralis*. *Microbes Infect* *16*, 502-511.

- Breloer, M., and Abraham, D. (2017). Strongyloides infection in rodents: immune response and immune regulation. *Parasitology* 144, 295-315.
- Breloer, M., Hartmann, W., Blankenhaus, B., Eschbach, M.L., Pfeffer, K., and Jacobs, T. (2015). Cutting Edge: the BTLA-HVEM regulatory pathway interferes with protective immunity to intestinal Helminth infection. *J. Immunol.* 194, 1413-1416.
- Brown, M., and Wittwer, C. (2000). Flow cytometry: principles and clinical applications in hematology. *Clin. Chem.* 46, 1221-1229.
- Cai, R., Pan, C., Ghasemigharagoz, A., Todorov, M.I., Foerster, B., Zhao, S., Bhatia, H.S., Mrowka, L., Theodorou, D., Rempfler, M., *et al.* (2018). Panoptic vDISCO imaging reveals neuronal connectivity, remote trauma effects and meningeal vessels in intact transparent mice. *bioRxiv*.
- Carriere, V., Roussel, L., Ortega, N., Lacorre, D.A., Americh, L., Aguilar, L., Bouche, G., and Girard, J.P. (2007). IL-33, the IL-1-like cytokine ligand for ST2 receptor, is a chromatin-associated nuclear factor in vivo. *Proc. Natl. Acad. Sci. U. S. A.* 104, 282-287.
- Cayrol, C., and Girard, J.P. (2009). The IL-1-like cytokine IL-33 is inactivated after maturation by caspase-1. *Proc. Natl. Acad. Sci. U. S. A.* 106, 9021-9026.
- Cayrol, C., and Girard, J.P. (2014). IL-33: an alarmin cytokine with crucial roles in innate immunity, inflammation and allergy. *Curr. Opin. Immunol.* 31, 31-37.
- Cayrol, C., and Girard, J.P. (2018). Interleukin-33 (IL-33): A nuclear cytokine from the IL-1 family. *Immunol. Rev.* 281, 154-168.
- Chackerian, A.A., Oldham, E.R., Murphy, E.E., Schmitz, J., Pflanz, S., and Kastelein, R.A. (2007). IL-1 receptor accessory protein and ST2 comprise the IL-33 receptor complex. *J. Immunol.* 179, 2551-2555.
- Chen, C.Y., Lee, J.B., Liu, B., Ohta, S., Wang, P.Y., Kartashov, A.V., Mugge, L., Abonia, J.P., Barski, A., Izuhara, K., *et al.* (2015). Induction of Interleukin-9-Producing Mucosal Mast Cells Promotes Susceptibility to IgE-Mediated Experimental Food Allergy. *Immunity* 43, 788-802.
- Cherry, W.B., Yoon, J., Bartemes, K.R., Iijima, K., and Kita, H. (2008). A novel IL-1 family cytokine, IL-33, potently activates human eosinophils. *J. Allergy Clin. Immunol.* 121, 1484-1490.
- Daley, J.M., Thomay, A.A., Connolly, M.D., Reichner, J.S., and Albina, J.E. (2008). Use of Ly6G-specific monoclonal antibody to deplete neutrophils in mice. *J. Leukoc. Biol.* 83, 64-70.
- Dawkins, H.J., and Grove, D.I. (1981a). Kinetics of primary and secondary infections with *Strongyloides ratti* in mice. *Int. J. Parasitol.* 11, 89-96.
- Dawkins, H.J., and Grove, D.I. (1981b). Transfer by serum and cells of resistance to infection with *Strongyloides ratti* in mice. *Immunology* 43, 317-322.



- Dawkins, H.J., Grove, D.I., Dunsmore, J.D., and Mitchell, G.F. (1980). Strongyloides ratti: susceptibility to infection and resistance to reinfection in inbred strains of mice as assessed by excretion of larvae. *Int. J. Parasitol.* *10*, 125-129.
- Dawkins, H.J., Mitchell, G.F., and Grove, D.I. (1982a). Strongyloides ratti infections in congenitally hypothyroid (nude) mice. *Aust. J. Exp. Biol. Med. Sci.* *60*, 181-186.
- Dawkins, H.J., Muir, G.M., and Grove, D.I. (1981). Histopathological appearances in primary and secondary infections with Strongyloides ratti in mice. *Int. J. Parasitol.* *11*, 97-103.
- Dawkins, H.J., Robertson, T.A., Papadimitriou, J.M., and Grove, D.I. (1983). Light and electron microscopical studies of the location of Strongyloides ratti in the mouse intestine. *Z. Parasitenkd.* *69*, 357-370.
- Dawkins, H.J., Thomason, H.J., and Grove, D.I. (1982b). The occurrence of Strongyloides ratti in the tissues of mice after percutaneous infection. *J. Helminthol.* *56*, 45-50.
- Dogan, C., Gayaf, M., Ozsoz, A., Sahin, B., Aksel, N., Karasu, I., Aydogdu, Z., and Turgay, N. (2014). Pulmonary Strongyloides stercoralis infection. *Respir Med Case Rep* *11*, 12-15.
- El-Malky, M.A., Maruyama, H., Al-Harhi, S.A., El-Beshbishi, S.N., and Ohta, N. (2013). The role of B-cells in immunity against adult Strongyloides venezuelensis. *Parasites & vectors* *6*, 148.
- Eller, K., Wolf, D., Huber, J.M., Metz, M., Mayer, G., McKenzie, A.N., Maurer, M., Rosenkranz, A.R., and Wolf, A.M. (2011). IL-9 production by regulatory T cells recruits mast cells that are essential for regulatory T cell-induced immune suppression. *J. Immunol.* *186*, 83-91.
- Enoksson, M., Lyberg, K., Moller-Westerberg, C., Fallon, P.G., Nilsson, G., and Lunderius-Andersson, C. (2011). Mast cells as sensors of cell injury through IL-33 recognition. *J. Immunol.* *186*, 2523-2528.
- Enoksson, M., Moller-Westerberg, C., Wicher, G., Fallon, P.G., Forsberg-Nilsson, K., Lunderius-Andersson, C., and Nilsson, G. (2013). Intraperitoneal influx of neutrophils in response to IL-33 is mast cell-dependent. *Blood* *121*, 530-536.
- Eschbach, M.L., Klemm, U., Kolbaum, J., Blankenhaus, B., Brattig, N., and Breloer, M. (2010). Strongyloides ratti infection induces transient nematode-specific Th2 response and reciprocal suppression of IFN-gamma production in mice. *Parasite Immunol.* *32*, 370-383.
- Everts, B., Perona-Wright, G., Smits, H.H., Hokke, C.H., van der Ham, A.J., Fitzsimmons, C.M., Doenhoff, M.J., van der Bosch, J., Mohrs, K., Haas, H., *et al.* (2009). Omega-1, a glycoprotein secreted by Schistosoma mansoni eggs, drives Th2 responses. *J. Exp. Med.* *206*, 1673-1680.
- Fallon, P.G., Ballantyne, S.J., Mangan, N.E., Barlow, J.L., Dasvarma, A., Hewett, D.R., McIlgorm, A., Jolin, H.E., and McKenzie, A.N. (2006). Identification of an interleukin (IL)-

25-dependent cell population that provides IL-4, IL-5, and IL-13 at the onset of helminth expulsion. *J. Exp. Med.* *203*, 1105-1116.

Feyerabend, T.B., Weiser, A., Tietz, A., Stassen, M., Harris, N., Kopf, M., Radermacher, P., Moller, P., Benoist, C., Mathis, D., *et al.* (2011). Cre-mediated cell ablation contests mast cell contribution in models of antibody- and T cell-mediated autoimmunity. *Immunity* *35*, 832-844.

Franke-Fayard, B., Waters, A.P., and Janse, C.J. (2006). Real-time in vivo imaging of transgenic bioluminescent blood stages of rodent malaria parasites in mice. *Nat. Protoc.* *1*, 476-485.

Gajardo, T., Morales, R.A., Campos-Mora, M., Campos-Acuna, J., and Pino-Lagos, K. (2015). Exogenous interleukin-33 targets myeloid-derived suppressor cells and generates periphery-induced Foxp3(+) regulatory T cells in skin-transplanted mice. *Immunology* *146*, 81-88.

Galioto, A.M., Hess, J.A., Nolan, T.J., Schad, G.A., Lee, J.J., and Abraham, D. (2006). Role of eosinophils and neutrophils in innate and adaptive protective immunity to larval *Strongyloides stercoralis* in mice. *Infect. Immun.* *74*, 5730-5738.

Gause, W.C., Wynn, T.A., and Allen, J.E. (2013). Type 2 immunity and wound healing: evolutionary refinement of adaptive immunity by helminths. *Nat. Rev. Immunol.* *13*, 607-614.

Goncalves, A.L., Rodrigues, R.M., Silva, N.M., Goncalves, F.A., Cardoso, C.R., Beletti, M.E., Ueta, M.T., Silva, J.S., and Costa-Cruz, J.M. (2008). Immunolocalization and pathological alterations following *Strongyloides venezuelensis* infection in the lungs and the intestine of MHC class I or II deficient mice. *Vet. Parasitol.* *158*, 319-328.

Grimbaldeston, M.A., Chen, C.C., Piliponsky, A.M., Tsai, M., Tam, S.Y., and Galli, S.J. (2005). Mast cell-deficient *W-sash* c-kit mutant *Kit W-sh/W-sh* mice as a model for investigating mast cell biology in vivo. *Am. J. Pathol.* *167*, 835-848.

Guimaraes-Costa, A.B., Nascimento, M.T., Wardini, A.B., Pinto-da-Silva, L.H., and Saraiva, E.M. (2012). ETosis: A Microbicidal Mechanism beyond Cell Death. *Journal of parasitology research* *2012*, 929743.

Hepworth, M.R., Danilowicz-Luebert, E., Rausch, S., Metz, M., Klotz, C., Maurer, M., and Hartmann, S. (2012). Mast cells orchestrate type 2 immunity to helminths through regulation of tissue-derived cytokines. *Proc. Natl. Acad. Sci. U. S. A.* *109*, 6644-6649.

Herbert, D.R., Lee, J.J., Lee, N.A., Nolan, T.J., Schad, G.A., and Abraham, D. (2000). Role of IL-5 in innate and adaptive immunity to larval *Strongyloides stercoralis* in mice. *J. Immunol.* *165*, 4544-4551.

Herbert, D.R., Nolan, T.J., Schad, G.A., and Abraham, D. (2002). The role of B cells in immunity against larval *Strongyloides stercoralis* in mice. *Parasite Immunol.* *24*, 95-101.

Higuchi, R., Fockler, C., Dollinger, G., and Watson, R. (1993). Kinetic PCR analysis: real-time monitoring of DNA amplification reactions. *Biotechnology. (N. Y.)* *11*, 1026-1030.

- Hira, P.R., and Patel, B.G. (1980). Human strongyloidiasis due to the primate species *Strongyloides fulleborni*. *Trop. Geogr. Med.* *32*, 23-29.
- Hueber, A.J., Alves-Filho, J.C., Asquith, D.L., Michels, C., Millar, N.L., Reilly, J.H., Graham, G.J., Liew, F.Y., Miller, A.M., and McInnes, I.B. (2011). IL-33 induces skin inflammation with mast cell and neutrophil activation. *Eur. J. Immunol.* *41*, 2229-2237.
- Humphreys, N.E., Xu, D., Hepworth, M.R., Liew, F.Y., and Grencis, R.K. (2008). IL-33, a potent inducer of adaptive immunity to intestinal nematodes. *J. Immunol.* *180*, 2443-2449.
- Hung, L.Y., Lewkowich, I.P., Dawson, L.A., Downey, J., Yang, Y., Smith, D.E., and Herbert, D.R. (2013). IL-33 drives biphasic IL-13 production for noncanonical Type 2 immunity against hookworms. *Proc. Natl. Acad. Sci. U. S. A.* *110*, 282-287.
- Katzwinkel-Wladarsch, S., Loscher, T., and Rinder, H. (1994). Direct amplification and differentiation of pathogenic and nonpathogenic *Entamoeba histolytica* DNA from stool specimens. *Am. J. Trop. Med. Hyg.* *51*, 115-118.
- Khan, A.I., Horii, Y., Tiuria, R., Sato, Y., and Nawa, Y. (1993). Mucosal mast cells and the expulsive mechanisms of mice against *Strongyloides venezuelensis*. *Int. J. Parasitol.* *23*, 551-555.
- Khan, W.I., Richard, M., Akiho, H., Blennerhasset, P.A., Humphreys, N.E., Grencis, R.K., Van Snick, J., and Collins, S.M. (2003). Modulation of intestinal muscle contraction by interleukin-9 (IL-9) or IL-9 neutralization: correlation with worm expulsion in murine nematode infections. *Infect. Immun.* *71*, 2430-2438.
- Krautz-Peterson, G., Ndegwa, D., Vasquez, K., Korideck, H., Zhang, J., Peterson, J.D., and Skelly, P.J. (2009). Imaging schistosomes in vivo. *FASEB J.* *23*, 2673-2680.
- Kuchler, A.M., Pollheimer, J., Balogh, J., Sponheim, J., Manley, L., Sorensen, D.R., De Angelis, P.M., Scott, H., and Haraldsen, G. (2008). Nuclear interleukin-33 is generally expressed in resting endothelium but rapidly lost upon angiogenic or proinflammatory activation. *Am. J. Pathol.* *173*, 1229-1242.
- Kurowska-Stolarska, M., Stolarski, B., Kewin, P., Murphy, G., Corrigan, C.J., Ying, S., Pitman, N., Mirchandani, A., Rana, B., van Rooijen, N., *et al.* (2009). IL-33 amplifies the polarization of alternatively activated macrophages that contribute to airway inflammation. *J. Immunol.* *183*, 6469-6477.
- Le, H.T., Tran, V.G., Kim, W., Kim, J., Cho, H.R., and Kwon, B. (2012). IL-33 Priming Regulates Multiple Steps of the Neutrophil-Mediated Anti-*Candida albicans* Response by Modulating TLR and Dectin-1 Signals. *The Journal of Immunology* *189*, 287-295.
- Lefrancais, E., Duval, A., Mirey, E., Roga, S., Espinosa, E., Cayrol, C., and Girard, J.P. (2014). Central domain of IL-33 is cleaved by mast cell proteases for potent activation of group-2 innate lymphoid cells. *Proc. Natl. Acad. Sci. U. S. A.* *111*, 15502-15507.
- Lefrancais, E., Roga, S., Gautier, V., Gonzalez-de-Peredo, A., Monsarrat, B., Girard, J.P., and Cayrol, C. (2012). IL-33 is processed into mature bioactive forms by neutrophil elastase and cathepsin G. *Proc. Natl. Acad. Sci. U. S. A.* *109*, 1673-1678.

- Liang, Y., Yi, P., Yuan, D.M.K., Jie, Z., Kwota, Z., Soong, L., Cong, Y., and Sun, J. (2018). IL-33 induces immunosuppressive neutrophils via a type 2 innate lymphoid cell/IL-13/STAT6 axis and protects the liver against injury in LCMV infection-induced viral hepatitis. *Cell. Mol. Immunol.*
- Licona-Limon, P., Arias-Rojas, A., and Olguin-Martinez, E. (2017). IL-9 and Th9 in parasite immunity. *Semin. Immunopathol.* *39*, 29-38.
- Licona-Limon, P., Henao-Mejia, J., Temann, A.U., Gagliani, N., Licona-Limon, I., Ishigame, H., Hao, L., Herbert, D.R., and Flavell, R.A. (2013). Th9 Cells Drive Host Immunity against Gastrointestinal Worm Infection. *Immunity* *39*, 744-757.
- Liew, F.Y., Girard, J.P., and Turnquist, H.R. (2016). Interleukin-33 in health and disease. *Nat. Rev. Immunol.* *16*, 676-689.
- Luthi, A.U., Cullen, S.P., McNeela, E.A., Duriez, P.J., Afonina, I.S., Sheridan, C., Brumatti, G., Taylor, R.C., Kersse, K., Vandenabeele, P., *et al.* (2009). Suppression of interleukin-33 bioactivity through proteolysis by apoptotic caspases. *Immunity* *31*, 84-98.
- Maizels, R.M., Hewitson, J.P., and Smith, K.A. (2012). Susceptibility and immunity to helminth parasites. *Curr. Opin. Immunol.* *24*, 459-466.
- Massacand, J.C., Stettler, R.C., Meier, R., Humphreys, N.E., Grencis, R.K., Marsland, B.J., and Harris, N.L. (2009). Helminth products bypass the need for TSLP in Th2 immune responses by directly modulating dendritic cell function. *Proc. Natl. Acad. Sci. U. S. A.* *106*, 13968-13973.
- McHugh, T.D., Jenkins, T., and McLaren, D.J. (1989). *Strongyloides ratti*: studies of cutaneous reactions elicited in naive and sensitized rats and of changes in surface antigenicity of skin-penetrating larvae. *Parasitology* *98 ( Pt 1)*, 95-103.
- Miller, A.M. (2011). Role of IL-33 in inflammation and disease. *Journal of inflammation (London, England)* *8*, 22.
- Mogensen, T.H. (2009). Pathogen recognition and inflammatory signaling in innate immune defenses. *Clin. Microbiol. Rev.* *22*, 240-273, Table of Contents.
- Mohapatra, A., Van Dyken, S.J., Schneider, C., Nussbaum, J.C., Liang, H.E., and Locksley, R.M. (2016). Group 2 innate lymphoid cells utilize the IRF4-IL-9 module to coordinate epithelial cell maintenance of lung homeostasis. *Mucosal Immunol.* *9*, 275-286.
- Molofsky, A.B., Savage, A.K., and Locksley, R.M. (2015). Interleukin-33 in Tissue Homeostasis, Injury, and Inflammation. *Immunity* *42*, 1005-1019.
- Moussion, C., Ortega, N., and Girard, J.P. (2008). The IL-1-like cytokine IL-33 is constitutively expressed in the nucleus of endothelial cells and epithelial cells in vivo: a novel 'alarmin'? *PLoS One* *3*, e3331.
- Mullis, K.B. (1990). The unusual origin of the polymerase chain reaction. *Sci. Am.* *262*, 56-61, 64-55.

- Nausch, N., and Mutapi, F. (2018). Group 2 ILCs: A way of enhancing immune protection against human helminths? *Parasite Immunol.* *40*.
- Noelle, R.J., and Nowak, E.C. (2010). Cellular sources and immune functions of interleukin-9. *Nat. Rev. Immunol.* *10*, 683-687.
- O'Connell, A.E., Hess, J.A., Santiago, G.A., Nolan, T.J., Lok, J.B., Lee, J.J., and Abraham, D. (2011). Major basic protein from eosinophils and myeloperoxidase from neutrophils are required for protective immunity to *Strongyloides stercoralis* in mice. *Infect. Immun.* *79*, 2770-2778.
- Obata-Ninomiya, K., Ishiwata, K., Tsutsui, H., Nei, Y., Yoshikawa, S., Kawano, Y., Minegishi, Y., Ohta, N., Watanabe, N., Kanuka, H., *et al.* (2013). The skin is an important bulwark of acquired immunity against intestinal helminths. *J. Exp. Med.* *210*, 2583-2595.
- Oboki, K., Ohno, T., Kajiwara, N., Saito, H., and Nakae, S. (2010). IL-33 and IL-33 receptors in host defense and diseases. *Allergology international : official journal of the Japanese Society of Allergology* *59*, 143-160.
- Ohnmacht, C., Schwartz, C., Panzer, M., Schiedewitz, I., Naumann, R., and Voehringer, D. (2010). Basophils orchestrate chronic allergic dermatitis and protective immunity against helminths. *Immunity* *33*, 364-374.
- Oliphant, C.J., Barlow, J.L., and McKenzie, A.N. (2011). Insights into the initiation of type 2 immune responses. *Immunology* *134*, 378-385.
- Osbourn, M., Soares, D.C., Vacca, F., Cohen, E.S., Scott, I.C., Gregory, W.F., Smyth, D.J., Toivakka, M., Kemter, A.M., le Bihan, T., *et al.* (2017). HpARI Protein Secreted by a Helminth Parasite Suppresses Interleukin-33. *Immunity* *47*, 739-751.e735.
- Padigel, U.M., Lee, J.J., Nolan, T.J., Schad, G.A., and Abraham, D. (2006). Eosinophils can function as antigen-presenting cells to induce primary and secondary immune responses to *Strongyloides stercoralis*. *Infect. Immun.* *74*, 3232-3238.
- Pampiglione, S., and Ricciardi, M.L. (1972). Geographic distribution of *Strongyloides fuelleborni* in humans in tropical Africa. *Parasitologia* *14*, 329-338.
- Percopo, C.M., Brenner, T.A., Ma, M., Kraemer, L.S., Hakeem, R.M., Lee, J.J., and Rosenberg, H.F. (2017). SiglecF<sup>+</sup>Gr1<sup>hi</sup> eosinophils are a distinct subpopulation within the lungs of allergen-challenged mice. *J. Leukoc. Biol.* *101*, 321-328.
- Perrigoue, J.G., Marshall, F.A., and Artis, D. (2008). On the hunt for helminths: innate immune cells in the recognition and response to helminth parasites. *Cell. Microbiol.* *10*, 1757-1764.
- Pichery, M., Mirey, E., Mercier, P., Lefrancais, E., Dujardin, A., Ortega, N., and Girard, J.P. (2012). Endogenous IL-33 is highly expressed in mouse epithelial barrier tissues, lymphoid organs, brain, embryos, and inflamed tissues: in situ analysis using a novel IL-33-LacZ gene trap reporter strain. *J. Immunol.* *188*, 3488-3495.
- Ramalingam, T.R., Pesce, J.T., Mentink-Kane, M.M., Madala, S., Cheever, A.W., Comeau, M.R., Ziegler, S.F., and Wynn, T.A. (2009). Regulation of helminth-induced Th2 responses by thymic stromal lymphopoietin. *J. Immunol.* *182*, 6452-6459.

- Rank, M.A., Kobayashi, T., Kozaki, H., Bartemes, K.R., Squillace, D.L., and Kita, H. (2009). IL-33-activated dendritic cells induce an atypical TH2-type response. *J. Allergy Clin. Immunol.* *123*, 1047-1054.
- Rauber, S., Lubber, M., Weber, S., Maul, L., Soare, A., Wohlfahrt, T., Lin, N.Y., Dietel, K., Bozec, A., Herrmann, M., *et al.* (2017). Resolution of inflammation by interleukin-9-producing type 2 innate lymphoid cells. *Nat. Med.* *23*, 938-944.
- Reber, L.L., Marichal, T., and Galli, S.J. (2012). New models for analyzing mast cell functions in vivo. *Trends Immunol.* *33*, 613-625.
- Reitz, M., Brunn, M.L., Rodewald, H.R., Feyerabend, T.B., Roers, A., Dudeck, A., Voehringer, D., Jonsson, F., Kuhl, A.A., and Breloer, M. (2017). Mucosal mast cells are indispensable for the timely termination of *Strongyloides ratti* infection. *Mucosal Immunol.* *10*, 481-492.
- Reitz, M., Hartmann, W., Rudiger, N., Orinska, Z., Brunn, M.L., and Breloer, M. (2018). Interleukin-9 promotes early mast cell-mediated expulsion of *Strongyloides ratti* but is dispensable for generation of protective memory. *Sci. Rep.* *8*, 8636.
- Reynolds, D.S., Stevens, R.L., Lane, W.S., Carr, M.H., Austen, K.F., and Serafin, W.E. (1990). Different mouse mast cell populations express various combinations of at least six distinct mast cell serine proteases. *Proc. Natl. Acad. Sci. U. S. A.* *87*, 3230-3234.
- Rodewald, H.R., and Feyerabend, T.B. (2012). Widespread immunological functions of mast cells: fact or fiction? *Immunity* *37*, 13-24.
- Rodrigues, R.M., Cardoso, C.R., Goncalves, A.L., Silva, N.M., Massa, V., Alves, R., Ueta, M.T., Silva, J.S., and Costa-Cruz, J.M. (2013). Increased susceptibility to *Strongyloides venezuelensis* infection is related to the parasite load and absence of major histocompatibility complex (MHC) class II molecules. *Exp. Parasitol.* *135*, 580-586.
- Rodrigues, R.M., Silva, N.M., Goncalves, A.L., Cardoso, C.R., Alves, R., Goncalves, F.A., Beletti, M.E., Ueta, M.T., Silva, J.S., and Costa-Cruz, J.M. (2009). Major histocompatibility complex (MHC) class II but not MHC class I molecules are required for efficient control of *Strongyloides venezuelensis* infection in mice. *Immunology* *128*, e432-441.
- Rotman, H.L., Schnyder-Candrian, S., Scott, P., Nolan, T.J., Schad, G.A., and Abraham, D. (1997). IL-12 eliminates the Th-2 dependent protective immune response of mice to larval *Strongyloides stercoralis*. *Parasite Immunol.* *19*, 29-39.
- Roussel, L., Erard, M., Cayrol, C., and Girard, J.P. (2008). Molecular mimicry between IL-33 and KSHV for attachment to chromatin through the H2A-H2B acidic pocket. *EMBO reports* *9*, 1006-1012.
- Saeij, J.P., Boyle, J.P., Grigg, M.E., Arrizabalaga, G., and Boothroyd, J.C. (2005). Bioluminescence imaging of *Toxoplasma gondii* infection in living mice reveals dramatic differences between strains. *Infect. Immun.* *73*, 695-702.
- Saenz, S.A., Siracusa, M.C., Perrigoue, J.G., Spencer, S.P., Urban, J.F., Jr., Tocker, J.E., Budelsky, A.L., Kleinschek, M.A., Kastelein, R.A., Kambayashi, T., *et al.* (2010). IL25

- elicits a multipotent progenitor cell population that promotes T(H)2 cytokine responses. *Nature* *464*, 1362-1366.
- Saenz, S.A., Taylor, B.C., and Artis, D. (2008). Welcome to the neighborhood: epithelial cell-derived cytokines license innate and adaptive immune responses at mucosal sites. *Immunol. Rev.* *226*, 172-190.
- Sandground, J. (1925). Speciation and specificity in the nematode genus *Strongyloides*. *Journal of Parasitology* *12*, 59-81.
- Sasaki, Y., Yoshimoto, T., Maruyama, H., Tegoshi, T., Ohta, N., Arizono, N., and Nakanishi, K. (2005). IL-18 with IL-2 protects against *Strongyloides venezuelensis* infection by activating mucosal mast cell-dependent type 2 innate immunity. *J. Exp. Med.* *202*, 607-616.
- Sato, Y., and Toma, H. (1990). *Strongyloides venezuelensis* infections in mice. *Int. J. Parasitol.* *20*, 57-62.
- Schad, G.A. (1989). Morphology and life history of *Strongyloides stercoralis*. In *Strongyloidiasis a major roundworm infection of man*. D.I. Grove, ed. (London: Taylor and Francis), 85–104.
- Schmitz, J., Owyang, A., Oldham, E., Song, Y., Murphy, E., McClanahan, T.K., Zurawski, G., Moshrefi, M., Qin, J., Li, X., *et al.* (2005). IL-33, an interleukin-1-like cytokine that signals via the IL-1 receptor-related protein ST2 and induces T helper type 2-associated cytokines. *Immunity* *23*, 479-490.
- Schramm, G., Gronow, A., Knobloch, J., Wippersteg, V., Grevelding, C.G., Galle, J., Fuller, H., Stanley, R.G., Chiodini, P.L., Haas, H., *et al.* (2006). IPSE/alpha-1: a major immunogenic component secreted from *Schistosoma mansoni* eggs. *Mol. Biochem. Parasitol.* *147*, 9-19.
- Schramm, G., Mohrs, K., Wodrich, M., Doenhoff, M.J., Pearce, E.J., Haas, H., and Mohrs, M. (2007). Cutting edge: IPSE/alpha-1, a glycoprotein from *Schistosoma mansoni* eggs, induces IgE-dependent, antigen-independent IL-4 production by murine basophils in vivo. *J. Immunol.* *178*, 6023-6027.
- Shimokawa, C., Kanaya, T., Hachisuka, M., Ishiwata, K., Hisaeda, H., Kurashima, Y., Kiyono, H., Yoshimoto, T., Kaisho, T., and Ohno, H. (2017). Mast Cells Are Crucial for Induction of Group 2 Innate Lymphoid Cells and Clearance of Helminth Infections. *Immunity* *46*, 863-874.e864.
- Shintoku, Y., Kadosaka, T., Kimura, E., Takagi, H., Kondo, S., and Itoh, M. (2013). Intestinal mast cells and eosinophils in relation to *Strongyloides ratti* adult expulsion from the small and large intestines of rats. *Parasitology* *140*, 626-631.
- Siddiqui, A.A., and Berk, S.L. (2001). Diagnosis of *Strongyloides stercoralis* infection. *Clin. Infect. Dis.* *33*, 1040-1047.

- Smithgall, M.D., Comeau, M.R., Yoon, B.R., Kaufman, D., Armitage, R., and Smith, D.E. (2008). IL-33 amplifies both Th1- and Th2-type responses through its activity on human basophils, allergen-reactive Th2 cells, iNKT and NK cells. *Int. Immunol.* *20*, 1019-1030.
- Sorobetea, D., Svensson-Frej, M., and Grecis, R. (2018). Immunity to gastrointestinal nematode infections. *Mucosal Immunol.* *11*, 304.
- Speare, R. (1989). Identification of species of *Strongyloides*. In *Strongyloidiasis a major roundworm infection of man*. D.I. Grove, ed. (London: Taylor and Francis), 11–84.
- Steenwinckel, V., Louahed, J., Orabona, C., Huaux, F., Warnier, G., McKenzie, A., Lison, D., Levitt, R., and Renaud, J.C. (2007). IL-13 mediates in vivo IL-9 activities on lung epithelial cells but not on hematopoietic cells. *J. Immunol.* *178*, 3244-3251.
- Stein, L.H., Redding, K.M., Lee, J.J., Nolan, T.J., Schad, G.A., Lok, J.B., and Abraham, D. (2009). Eosinophils utilize multiple chemokine receptors for chemotaxis to the parasitic nematode *Strongyloides stercoralis*. *J. Innate Immun.* *1*, 618-630.
- Streit, A. (2008). Reproduction in *Strongyloides* (Nematoda): a life between sex and parthenogenesis. *Parasitology* *135*, 285-294.
- Talabot-Ayer, D., Lamacchia, C., Gabay, C., and Palmer, G. (2009). Interleukin-33 is biologically active independently of caspase-1 cleavage. *J. Biol. Chem.* *284*, 19420-19426.
- Taylor, B.C., Zaph, C., Troy, A.E., Du, Y., Guild, K.J., Comeau, M.R., and Artis, D. (2009). TSLP regulates intestinal immunity and inflammation in mouse models of helminth infection and colitis. *J. Exp. Med.* *206*, 655-667.
- Thomas, P.G., Carter, M.R., Atochina, O., Da'Dara, A.A., Piskorska, D., McGuire, E., and Harn, D.A. (2003). Maturation of dendritic cell 2 phenotype by a helminth glycan uses a Toll-like receptor 4-dependent mechanism. *J. Immunol.* *171*, 5837-5841.
- Townsend, J.M., Fallon, G.P., Matthews, J.D., Smith, P., Jolin, E.H., and McKenzie, N.A. (2000a). IL-9-deficient mice establish fundamental roles for IL-9 in pulmonary mastocytosis and goblet cell hyperplasia but not T cell development. *Immunity* *13*, 573-583.
- Townsend, M.J., Fallon, P.G., Matthews, D.J., Jolin, H.E., and McKenzie, A.N. (2000b). T1/ST2-deficient mice demonstrate the importance of T1/ST2 in developing primary T helper cell type 2 responses. *J. Exp. Med.* *191*, 1069-1076.
- Turner, J.E., Morrison, P.J., Wilhelm, C., Wilson, M., Ahlfors, H., Renaud, J.C., Panzer, U., Helmbj, H., and Stockinger, B. (2013). IL-9-mediated survival of type 2 innate lymphoid cells promotes damage control in helminth-induced lung inflammation. *J. Exp. Med.* *210*, 2951-2965.
- Turnquist, H.R., Zhao, Z., Rosborough, B.R., Liu, Q., Castellaneta, A., Isse, K., Wang, Z., Lang, M., Stolz, D.B., Zheng, X.X., *et al.* (2011). IL-33 expands suppressive CD11b+ Gr-1(int) and regulatory T cells, including ST2L+ Foxp3+ cells, and mediates regulatory T cell-dependent promotion of cardiac allograft survival. *J. Immunol.* *187*, 4598-4610.



- Verri, W.A., Jr., Souto, F.O., Vieira, S.M., Almeida, S.C., Fukada, S.Y., Xu, D., Alves-Filho, J.C., Cunha, T.M., Guerrero, A.T., Mattos-Guimaraes, R.B., *et al.* (2010). IL-33 induces neutrophil migration in rheumatoid arthritis and is a target of anti-TNF therapy. *Ann. Rheum. Dis.* *69*, 1697-1703.
- Viney, M., and Kikuchi, T. (2017). *Strongyloides ratti* and *S. venezuelensis* - rodent models of *Strongyloides* infection. *Parasitology* *144*, 285-294.
- Viney, M.E. (1999). Exploiting the life cycle of *Strongyloides ratti*. *Parasitol. Today* *15*, 231-235.
- Viney, M.E., and Lok, J.B. (2007). *Strongyloides* spp. *WormBook*, 1-15.
- Voehringer, D. (2013). Protective and pathological roles of mast cells and basophils. *Nat. Rev. Immunol.* *13*, 362-375.
- Wang, J.X., Kaieda, S., Ameri, S., Fishgal, N., Dwyer, D., Dellinger, A., Kepley, C.L., Gurish, M.F., and Nigrovic, P.A. (2014). IL-33/ST2 axis promotes mast cell survival via BCLXL. *Proc. Natl. Acad. Sci. U. S. A.* *111*, 10281-10286.
- Watanabe, K., Noda, K., Hamano, S., Koga, M., Kishihara, K., Nomoto, K., and Tada, I. (2000). The crucial role of granulocytes in the early host defense against *Strongyloides ratti* infection in mice. *Parasitol. Res.* *86*, 188-193.
- Watanabe, K., Sasaki, O., Hamano, S., Kishihara, K., Nomoto, K., Tada, I., and Aoki, Y. (2003). *Strongyloides ratti*: the role of interleukin-5 in protection against tissue migrating larvae and intestinal adult worms. *J. Helminthol.* *77*, 355-361.
- Wilhelm, C., Hirota, K., Stieglitz, B., Van Snick, J., Tolaini, M., Lahl, K., Sparwasser, T., Helmbj, H., and Stockinger, B. (2011). An IL-9 fate reporter demonstrates the induction of an innate IL-9 response in lung inflammation. *Nat. Immunol.* *12*, 1071-1077.
- Wojtasiak, M., Pickett, D.L., Tate, M.D., Londrigan, S.L., Bedoui, S., Brooks, A.G., and Reading, P.C. (2010). Depletion of Gr-1+, but not Ly6G+, immune cells exacerbates virus replication and disease in an intranasal model of herpes simplex virus type 1 infection. *J. Gen. Virol.* *91*, 2158-2166.
- Xu, J., Guardado, J., Hoffman, R., Xu, H., Namas, R., Vodovotz, Y., Xu, L., Ramadan, M., Brown, J., Turnquist, H.R., *et al.* (2017). IL33-mediated ILC2 activation and neutrophil IL5 production in the lung response after severe trauma: A reverse translation study from a human cohort to a mouse trauma model. *PLoS Med.* *14*, e1002365.
- Yap, G.S., and Gause, W.C. (2018). Helminth Infections Induce Tissue Tolerance Mitigating Immunopathology but Enhancing Microbial Pathogen Susceptibility. *Front. Immunol.* *9*, 2135.
- Yasuda, K., Muto, T., Kawagoe, T., Matsumoto, M., Sasaki, Y., Matsushita, K., Taki, Y., Futatsugi-Yumikura, S., Tsutsui, H., Ishii, K.J., *et al.* (2012). Contribution of IL-33-activated type II innate lymphoid cells to pulmonary eosinophilia in intestinal nematode-infected mice. *Proc. Natl. Acad. Sci. U. S. A.* *109*, 3451-3456.
- Yazdani, H.O., Chen, H.W., Tohme, S., Tai, S., van der Windt, D.J., Loughran, P., Rosborough, B.R., Sud, V., Beer-Stolz, D., Turnquist, H.R., *et al.* (2017). IL-33

## List of references

---

exacerbates liver sterile inflammation by amplifying neutrophil extracellular trap formation. *J. Hepatol.*

Yu, C., Cantor, A.B., Yang, H., Browne, C., Wells, R.A., Fujiwara, Y., and Orkin, S.H. (2002). Targeted deletion of a high-affinity GATA-binding site in the GATA-1 promoter leads to selective loss of the eosinophil lineage in vivo. *J. Exp. Med.* *195*, 1387-1395.